

COMPARING PHOTOGRAMMETRIC AND SPECTRAL DEPTH TECHNIQUES IN
EXTRACTING BATHYMETRIC DATA FROM A GRAVEL-BED RIVER

by

CHRISTINA MARIE SHINTANI

A THESIS

Presented to the Department of Geography
and the Graduate School of the University of Oregon
in partial fulfillment of the requirements
for the degree of
Master of Science

June 2016

THESIS APPROVAL PAGE

Student: Christina Marie Shintani

Title: Comparing Photogrammetric and Spectral Depth Techniques in Extracting Bathymetric Data from a Gravel-Bed River

This thesis has been accepted and approved in partial fulfillment of the requirements for the Master of Science degree in the Department of Geography by:

Dr. Mark Fonstad	Chairperson
Dr. Patricia McDowell	Member

and

Scott L. Pratt	Dean of the Graduate School
----------------	-----------------------------

Original approval signatures are on file with the University of Oregon Graduate School.

Degree awarded June 2016

© 2016 Christina Marie Shintani

THESIS ABSTRACT

Christina Marie Shintani

Master of Science

Department of Geography

June 2016

Title: Comparing Photogrammetric and Spectral Depth Techniques in Extracting Bathymetric Data from a Gravel-Bed River

Recent advances in through-water photogrammetry and optical imagery indicate that accurate, continuous bathymetric mapping may be possible in shallow, clear streams. This research directly compares the ability of through-water photogrammetry and spectral depth approaches to extract water depth for monitoring fish habitat. Imagery and cross sections were collected on a 140 meter reach of the Salmon River, Oregon, using an unmanned aerial vehicle (UAV) and rtk-GPS. Structure-from-Motion (SfM) software produced a digital elevation model (DEM) (1.5 cm) and orthophoto (0.37 cm). The photogrammetric approach of applying a site-specific refractive index provided the most accurate (mean error 0.009 m) and precise (standard deviation of error 0.17 m) bathymetric data ($R^2 = 0.67$) over the spectral depth and the 1.34 refractive index approaches. This research provides a quantitative comparison between and within bathymetric mapping methods, and suggests that a site-specific refractive index may be appropriate for similar gravel-bed, relatively shallow, clear streams.

CURRICULUM VITAE

NAME OF AUTHOR: Christina Marie Shintani

GRADUATE AND UNDERGRADUATE SCHOOLS ATTENDED:

University of Oregon, Eugene, OR
The College of William and Mary, Williamsburg, VA

DEGREES AWARDED:

Master of Science, Geography, 2016, University of Oregon
Bachelor of Science, Physical Geography, 2014, The College of William and Mary.

AREAS OF SPECIAL INTEREST:

Fluvial geomorphology
Fluvial remote sensing
River and habitat restoration
Cartography

PROFESSIONAL EXPERIENCE:

Science and Analytics Fellow, The Freshwater Trust, July – September 2016

Graduate Teaching Fellow, Department of Geography, University of Oregon, Fall 2014 – Winter 2015, Fall 2015 – Spring 2016

Graduate Teaching Fellow, Department of Geological Sciences, University of Oregon, Spring 2015

Research Assistant, The College of William and Mary, 2013 – 2014

GRANTS, AWARDS, AND HONORS:

Bill Loy Award for Excellence in Cartographic Design and Geographic Visualization, Restoring Fish Habitat in the Sandy River Basin, University of Oregon, 2016

Graduate Student Conference Support, University of Oregon, 2016

ASPRS Research Support, University of Oregon Student Chapter, 2016

Graduate Teaching Fellowship, University of Oregon, 2014 – 2016

ACKNOWLEDGMENTS

I want to thank my advisor Mark Fonstad for introducing me to the fluvial remote sensing world. He taught me how to contextualize details into the broader themes and obstacles of the fluvial geomorphology and remote sensing research. I could always rely on Mark to support and encourage me at every step. I would also like to thank my committee member Patricia McDowell for providing detailed feedback and for her support and encouragement throughout this process. This research would not have been possible without the support of Greg Wanner and the US Forest Service Zigzag Ranger Station and Bruce Zoellick with the Oregon Bureau of Land Management.

I would like to thank my fellow geography graduate students for their support, especially to the current and former fluvial geomorphology students. Not only have I appreciated your support and kindness, but also our day-to-day conversations about each other's research undoubtedly improved the way I conducted and analyzed my research. Last but not least, I would like to thank my parents, who have always encouraged my academic pursuits, and without whom I would not have had the educational opportunities or support I needed to be where I am today.

TABLE OF CONTENTS

Chapter	Page
I. INTRODUCTION	1
II. BACKGROUND.....	7
Fluvial Remote Sensing	7
Spectral Depth.....	9
Through-Water Photogrammetry	13
Study Site	16
III. METHODS	19
Image Acquisition and GPS Data Collection.....	19
Structure-from-Motion Processing	21
Water Surface Interpolation	23
Photogrammetric Approach	31
1.34 Refraction Coefficient.....	31
Site Specific Refraction Correction	32
Habitat Unit Refraction Correction.....	34
Spectral Depth Approach	36
IV. RESULTS	38
Photogrammetric Refraction Correction.....	38
Spectral Depth Regression	41
Comparison of Photogrammetric and Spectral Depth Approaches	44
Creating the Corrected DEM	48

Chapter	Page
V. DISCUSSION	52
Image Acquisition.....	52
Water Surface Interpolation.....	53
Photogrammetric Approach.....	55
Spectral Depth Approach.....	58
Comparison of the Approaches and Applicability in Surveying Fish Habitat.....	60
Suggestions for River Scientists and Managers.....	64
Limitations and Considerations	68
VI. CONCLUSION.....	72
APPENDICES	74
A. STRUCTURE-FROM-MOTION	74
B. RTK-GPS CHANNEL CROSS-SECTION DATA	76
C. WATER SURFACE INTERPOLATION.....	84
D. ERROR DISTRIBUTIONS	93
REFERENCES CITED.....	111

LIST OF FIGURES

Figure	Page
1. Study site location map.....	17
2. General workflow	20
3. Site orthophoto.....	22
4. Site DEM	23
5. Longitudinal profile of water surface elevations	25
6. Adjusted water surface elevations	27
7. Spline water surface.....	31
8. Refraction correction workflow	32
9. Habitat unit delineation.....	35
10. 1.34 Refraction coefficient scatterplot.....	39
11. Site-specific refraction correction.....	40
12. Site spectral depth regression.....	43
13. Non-shadow spectral depth regression	43
14. Final DEM corrected.....	49
15. Error distributions between predicted and observed water depths	50
16. Residual plot of depth differences	51

LIST OF TABLES

Table	Page
1. Previous depth mapping studies.....	10
2. Adjusted edge-of-water elevations	25
3. Comparing water surface elevations from the TIN and spline interpolation.....	30
4. Method of dividing data to derive site-specific coefficient	33
5. Refraction correction equations and goodness of fit.....	39
6. Refraction correction after removing more outliers.....	39
7. Refraction correction after removing shallow depths.....	40
8. Refraction correction for three habitat units	41
9. Refraction correction for three habitat units after removing outliers	41
10. Best refraction correction equations	41
11. Spectral depth regressions.....	42
12. Comparison of photogrammetric and spectral depth approaches	45
13. Mean error and standard deviation of photogrammetric and spectral depth regressions.....	45
14. Changes in mean error and standard deviation after refraction correction.....	45
15. T-tests measuring significant difference between mean error of site-specific coefficient and other approaches	46
16. Moran’s I statistic for 4 approaches.....	47
17. Best field surveying practices	65

CHAPTER I

INTRODUCTION

The understanding of physical and ecological processes that govern rivers and their biota are critical components of myriad studies and disciplines. River processes have significant controls on a wide range of geographical extents, from whole landscapes to a small side channel supporting life for hundreds of organisms. Quantifying bathymetry has been of particular concern of fluvial geomorphology and river management because it is a basic descriptor of channel morphology, as well as one of the major elements of a river that adjusts in response to fluctuations and disturbances (Montgomery and Buffington, 1998; Westaway et al., 2001; Woodget et al., 2014). Bathymetry and changes in bathymetry define the location of channel units, and therefore control the location of various habitat types and hydraulic variables that influence the rate of geomorphic change.

Understanding fluvial topography is, therefore, paramount in understanding river form, process, and function. Bathymetry is generally derived from spatially extensive but low density data, such as from total station or rtk-GPS surveys (Feurer et al., 2008; Marcus and Fonstad, 2008; Bangen et al., 2014). These traditional survey techniques to collect bathymetric data describe streams in a discontinuous manner, and can potentially overlook key physical features of the river that influence river behavior and affect biota at the sub-meter scale (Marcus and Fonstad, 2008; Dietrich, 2015). Our understanding and mapping of rivers across disciplines has been based on discontinuous data to describe a continuously varying system.

New applications to study rivers, including geomorphic change detection, physical habitat modeling, 2D hydraulic modeling, sediment budgeting, and restoration assessment and monitoring, are demanding more continuous, higher resolution bathymetric data in order to improve our knowledge of river form and process. All of these applications require an objective and repeatable technique that offers high resolution and spatially continuous data (Woodget et al., 2014). Aerial and satellite imagery may be an option for larger rivers in non-forested watersheds and when funding is available, but do not meet the spatial or temporal requirements for monitoring small streams (Lejot et al., 2007; Carbonneau and Piegay, 2012). Some areas may have bathymetric LiDAR data available, but these data are most accurate at depths greater than 0.50 meters (Feurer et al., 2008), as well as being expensive and infrequently collected. ADCPs (Acoustic Doppler Current Profilers) and sonar are commonly used as well, however cannot be used in very shallow depths or in some riffle habitats. When timing and extensive surveys are essential to observe morphological changes, non-continuous land surveys or infrequent aerial surveys to collect bathymetric data become inadequate. In order to understand the physical processes that occur following fluctuations and disturbances, we need higher resolution data, both spatially and temporally.

Recent advances in photogrammetry and optical imagery have demonstrated potential in meeting the demands for high spatial and temporal resolution bathymetric data and mapping as an alternative to orthodox field methods (Marcus and Fonstad, 2008; Legleiter, 2012), particularly for shallow rivers, where high spatial resolution is needed but little data have been collected (Feurer et al., 2008). These advances indicate that accurate, continuous mapping of depth and in-stream habitats should be possible (Marcus

and Fonstad, 2008), and numerous studies, given relatively shallow depths and clear water, reported results demonstrating the ability and potential of remote sensing methods to derive accurate and precise digital elevation models (DEMs) for submerged topography (Marcus et al., 2003; Carbonneau et al., 2006; Lejot et al., 2007; Feurer et al., 2008; Legleiter et al., 2009; Fonstad et al., 2013; Woodget et al., 2014; Dietrich, 2015).

Despite these advances and promising results, large gaps remain in the literature regarding the types of methods available and able to derive bathymetric data in different river systems. An overwhelming majority of published literature utilizes aerial photography and spectral depth methods. The use of aerial photography is inflexible and has been repeatedly cited as a logistical issue regarding planning, cost, and ability of repeat flights (Lejot et al., 2007; Feurer et al., 2008; Marcus et al., 2012). Unmanned aerial systems (UAS) are becoming increasingly popular as they offer flexibility for a much lower cost, however very few studies have used an unmanned aerial vehicle (UAV) or drone to collect imagery (Carbonneau and Piegay, 2012). Spectral depth may be the most widely used method for deriving water depth (Woodget et al., 2014), even though research has found spectral depth to be more effective where the streambed is homogeneous with little spatial variation in the streambed spectral properties (Feurer et al., 2008; Legletier et al., 2008). Shadow is well documented as a major limitation to using the spectral depth method, but there are no published methods to mitigate this shadow problem (Carbonneau et al., 2012), and quantitatively measuring the differences in accuracy and precision in shadow and non-shadow areas of the channel has not been thoroughly explored.

The photogrammetric technique is based on multiplying the predicted water depth by a refractive index to account for the light refraction occurring at the air-water interface. The accepted refractive index of 1.34 established by Jerlov (1976) has been applied in multiple publications using this technique, but some researchers also reported that in shallow depths of less than 0.4 meters, mean error of depths were negligible and similar to errors on exposed topography, and that depths greater than 0.4 meters produced larger errors that increased with depth (Westaway et al., 2001; Woodget et al., 2014). Additionally, Butler et al. (2002) stated that the simple application of Snell's Law is not sufficient to account for the refraction effect because the magnitude of the refractive index depends on the angle of incidence and the distance and angle of the sensor from the water surface. This questions the applicability of a single coefficient to correct for refraction on all clear, shallow streams, and that the coefficient encompasses all the variables at play that lead to varying error in a stream.

Photogrammetric and spectral depth methods succeed in extracting flow depths in different environments, but through-water photogrammetric methods are published far less often (Feurer et al., 2008), and the accuracy and precision of the two methods have not been directly quantitatively compared. Both methods require knowing the elevation of the water surface (Westaway et al., 2001; Butler et al., 2002; Javernick et al., 2014) and researchers have acknowledged that this step is crucial in extracting accurate water depths, yet most studies have only provided one to two sentences at best to justify their choice of water surface interpolation method, if an explanation is given at all. The accuracy and precision results produced by these methods must be contextualized with

the quality of the interpolated water surface, which often passes as an undiscussed topic (Williams et al., 2014).

This research seeks to quantitatively compare spectral depth and photogrammetric approaches and assess water surface interpolation methods in a gravel-bed stream. I used a UAV and structure-from-motion (SfM) software to acquire and process the imagery, and collected validation data with an rtk-GPS on a reach of the Salmon River, in northeast Clackamas County, Oregon. After deriving regression equations to estimate water depth with both approaches, I assessed which method extracts more accurate depth measurements at the study site. The data processing and results will indicate if these methods are ready for widespread application in collecting high resolution, spatially continuous bathymetric data, and how to improve these methods for future research. This thesis will present a methodological analysis of the advantages and disadvantages between two types of bathymetry measurements to answer the following research questions:

1. Given the site conditions, which remote sensing methods improve the accuracy of each bathymetric mapping technique?
 - a. For both the spectral depth and structure-from-motion photogrammetry techniques, which method of deriving a water surface lid produces the best results for deriving bathymetry?
 - b. Regarding the photogrammetric approach, what is the appropriate refraction coefficient for a test reach of the Salmon River, and how can it be applied to similar gravel-bed streams?

- c. Regarding the spectral depth approach, how does separating the river into shadow and non-shadow areas and habitat units affect the accuracy of the bathymetry?
2. Which remote sensing approach, structure-from-motion or spectral depth, extracts more accurate data from a gravel-bed stream and provides the highest quality data for monitoring fish habitat?

This research aims to identify methods that produce repeatable results for interpolating a water surface, and deriving water depths from photogrammetric and spectral depth methods to allow others to make the same assessments and comparisons on different types of rivers. The goal is to quantify the differences in accuracy and precision between the two methods, and to influence future research to compare these methods in order to develop guidelines for best practices and where these methods can be applied. Quantifying these differences would be an important contribution to any application that involves collecting high resolution bathymetric data, as well as to the broader remote sensing community in measuring aspects of submerged topography.

CHAPTER II

BACKGROUND

Fluvial Remote Sensing

Remote sensing has been used to characterize river forms and bathymetry for decades, which has coincided with the rapid increase in availability of high resolution digital imagery (Lejot et al., 2007; Feurer et al., 2008; Marcus et al., 2012). The use of remote sensing has become more popular in studying river processes due to the need for surveying larger extents more frequently, however its use is also limited by logistical and cost concerns (Marcus et al., 2012). While obstacles exist that hinder remote sensing methods from capturing high quality images in all environments, remote sensing is the only feasible method for measuring, mapping, and monitoring various river features at a sub-meter resolution (Marcus and Fonstad, 2008; Carbonneau and Piegay, 2012).

Among commonly used imagery are those collected from satellites, aerial photography, and bathymetric lidar. While there are advantages to each, all three methods are inadequate in measuring bathymetry in relatively small, shallow streams, and pose considerable logistical challenges. For streams located in forested watersheds, overhanging vegetation would prevent the full channel from being captured in the images acquired from above the canopy height. Satellite imagery is only viable for large rivers because even the spatial resolution of the best quality imagery is too coarse to identify detailed features in a small stream (Lejot et al., 2007; Carbonneau and Piegay, 2012). Bathymetric lidar, while it does not depend on illumination conditions, uses algorithms that make it nearly impossible to accurately measure depths shallower than 0.5 meters, and its minimum vertical accuracy is 0.2 meters (Feurer et al., 2008). Aerial photography

can be very expensive and difficult to plan logistically, and thus repeat flights are difficult to plan or fund. As for the sensors that are affordable and widely used, many do not penetrate water (Williams et al., 2014).

Using UASs to collect imagery gives researchers the flexibility and higher resolution imagery not always available by the previously discussed methods, and at a lower cost. Having access to a UAS allows control over timing of the flight that may change close to the planned flight day without losing money on an aerial flight. The water must be clear and visible at the time of photo acquisition, and weather and turbidity cannot always be predicted far enough in advance to plan an aerial flight. UAVs, helikites, and other platforms and sensors allow the researcher to control the flying height and capture imagery below overhanging canopy that would otherwise block visibility of the channel taken from a higher altitude. Given these difficulties, an increasing number of river researchers are obtaining their own sensor (Marcus and Fonstad, 2008). Despite the increase in flexibility and decrease in cost, UAVs and ‘drones’ are rarely used in studies to collect imagery (Carbonneau and Piegay, 2012) and the combination of UAS with SfM-photogrammetry has not been rigorously evaluated within fluvial geomorphology applications. Fonstad et al. (2013), Woodget et al. (2014), and Tamminga et al. (2015) are among the few researchers that have published results from UAS imagery that was processed by SfM software to quantify fluvial topography.

The three general approaches used to derive water depth with remotely sensed data are 1) photogrammetry, 2) spectral depth correlation, and 3) physically based models, and some research uses a hybrid of these approaches (Marcus and Fonstad, 2008; Marcus et al., 2012). Physically based models are outside the scope of this study, but can

be reviewed in the following articles (Legleiter et al., 2004, 2009; Fonstad and Marcus, 2005; Walther et al., 2011; Flener et al., 2012; Marcus et al., 2012; Legleiter, 2015). The following sections will discuss the previous research involving spectral depth and photogrammetry.

Spectral Depth

The spectral depth approach to estimate water depth from images was one of the first techniques that applied remote sensing technology to water environments (Lyzenga, 1978; Legleiter and Fonstad, 2012), and has now become one of the most commonly used approaches to measure water depth (Winterbottom and Gilvear, 1997; Marcus et al., 2003; Legleiter et al., 2004; Lejot et al., 2007; Feurer et al., 2008; Javernick et al., 2014). Optical bathymetric mapping requires a correlation to be established between the pixel value or spectral properties of an image at multiple locations and field depth measurements at the same locations (Winterbottom and Gilvear, 1997; Marcus et al., 2012). This correlation between water depth and water color creates a regression equation that can be applied to the rest of the image to estimate water depths on a spatially continuous scale. This relationship depends on the predictable attenuation rates of different wavelengths of light as it propagates through clear water. Longer wavelengths attenuate at a faster rate as depth increases in comparison to shorter wavelengths with weaker attenuation. Thus, a ratio using two bands of varying attenuation rates increases as depth increases (Legleiter and Fonstad, 2012). The most commonly used bands for this ratio are the natural log of the green band over the red band, which has been found to

correlate linearly with water depth across a large range of substrate albedos and types (Legleiter et al., 2004).

The radiometric signal is more successful at predicting water depth under certain conditions, including homogeneous substrate and water column conditions (Lejot et al., 2007), and is adversely affected by differences in illumination and shadow, turbidity, water surface roughness, and substrate (Winterbottom and Gilvear, 1997; Legleiter et al., 2004; Carbonneau et al., 2006). Despite these limitations that constrain its application on a wide range of river environments, most research reports that this method can estimate water depth fairly well. The highest levels of accuracy achieved in the fluvial remote sensing community range between 75 and 90%, as 100% is impossible to achieve given the inherent variability in natural rivers (Marcus et al., 2012). Among the highest accuracies for using spectral properties to estimate depth were achieved by Marcus et al. (2003), Lejot et al. (2007), and Javernick et al. (2014) (Table 1). The review of these three articles is not meant to be comprehensive, but rather a way to summarize varying data and accuracy results used, and to indicate the gaps in previous research that are found throughout the fluvial remote sensing discipline.

Table 1: Summary table of previous depth mapping studies from optical imagery. R² values represent estimated vs. observed water depth correlation

Site Features	Platform & Sensor	Spatial Resolution	Spectral Range	# Bands	R ² Value	Author(s)
Typical depths 0 – 0.6 m; pool riffle morphology	Helicopter – PROBE-1 sensor	1 m	400-2400 nm	128	0.20 – 0.99	Marcus et al., 2003
2 sites: sand and silt; gravel. Depths 0-5 m	Pixy drone, digital camera	5 cm, 7 cm	Visible	3 (r,g,b)	0.53 – 0.90	Lejot et al., 2007

Braided river; mean depth = 0.55 m	Helicopter, digital camera	0.12 m, 0.16 m	Visible	3 (r,g,b)	0.71 – 0.76	Javernick et al., 2014
--	----------------------------------	-------------------	---------	--------------	----------------	------------------------------

While Marcus et al. (2003) achieved high accuracies of estimating water depth within habitat units by using a maximum likelihood classification of principal component images. Depending on the habitat type, the R^2 value increased or decreased from the R^2 value for all the sites combined. This water depth estimation within habitat units is usually done using a classification system and hyperspectral data, and not using the simple spectral depth band ratio approach with 3-band imagery. Additionally, Marcus et al. (2003) described the site characteristics at length and included an on-the-ground photo of typical habitat types of interest to inform the reader of all the variables that would affect the viability of the method. This description is crucial to understanding the characteristics within which this approach may be successful, but is often not included in publications.

Javernick et al. (2014) conducted their study by using a basic 3-step process for optical bathymetric mapping: 1) collecting photographs and water depth measurements, 2) generating a water surface, and 3) developing a relationship between spectral properties and water depth in order to subtract the depth data from the water surface layer to create a river bed elevation map. The authors do not discuss their reasoning for choosing a particular water surface interpolation method, which is all too common for both spectral depth and photogrammetric bathymetric mapping literature. Some articles reference other articles as to which method they used (Javernick et al., 2014), and others give a short explanation as to the preference of one interpolation method over another (Westaway et al., 2001), but quantitative differences between the accuracy and precision

of water surfaces created from various interpolation methods are usually not described. Javernick et al. (2014) and Woodget et al. (2014) interpolated a TIN (triangulated irregular network) water surface by extracting elevation values along the water's edge, under the assumption that the study site has a planar water surface. Westaway et al. (2001) also interpolated a water surface from edge-of-water elevations, however they found that using an inexact interpolation algorithm, such as kriging, produced a smoother water surface than an exact interpolation (eg. triangulation), which produced an angular surface. However, Westaway et al. (2001) didn't elaborate whether the smoother water surface was also more accurate than the angular surface or discuss any further quantitative differences.

The paper by Williams et al. (2014) is an exception, where they acknowledged this widespread issue of under-reporting water surface elevation interpolation methods and compared the quality of two different water surfaces: the standard Delaunay triangulation method that interpolates a surface from field data, and a GIS method that identifies channel edge elevations and interpolates as surface across the channel. They found that the GIS method produced a more precise water surface elevation model, however both approaches relied on field measurements, and Williams et al. (2014) collected over 5,000 water surface elevation measurements. Legleiter (2012) found success in calculating water surface elevations from LiDAR data, however this method requires tedious and potentially inconsistent manual digitization, as well the expensive and infrequent LiDAR data.

Lejot et al. (2007) removed data points that were shaded or covered by riparian canopy, but did not compare how this removal changed the resulting regression

equations. Many articles similarly do not mention shadow at all or simply remove it completely from the data set. Lejot et al. (2007) also mentioned that the brightness between photos varied significantly, and minimized the differences by standardizing the brightness by redistributing the brightness histogram to match a reference image. This approach, however, assumes that the difference in brightness is the only optical property that is different between images (Carbonneau et al., 2012). Lejot et al. (2007) briefly speculated that their lowest R^2 value of 0.53 was in a reach with heterogeneous bottom and varying flow conditions; most researches limit this type of environment in their spectral depth experiments as much as possible. The authors concluded that this technology was ready to be applied to monitoring restored river reaches and supplying data for 2D hydraulic modeling. Like many other publications, they do not couple this information with what types of river environments this method can be applied to in order to derive similar levels of accuracy.

Through-Water Photogrammetry

Through-water photogrammetry will be discussed through the lens of structure-from-motion (SfM) multi-view stereo photogrammetry software. SfM operates under the same principles as stereoscopic photogrammetry, except the camera positions and scene geometry are automatically identified and reconstructed from a set of multiple overlapping images taken from a wide range of angles (Westoby et al., 2012). The development of free and low cost SfM software packages with more automated procedures make photogrammetry more accessible and simple to use by non-experts. SfM has the ability to produce high resolution orthophotos and DEMs that have the

accuracy and precision similar to LiDAR or better, collected by a low cost consumer grade camera (Fonstad et al., 2013). The use of SfM in fluvial geomorphology and remote sensing studies, however, is still in its infancy.

Both photogrammetric and spectral depth methods can use SfM software-derived orthophotos and DEMs to map bathymetry, however the photogrammetric method estimates water depth by correcting the original DEM with a simple refraction correction. The correction algorithm reduces the systematic bias caused by the refraction of light at the air-water interface (Westaway et al., 2001; Butler et al., 2002). Snell's Law explains the geometry of light refraction at the water surface and how this is translated into the DEM by overestimating the bed elevation, or underestimating water depth (Butler et al., 2002; Woodget et al., 2014). Jerlov (1976) established that the refractive index is 1.340, varying by +/- 0.007, for clear water between 0 and 30 degrees Celsius. This value has been accepted as the constant refractive index in the fluvial remote sensing field, and has been found to significantly reduce DEM errors (Westaway et al., 2001; Woodget et al., 2014; Tamminga et al., 2015).

Although this value is accepted and applied, multiple studies have stated that the refraction correction may not be necessary in shallow waters; the error in shallow depths are similar to those on exposed topography and that error increases with depth, even after applying the refraction correction (Westaway et al., 2001; Woodget et al., 2014; Tamminga et al., 2015). Some researchers attributed this increase in overestimating bed elevation with depth to a combination of light refraction effects and photogrammetric processes that may introduce error during point alignment (Westaway et al., 2001; Woodget et al., 2014). Butler et al. (2002) also stated that the magnitude of the refractive

index increased with distance between the sensor and the water surface, and that the index depended on the angle of incidence, or the angle at which light hits the water surface. These changes in the refractive index do not include other effects such as water surface roughness and turbidity. Butler et al. (2002) also found that elevations at greater depths received larger refraction corrections to compensate for greater height errors. It is reasonable, then, to question that 1.34 is an appropriate refractive index to measure submerged topography with digital photogrammetry, or to suggest that photogrammatrists should apply a corrective index that encompasses both refraction and any other associated errors.

This research will contribute to the baseline knowledge of studying river environments with digital photogrammetry and SfM, and will introduce a data-derived 'apparent' refractive index and compare it to the established 1.34 refractive index. To my knowledge, the only other researchers that have employed a UAS and SfM approach to which I can compare my results are Woodget et al. (2014) and Tamminga et al. (2015). Both studies measured fluvial topography with a UAV and digital photogrammetry, but Tamminga et al. (2015) quantitatively compared the error of submerged topography between using the 1.34 refractive index and spectral depth approaches. However, these studies validated their results by comparing the estimated and observed bed elevations, which introduces the relationship where elevation decreases in the downstream direction, thereby increasing the reported R^2 value instead of measuring this method's predictive power of water depth independently. Additionally, these studies did not explore accounting for light refraction using an index other than 1.34. Thus this research will also evaluate these methods by measuring the accuracy and precision between estimated and

observed water depths, which, as a new evaluative approach, makes it difficult to contextualize my results within published literature.

Study Site

The study site is a 140-meter reach of the Salmon River in the Sandy River Basin, Oregon (Figure 1). The Salmon River begins on the south slopes of Mount Hood and flows for 53 kilometers through a largely forested watershed, and it provides habitat for threatened fish species including Chinook Salmon, Coho Salmon, and Steelhead. The study site is approximately 2.4 kilometers upstream from the confluence with the Sandy River. The sediment type at the site consists of gravels and cobbles and it has pool-riffle morphology. Large boulders and log structures were placed before data collection as part of a restoration effort to improve salmonid habitat in August 2015. A large log structure was placed on the gravel bar on the left bank and an emulated landslide deposit was placed on the right bank downstream. Both structures were designed to enhance pool habitat, increase gravel deposition, accumulate large wood, and provide cover and peak flow refuge. The boulder placements were designed to improve glide habitat and promote spawning gravel deposition (Wanner, personal communication, 2015).

This river is different from previous rivers that are used to test bathymetric mapping methods because of the optical challenges that exist within this reach. The characteristics of the Salmon River are representative of other streams in the Pacific Northwest that could potentially benefit from the use of these methods, but the lack of studies on these streams limit our knowledge of the methods' abilities or what aspects of the method should be improved for successful application. This reach of the Salmon

River is a good candidate to use a UAV for image acquisition because of the canopy blocking visibility from a higher altitude, the small reach length would benefit from the use of SfM (Fonstad et al., 2013), and it is an ecologically important scale for physical habitat assessments (Woodget et al., 2013). While it is likely that the photogrammetric method will outperform the spectral depth method due to the Salmon's heterogeneous river bed, performing both approaches facilitates the development of guidelines for using these methods and which method should be preferred on this river environment over another.



Figure 1: Study site location map.

Collecting high-resolution and spatially continuous data on the Salmon River, where the salmonid habitat is a paramount concern to river managers, can encourage

others to provide the data necessary to detect unique habitats or disturbances that can affect fish distribution and abundance; management decisions are often based on studies with spatially discontinuous data, which may have contributed to the decline of some fish populations (Bergeron and Carbonneau, 2012). Depth is an important habitat characteristic to measure and monitor because salmonids of different life stages exhibit preferences for various depths. This reach of the Salmon River has relatively shallow flows that juvenile salmon prefer, which can potentially be measured by these remote sensing techniques. Many articles have stated that these methods are ready to be used and applied, so testing these methods on a site that is in need of monitoring is a good place to start assessing whether these methods are ready for widespread application, particularly for monitoring fish habitat.

CHAPTER III

METHODS

Figure 2 provides a general outline of the methods used in this research, which are detailed in the following sections. The structure-from-motion and water surface interpolation sections include methods and results because the results are needed to extract bathymetric data in subsequent methods.

Image acquisition and GPS data collection

Before I collected my primary data, I established six control points for surveying and determined their coordinates using static occupation with an rtk-GPS. I chose the single most accurate control point as a base station to collect the rest of my data with an rtk-GPS. I conducted my field work between September 15th and 18th, 2015, after restoration activities were completed in August, including image acquisition, and cross section and ground control point (GCP) locations with an rtk-GPS. I surveyed 12 channel cross sections over three days, including the gravel bars up to the edge of vegetation on the floodplain. The cross sections are relatively evenly spaced, with cross sections between each of the steps in the riffle to capture the changes in the bed topography and water surface elevation. The original cross section data are in Appendix B.

On a sunny day, I distributed cards to mark ground control points across the site, both on the dry gravel bars and on the channel bed. I flew a DJI Phantom III Pro UAV over my study site between 5 and 25 meters above the channel and collected still pictures with the 12 megapixel camera attached to the UAV. Given the time constraints determined by the 4 UAS batteries available, I aimed to collect images with at least 60%

- 1. Data Acquisition**
 - a. Collect cross-section data (rtk-GPS)
 - b. Distribute GCPs throughout site and survey locations with rtk-GPS
 - c. Collect images with a UAV
- 2. SfM Processing**
 - a. See appendix for detailed Agisoft PhotoScan methods
 - b. Align points, and generate dense point cloud, orthophoto, and DEM
- 3. Water Surface**
 - a. Adjust cross section edge-of-water elevations
 - b. Extract edge-of-water elevations from the DEM (2b)
 - c. Used 3a and 3b to interpolate water surface using TIN and Spline methods
 - d. Qualitatively chose 2 best water surfaces based on amount and location of channel covered by the surface
 - e. Quantitatively compared the surfaces and selected the best water surface
- 4. Photogrammetric Approach: Refraction Correction**
 - a. Derive observed water depth by subtracting GPS bed elevation data (1a) from the water surface (3e)
 - b. Derive predicted water depth by subtracting DEM bed elevations (2b) from the water surface (3e)
 - c. 1.34 coefficient
 - i. Multiply (4b) by 1.34
 - ii. Compare (4ci) to (4a) to determine goodness of fit
 - d. Site specific coefficient
 - i. Derive linear regression between (4a) and (4b) to randomly selected calibration data
 - ii. Apply regression equation (4di) to remaining validation data to determine goodness of fit
 - e. Coefficient by habitat unit
 - i. Divide channel into 3 classifications based on water surface roughness and apparent depth
 - ii. Divide GPS elevation data (1a) into these classifications and apply (4d) to each
- 5. Spectral Depth Approach**
 - a. Extract RGB values from orthophoto at cross section GPS locations
 - b. Derive $\ln(G/R)$ for each GPS data point
 - c. Derive linear regression between (5b) and (4a) to randomly selected calibration data
 - d. Apply regression equation (5c) to remaining validation data to determine goodness of fit
 - e. Divide data into shadow and non-shadow, and by habitat unit, and repeat (5a – d) for each group, similar to (4d and 4e)
- 6. Comparison of DEM accuracy and precision between methods**
 - a. Determine goodness of fit, mean error, and standard deviation for each method
 - b. Choose best methods for (4) and (5) based on results from (6a)

Figure 2: General workflow used to compare the accuracy and precision between photogrammetric and spectral depth approaches.

overlap in order to ensure that any given point was captured from different perspectives to aid 3-D point cloud generation with SfM software (James and Robson, 2012; Westoby et al., 2012; Fonstad et al., 2013; Dietrich, 2015). While flying at low altitudes produces high point cloud densities, I flew the UAS at varying altitudes to reduce systematic distortions (Fonstad et al., 2013) and I angled the camera just off nadir to reduce the doming error in the images (James and Robson, 2014; Woodget et al., 2014). The entire

flight occurred in less than one hour in order to reduce the amount of potential changes in water surface elevation, atmospheric conditions (Lejot et al., 2007), and sun angle that could affect the quality of the point cloud and DEM.

Theoretically, the georeferencing process using SfM only requires a minimum of 3 GCPs, however, because the appropriate amount and distribution of GCPs has not been established (Woodget et al., 2014), I assumed a 1:10 ratio between GCPs and photographs based on my estimation of collecting no more than 300 photographs for a 140 meter reach. I placed 30 GCPs throughout the field site, both on the dry gravel bars and in the channel. I used the rtk-GPS to collect GPS locations at the GCPs as close to the time of image acquisition as possible, and I used a stadia rod to collect water depths at the GCPs located under water.

Structure-from-Motion Processing

I used commercial SfM software PhotoScan Professional v.1.0.4 by Agisoft (Agisoft LLC, 2015) to process my images. This software performs digital photogrammetry by processing images and producing 3D spatial data. After image acquisition, I inspected all the photographs and removed any that were blurry or extended beyond the study area. I added the remaining photographs to Photoscan and used the 'Estimate Image Quality' tool to further ensure the photos are of high enough quality to use in alignment. The DJI Phantom III Pro collects images in the WGS-84 coordinated system, and thus I converted the geotagged photos to NAD83 UTM Zone 10, the coordinate system used to collect GPS data in the field. I aligned the photos, disabled photos that could not be aligned correctly, and removed any points that were too far away

from the main point cloud to be accurate. This process resulted in 163 photos being used to create the final dense point cloud. I imported the ground control point GPS locations and assigned the locations to the appropriate locations in the images. After optimization, I removed any ground control points that caused higher error in the point cloud, resulting in 23 of the 30 ground control points used to georeference the point cloud. Then I built the dense point cloud, mesh, and texture, from which it derived an orthophoto (Figure 3) and digital elevation model (DEM) (Figure 4). For a more detailed Agisoft PhotoScan workflow, see Appendix A. There is a large gap in both the orthophoto and DEM on the right bank. This is likely due to a lack of high quality photos with enough overlap to align matching points.

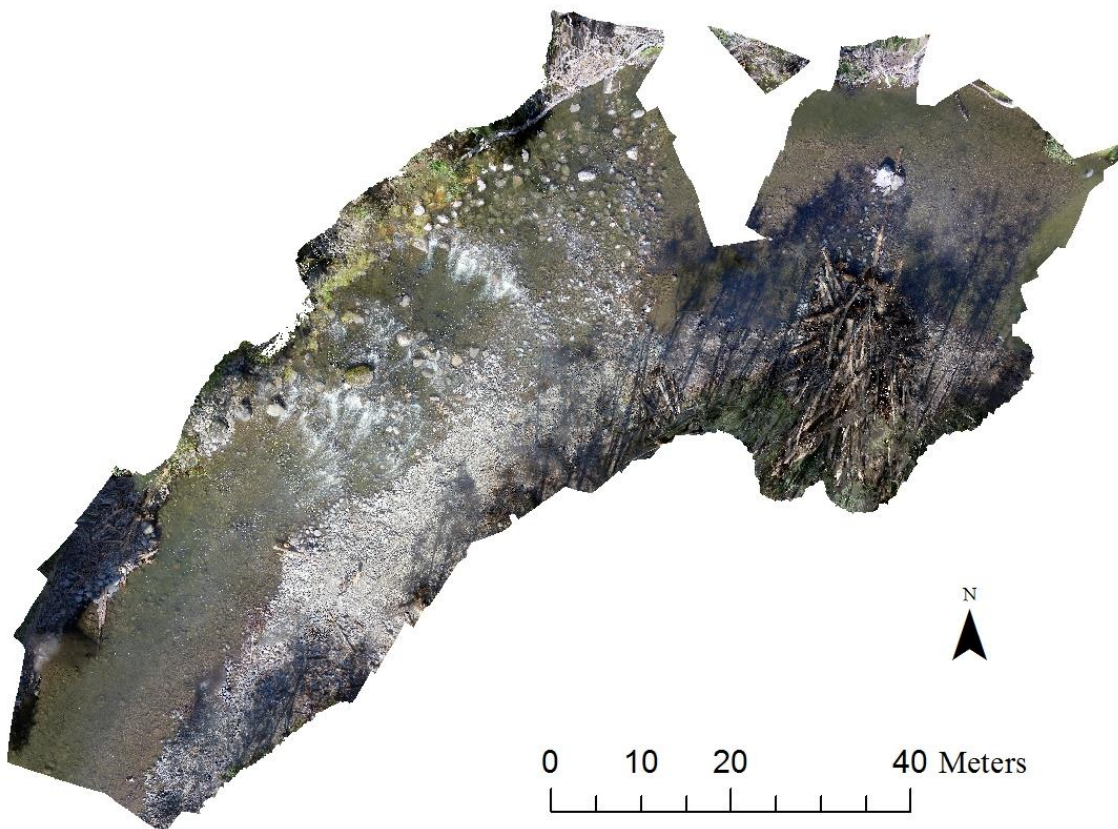


Figure 3: Site orthophoto output. Cell size of 0.37 cm. Water flows from the upper right to the lower left of the image.

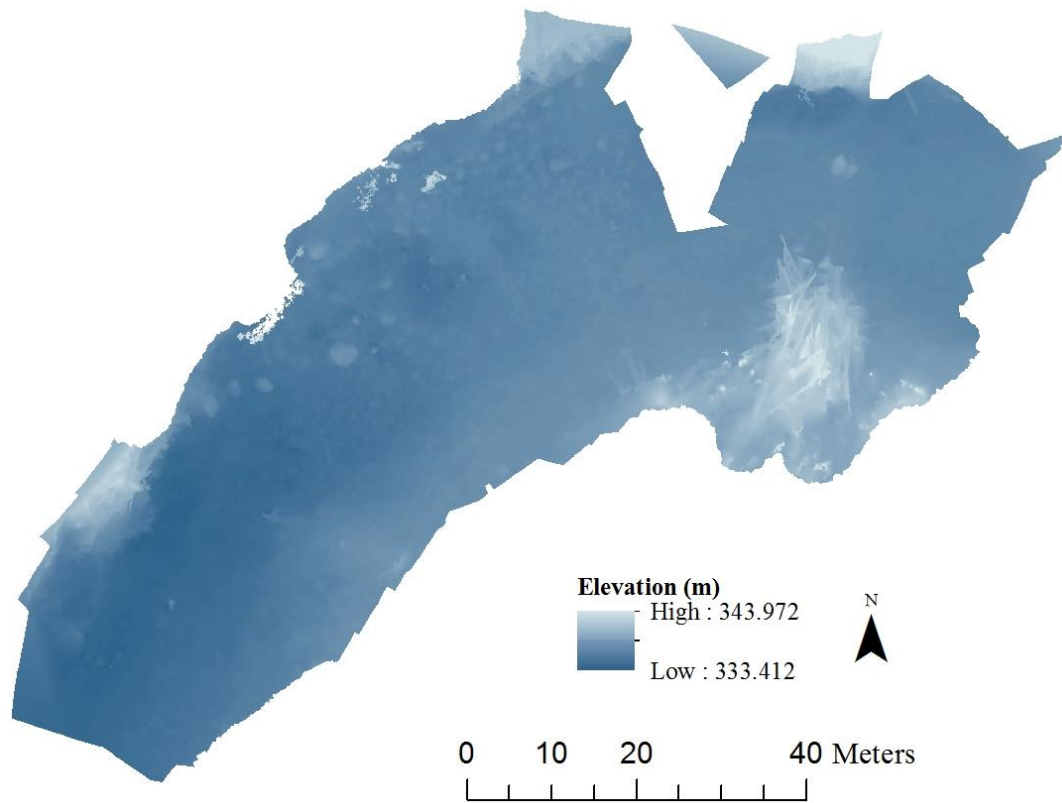


Figure 4: Site DEM output from PhotoScan prior to correction. Spatial resolution of 1.50 cm.

Water Surface Interpolation

In order to extract bathymetric data from the DEM and orthophoto, a model of the water surface needs to be created. In the photogrammetric approach, bed elevations are subtracted from this water surface to calculate water depths, and in the spectral depth approach, water depths are subtracted from the water surface to derive bed elevations (Westaway et al., 2001; Javernick et al., 2014). The accuracy of the water surface directly affects the results of extracting bathymetry for all subsequent methods, and therefore it is important to explore the most accurate yet repeatable method in deriving the water surface. While in the field, I collected edge-of-water elevations with the rtk-GPS on both banks of the cross sections whenever possible. It was often not possible to collect edge-

of-water elevations on the right bank of some cross sections because the tree canopy reduced the accuracy of the GPS location. 11 of the 12 cross sections collected fall within the usable extent of the orthophoto and DEM, and of those cross sections there are 14 edge-of-water elevations collected. The edge-of-water elevations do not all decrease in the downstream direction. This error could have been due to the expected vertical error associated with the rtk-GPS (vertical error ranges 0.7 – 2.9 cm) or equipment error while collecting the data in the field (Appendix B). In order to reduce this error, I altered water surface elevation measurements to make a more realistic water surface that decreases in elevation in the downstream direction by comparing all the elevations as a whole.

Figure 5 shows the longitudinal profile of water surface elevations from the edge-of-water elevations collected by the rtk-GPS, and water surface elevations (WSEs) collected at ground control points (GCPs) in the channel, calculated by adding the recorded water depth to the bed elevation. WSEs at cross sections 5 and 12 do not decrease in elevation in the downstream direction (Table 2). The two edge-of-water elevations at cross section 5 are 337.20 m and 337.22 m, which are both slightly higher than the one edge-of-water elevation at cross section 4 upstream. Both elevations at cross section 5 are higher, and both cross sections are located in a glide where there is a relatively smooth water surface. For these reasons, I increased the WSE on the left bank of cross section 4 to 337.21 m, the average of the two elevations at cross section 5 (Table 2). While the GCPs upstream and downstream also have a higher elevation than cross section 4, I did not use the GCP elevations in the averaging of the altered edge-of-water elevation because the GCP elevations in the relatively flat areas of the reach appear to be systematically higher than most other edge-of-water elevations.

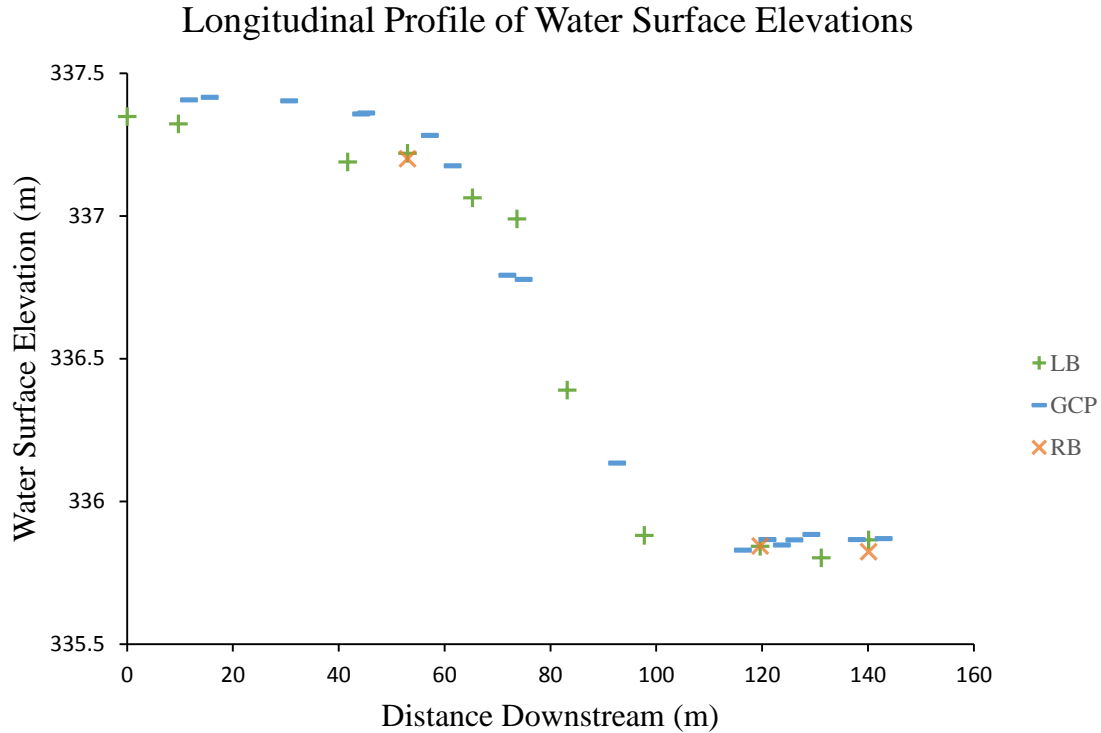


Figure 5: Longitudinal profile of water surface elevations at the left and right banks (LB and RB) of the cross sections and the water surface elevations measured at the GCPs in the channel.

Table 2: Adjusted edge-of-water elevations at cross sections to ensure the decrease in elevation in the downstream direction. An ‘x’ denotes that an edge-of-water elevation not collected at that side of the cross section due to poor GPS quality or inaccessibility. For the original WSEs, I used the original rtk-GPS-collected elevations at the sub-meter scale, but only included centimeter scale elevations in the table.

Cross Section	LB Original WSE (m)	RB Original WSE (m)	Altered WSE (m)
2	337.32	x	
3	x	x	
4	337.19	x	337.21 (LB)
5	337.22	337.20	
6	337.06	x	
7	336.99	x	
8	336.39	x	
9	335.88	x	
10	335.84	335.84	335.84 (both)
11	335.80	x	335.84 (LB)
12	335.87	335.82	335.84 (both)

Cross sections 10, 11, and 12 are located below the riffle where the WSE was observed to be relatively flat. The elevations decreased almost half a meter in a short distance between cross sections 10 and 11, and subsequently increased almost half a meter between cross sections 11 and 12 (given the average of edge-of-water elevations at cross section 12, Table 2). Although the left and right bank elevations at cross section 12 differ by about 4 cm, the average elevation of the two is 335.85 m, which is one centimeter different from the average of the elevations at cross section 10, 335.84 m. Thus, the average elevation between all edge-of-water elevations at cross sections 10 and 12 (335.84 m) was applied to cross sections 10, 11, and 12 (Table 2, Figure 6). Including the GCPs adjacent to these cross sections in the averaging of the edge-of-water elevations would have increased the average to an elevation higher than 4 of the 5 edge-of-water elevations collected at the 3 cross sections; therefore, including the GCP elevations in the edge-of-water elevation average for the 3 cross sections could not be supported.

In addition to the altered WSEs from Table 2, I also extracted water surface elevations from the DEM in areas where I could clearly see the boundary between water and dry topography, and in areas where the flow velocity was very low so the water surface elevation wasn't influenced by surface turbulence. Between extracted elevations from the DEM and the edge-of-water elevations from the cross section data, there were 60 locations with WSE data that could be used to interpolate a water surface layer across the wetted channel (Appendix C).

Adjusted Longitudinal Profile of Water Surface Elevations

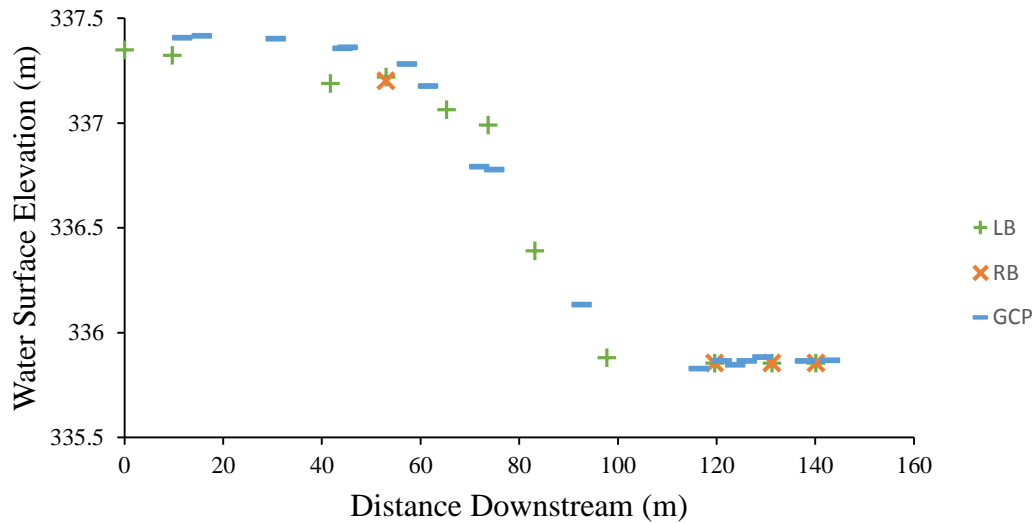


Figure 6: Adjusted water surface elevations from Table 2 used in creating a water surface.

Given the synopsis of current water surface interpolation methods in Chapter II, I created water surfaces from TIN and spline interpolation methods. Kriging interpolation, supported by Westaway et al. (2001), is based on spatial autocorrelation, and therefore an even spacing of points is ideal to result in an accurate water surface. My data set did not allow for evenly spaced edge-of-water elevations because the tree canopy reduced the GPS accuracy and photo overlap on the right bank, consequently reducing the number of accurate elevations in certain areas of the channel collected from either the GPS data or the DEM. It is possible that kriging is more appropriate when the edge-of-water elevations used are extracted from the DEM because there is more error introduced from the georeferencing from the orthophoto, and thus creating a surface based on a group of proximate elevations would be more applicable instead of forcing the surface through each point. However, my data were collected with a highly accurate rtk-GPS, and

therefore a spline or triangulated interpolation would ensure the surface passed through these elevations. For these reasons, I interpolated water surfaces using TIN and Spline interpolation methods in ArcGIS, using the 60 water WSEs described above.

The first TIN surface created (Appendix C) in ArcGIS showed some irregularities in the surface, where the WSEs were not consistent in some cross sections. Upon closer inspection of the DEM-extracted elevation points, five of the points were surrounded by points that had more similar elevations. The agreement of multiple surrounding elevations led me to remove the inconsistent elevations and to create a second TIN surface with only the agreeing elevation points (Appendix C). While there is still some variation in WSEs across any given cross section, the removal of a few DEM elevation points that disagreed with multiple adjacent elevations promoted generally level water surfaces that decreased in the downstream direction.

Using the spline interpolation tool, I created another water surface using the same WSE points used to create the second TIN surface (Appendix C). I specified this surface to be a tension spline, assuming a planar water surface, and accepted all other default parameters in ArcGIS. Even though this assumption is certainly not true in the riffle units and most likely not true in other areas of the channel, these methods were intentionally developed to be simple in order to create steps that could be easily followed, reproduced, and accessible to non-experts; therefore, incorporating water surface roughness into the water surface layer was not included in this study.

When comparing the two surfaces in ArcMap, they both seem to show elevation breaks in similar points in the riffle. The spline's elevation is slightly higher than the TIN in the glide upstream, and slightly lower in the channel downstream of the riffle

(Appendix C). To further qualitatively assess the water surfaces, I examined the TIN and spline surfaces in 3D in ArcScene to see the extent of the water surface, and to ensure the surface did not overflow the banks or cover protruding boulders (within the red boundary in Appendix C). The spline appears to cover more of the submerged channel, particularly on the right bank in the riffle section, although much of the orthophoto in this section appears fuzzy, indicating poor DEM quality here. Both surfaces do not cover parts of the channel just downstream of the log structure on river left. The DEM and orthophoto quality in this part of the channel is also quite poor, as demonstrated by the elevations along the water's edge in the DEM that are much higher than surrounding elevations. Due to these inaccuracies in the DEM, adjusting the water surface such that it covers these areas would make the water surface elevations in areas with a clearer DEM less accurate. Because the purpose of this research is to determine the most accurate method for extracting bathymetric data, the water surface must be chosen based on the parts of the channel with the best DEM and orthophoto.

The visual comparison between the two surfaces did not reveal one surface to be significantly more accurate, and so I ran a quantitative test. Because there is no data to compare the elevation data set to, I randomly selected half of the WSE data and created one TIN and one spline water surface with this half of the data. Ensuring that the random sampling of water surface calibration and validation data were relatively evenly distributed throughout the channel (Appendix C), I compared the remaining half of the data points to the interpolated WSEs from the water surfaces at those locations (Table 3).

Table 3: Comparing the water surface elevations from GPS data and DEM vs. the water surface elevations determined by the TIN and spline interpolation, demonstrated by the slope and R^2 values. Y represents the validation WSE, and X represents the elevation extracted from the interpolated water surface. The slopes equal to 1 demonstrate that the validation elevations are almost identical to the elevations created by the water surface at the same location.

	TIN	Spline
Regression equation	$y = 1x$	$y = 0.999x$
R^2	0.990	0.991

Table 3 demonstrates that there is no significant difference between the accuracies of the TIN and spline water surfaces. I chose the spline for the purpose of developing repeatable methods based on the data requirements for spline versus TIN surfaces. While both splines and TIN algorithms are deterministic interpolations, splines can include barriers that allow interpolation across linearly discontinuous features, such as river banks. Splines force the surface through the elevation data points and create a smooth surface while minimizing curvature of the surface, which may better represent a water surface in a river than an angular TIN surface. Unlike TIN surfaces, splines do not require relatively evenly spaced points, which is an important consideration for rivers such as the Salmon that has canopy coverage that prevents the collection of accurate GPS points or enough photo overlap to create an accurate dense point cloud. Figure 7 shows the final spline surface chosen to make subsequent calculations regarding water depth.

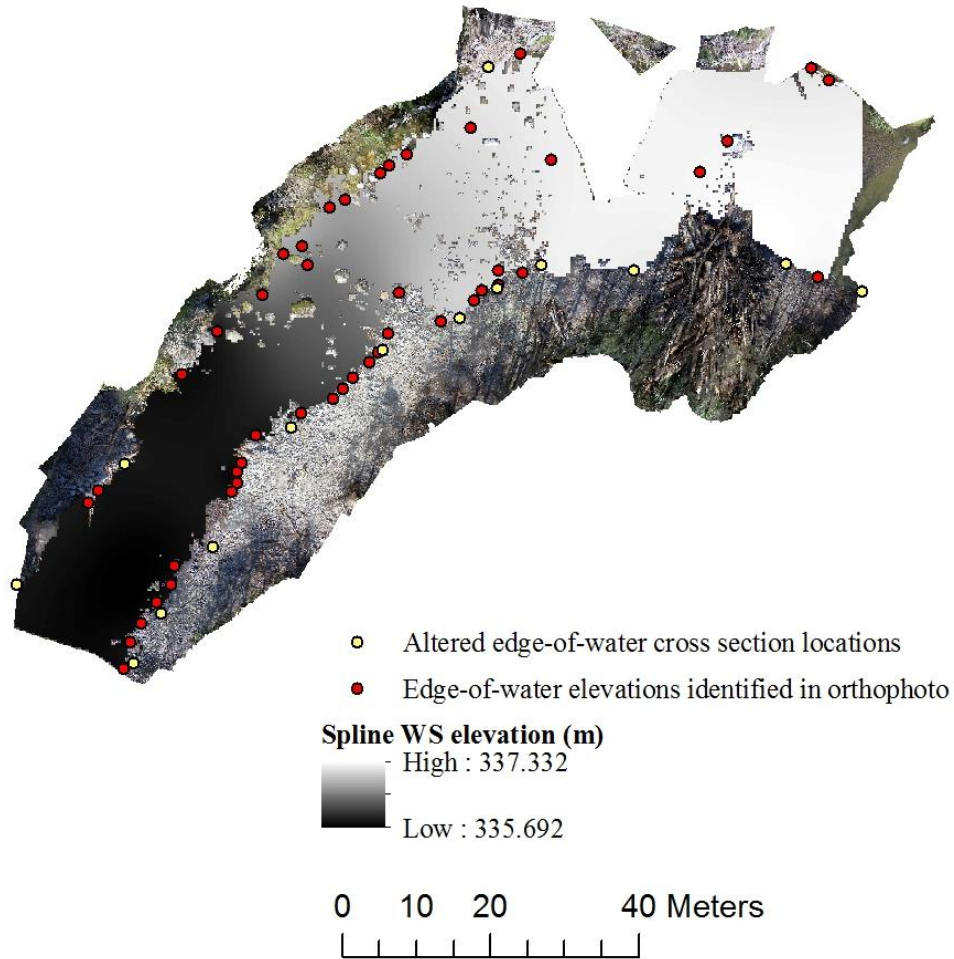


Figure 7: Spline water surface chosen to execute the photogrammetric and spectral depth approaches with the locations of the WSEs used to create the spline.

Photogrammetric Approach

1.34 Refraction Correction

Step 4a-c in Figure 2 describes the basic method of calculating the water depth after applying the refractive index of 1.34 to clear, nonturbid water (Jerlov, 1976; Westaway et al., 2001; Butler et al., 2002; Woodget et al., 2014). A refraction correction is applied by multiplying the predicted water depth, or the depth calculated from the original DEM that does not account for the effects of light refraction in water, by the refractive index. Comparing the estimated water depth to the validation water depth data,

or the water depth measured in the field, is a measure of how well the refractive index can correct for the refraction of light in water. The measured or observed water depth is calculated by subtracting the GPS measured bed elevations in the cross section data from the water surface, and the predicted water depth is calculated by subtracting the DEM elevations in the submerged channel from the water surface. This predicted depth is multiplied by 1.34, and then compared to the measured water depths at the same locations to determine the goodness of fit of this refractive index on this reach of the Salmon River (Figure 8). Before the multiplication, I removed 21 data points from the analysis due to being located in areas of the channel where the DEM quality was low, such as areas in extreme shadow, white water, low photo overlap, or negative actual water depths. Negative actual water depths could have occurred from poor DEM quality, inaccurate water surface at this location, or both. I performed these processes in ArcGIS by subtracting and multiplying the appropriate layers.

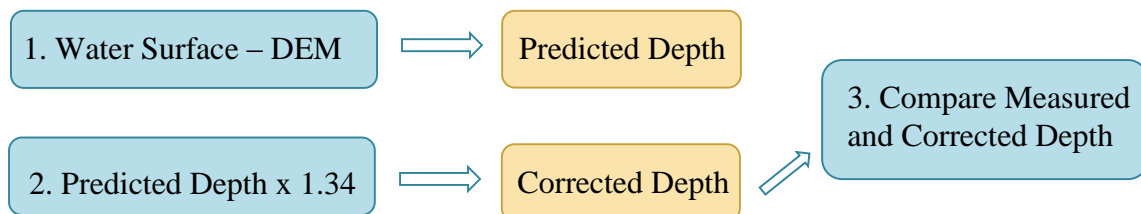


Figure 8: Refraction correction workflow to derive water depth.

Site-Specific Refraction Correction

Applying a site-specific refraction correction outlined in step 4d of workflow Figure 8 is similar to applying the 1.34 coefficient, however, first the refractive index that best estimates depth for the data set needs to be determined. The cross section data must

be randomly divided into calibration and validation data in order to derive a linear regression equation between predicted and measured water depth and to test how well that equation corrects for light refraction in water, respectively. Multiple combinations of the data were used to derive a regression equation in order to determine the most accurate refraction correction. The combinations included using 2/3 of the data for calibration and 1/3 for validation and dividing the data in half, as well as varying levels of excluding outliers from the data set before calibration (Table 4). Because these methods are being tested to determine how well a refractive index can predict water depth, any negative measured depths were not included in the calibration or validation of the regression equation. ‘Obvious outliers removed’ in Table 4 refers to any data point that overlaps with a physical characteristic of the orthophoto that would cause the elevation in the DEM to be inaccurate, such as white water, extreme shadow, and poor photo overlap (represented as fuzzy image quality in the orthophoto).

Table 4: Method of dividing data to derive site-specific refraction coefficient.

Division of Data	Data used
2/3 calibration, 1/3 validation	All data, except negative measured depths
	Obvious outliers removed
1/2 calibration, 1/2 validation	All data, except negative measured depths
	Obvious outliers removed

Once the best regression equation was determined from the four resulting R^2 values of the validation data set, I took the data set that resulted in highest R^2 and removed more outliers from the calibration data set. The purpose was to test whether only using ideal data that occurred in locations of the channel with adequate sunlight, smooth water surface, and sufficient photo overlap could better predict water depth for all the validation data set, including outliers.

Some studies have suggested that light refraction in water is minimal for depths of less than about 0.2 meters, and thus a refraction correction for these areas may not be necessary (Westaway et al., 2001; Woodget et al., 2014). I developed new regression equations for the data set that produced the best results to test if excluding shallow depths from the calibration would improve the estimation power of the refractive index.

Habitat Unit Refraction Correction

A third way of categorizing the data to derive the most accurate refractive index is by habitat units. Limitations to remote sensing of rivers with close-range photogrammetry are associated with physical and flow features that obscure the bottom of the bed, such as water surface roughness and greater water depths (Lyzenga, 1978; Winterbottom and Gilvear, 1997; Westaway et al., 2001; Fonstad et al., 2013; Woodget et al., 2014) where light may not penetrate enough to be detected by a sensor (Marcus et al., 2012) and therefore make it difficult for SfM to detect edges at deeper depths. While channel units are not defined by fixed physical characteristics, channel units often have associated morphologies that overlap with flow characteristics (Montgomery and Buffington, 1998; Harvey et al., 2007). It would be possible to delineate the channel into many specific units by which to derive refractive indexes, however for the sake of simplicity and repeatability by river managers, dividing this reach into three habitat units visually encompasses the varying surface flow and depth characteristics that appear to occur in the orthophoto:

- 1) Glide - shallow apparent depth and relatively low water surface roughness;
- 2) Riffle – shallow apparent depth and relatively high water surface roughness;

- 3) Pool – deep apparent depth and relatively low to medium water surface roughness.

For the purposes of the initial test, I viewed each individual cross section point and determined its habitat unit based on the water surface roughness and apparent depth at each location (Figure 9). Once the cross section data has been divided, the same procedures are applied here as in the previous sections to develop a refraction correction for each habitat unit (Step 4e, Figure 2). If this method produced the best estimated water depths, then the whole channel should be delineated into habitat units in order to create a corrected DEM.

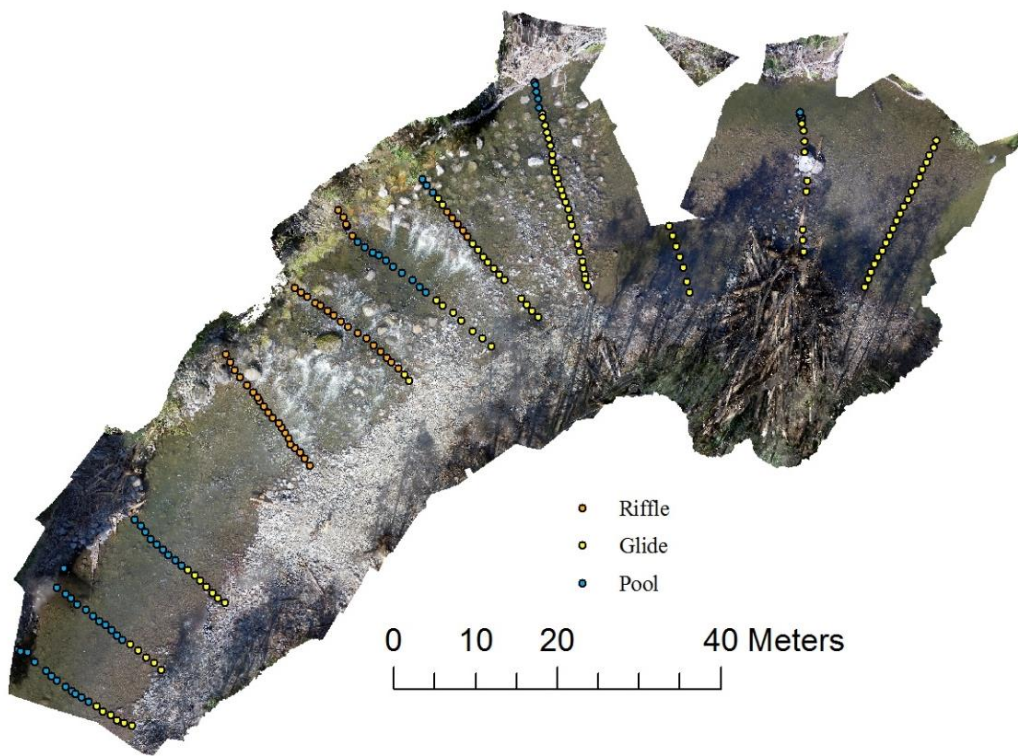


Figure 9: Habitat unit delineation based on water surface roughness and apparent depth differences.

Spectral Depth Approach

The spectral depth approach requires similar data sets as the photogrammetric approach, and a majority of the initial methods for optical bathymetric mapping are the same (Javernick et al., 2014). The orthophoto, GPS elevations, and water surface interpolation provide the information needed to establish a correlation between the spectral properties and measured depth (Winterbottom and Gilbear, 1997; Legleiter 2004; Lejot et al., 2007; Javernick et al., 2014). First, the natural log of the green divided by the red DN values should be calculated for each GPS location (Figure 2). If this value equaled 0, or where the red and green values were equal for a given pixel, then this value was removed from the data set because it does not report any information about the depth at that location. When these data are randomly split for calibration and validation data sets, the calibration data is used to create a regression equation between the $\ln(G/R)$ and the measured water depths calculated in step 4a (Figure 2). The resulting linear regression equation is applied to the remaining validation data, where the $\ln(G/R)$ value is entered as the 'x' variable, or the slope, in the regression equation. The R^2 value of this relationship determines the goodness of fit of the regression equation.

Similarly to the photogrammetric approach, the data was split into habitat units using the same deliniation (Figure 9). Because spectral properties are strongly affected by shadow, the data were also split into shadow and non-shadow in order to test the effect of shadow. Shadow was defined as any part of the channel where there was an object between the sun's rays and the water surface, whereas for non-shadow areas, there is a direct path from the sun to the water surface, disregarding atmosphere as an obstacle. The correlation between measured water depth and $\ln(g/r)$ is applied to these groups in the

same way as it was applied to all the data (Figure 2, Steps 4a-d), resulting in 6 spectral depth regression equations.

CHAPTER IV

RESULTS

This chapter will explore the results of the goodness of fit, accuracy, and precision of the photogrammetric and spectral depth bathymetric mapping methods in estimating water depth. The structure-from-motion processing and water surface interpolation results are discussed in the respective sections of Chapter III, as the results from these sections were used in deriving the bathymetric data.

Photogrammetric Refraction Correction

Figure 10 shows that the 1.34 refractive index compared to the measured water depths has an R^2 value of about 0.60, with some systematic error shown in the deviation from 0 and 1 in the y-intercept and slope values, respectively. Table 5 contains various site-specific refraction corrections created from the data (linear regression equations in the calibration column) and how well the refraction correction equations estimated water depth (R^2 in the validation column). The calibration equation that resulted in the highest R^2 of 0.67 was created after removing data outliers and then randomly splitting the data into 2/3 and 1/3 for calibration and validation, respectively. After removing more outliers from this best-fitting site-specific calibration data, the R^2 value remained the same, however the slope of the validation equation became closer to one and the y-intercept became closer to zero (Table 6). Thus the refraction correction with more outliers removed from the calibration data set was chosen as the best-fitting site-specific refraction correction (bolded in Table 6), shown in Figure 11. I also removed shallow depths less than 0.2 meters to test the hypothesis that these shallow depths may not be

affected by light refraction in water to the same extent as deeper water depths, however these results show no significant improvement (Table 7).

1.34 Refraction Coefficient: Estimated vs. Measured Water Depths

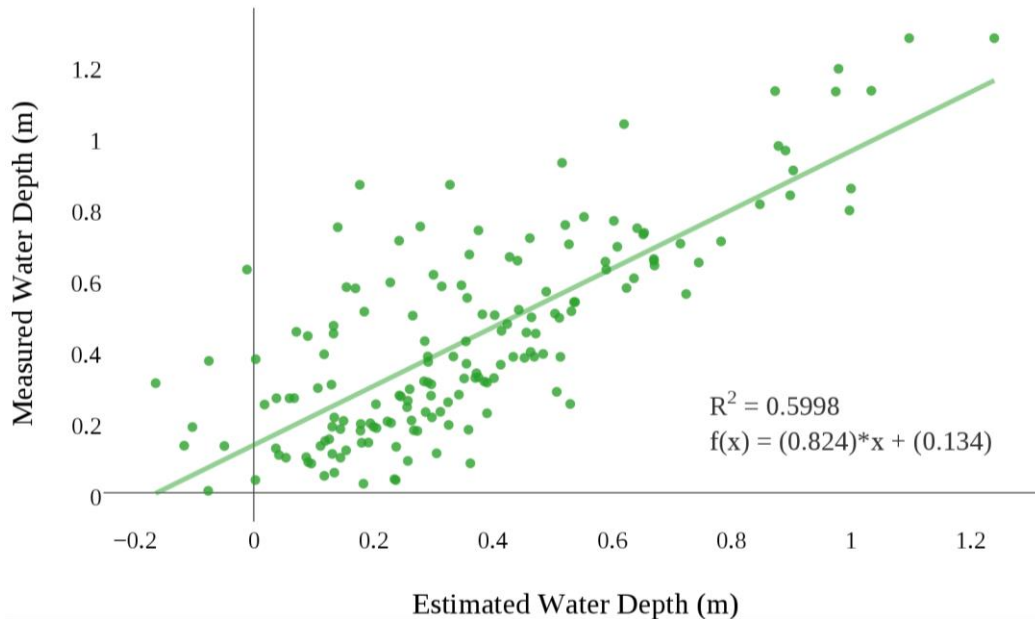


Figure 10: 1.34 Refraction coefficient. Scatterplot of the estimated water depths by the 1.34 refractive index vs. the measured water depths.

Table 5: Refraction correction equations (calibration column) and its goodness of fit (validation column) for various combinations of the data. The highest

	Data	Calibration	Validation
2/3 calibration, 1/3 validation	All data	$d = 1.06x + 0.17$ $R^2 = 0.60$	$d = 0.94x - 0.002$ $R^2 = 0.46$
	Outliers removed	$d = 1.08x + 0.15$ $R^2 = 0.55$	$d = 1.11x - 0.09$ $R^2 = 0.67$
1/2 calibration, 1/2 validation	All data	$d = 1.04x + 0.18$ $R^2 = 0.54$	$d = 0.98x - 0.02$ $R^2 = 0.56$
	Outliers removed	$d = 1.06x + 0.16$ $R^2 = 0.66$	$d = 1.09x - 0.06$ $R^2 = 0.53$

Table 6: Refraction correction after removing more outliers.

	Calibration	Validation
Original best fit equation	$d = 1.08x + 0.15$ $R^2 = 0.55$	$d = 1.11x - 0.09$ $R^2 = 0.67$
More outliers removed to create regression	$d = 1.21x + 0.09$ $R^2 = 0.62$	$d = 0.96x + 0.009$ $R^2 = 0.67$

Site Specific Refraction Correction: Estimated vs. Measured Water Depths

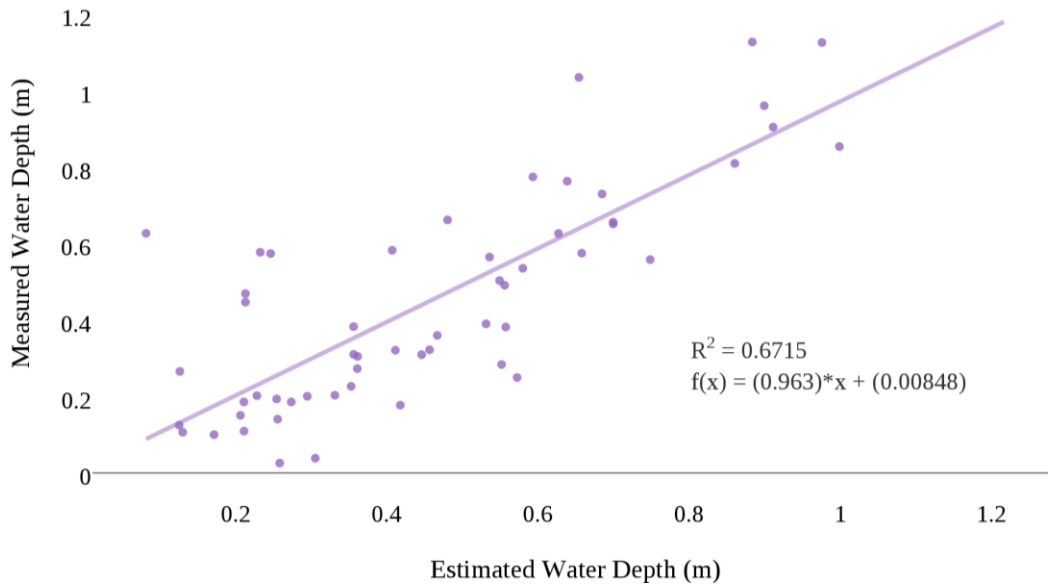


Figure 11: Best-fitting site-specific refraction correction to estimate water depth (equation bolded in Table 6).

Table 7: Refraction correction after removing shallow depths.

Included Water Depths	Calibration	Validation
Depths >0.2 m	$d = 1.08x + 0.17$ $R^2 = 0.55$	$d = 0.99x - 0.004$ $R^2 = 0.59$
Depths >0.15 m	$d = 1.13x + 0.14$ $R^2 = 0.58$	$d = 0.98x + 0.01$ $R^2 = 0.62$
Depths >0.10 m	$d = 1.16x + 0.12$ $R^2 = 0.61$	$d = 1.01x - 0.01$ $R^2 = 0.66$

Table 8 shows the calibration equations and validation R^2 after dividing the data into habitat units based on apparent depth and water surface roughness. The R^2 values decreased in comparison with non-habitat divided data, ranging from 0.34 in glides to 0.46 in pools. Outliers were also removed from the calibration data sets for the three habitat units before deriving a refraction correction equation (Table 9). While all the R^2 values stayed the same, the slope and y-intercept values of the validation equation showed an increase in accuracy for glide habitats, and a decrease in accuracy for riffle

and pool habitats (Table 9). Table 10 shows the best refraction correction equations and validation equations and R^2 values for the whole site and for each habitat unit.

Table 8: Refraction correction for data in three habitat units.

Habitat (# pts)	Calibration	Validation
Glide (88)	$d = 0.65x + 0.16$ $R^2 = 0.15$	$d = 1.08x - 0.02$ $R^2 = 0.34$
Riffle (34)	$d = 1.14x + 0.18$ $R^2 = 0.59$	$d = 0.69x + 0.11$ $R^2 = 0.34$
Pool (45)	$d = 0.90x + 0.26$ $R^2 = 0.45$	$d = 0.87x + 0.21$ $R^2 = 0.46$

Table 9: Refraction correction for data in three habitat units after removing outliers from calibration data.

Habitat	Calibration	Validation
Glide	$d = 0.67X + 0.14$ $R^2 = 0.12$	$d = 1.05X + 0.008$ $R^2 = 0.33$
Riffle	$d = 1.37X + 0.11$ $R^2 = 0.70$	$d = 0.57X + 0.17$ $R^2 = 0.34$
Pool	$d = 1.46X - 0.08$ $R^2 = 0.70$	$d = 0.54X + 0.48$ $R^2 = 0.46$

Table 10: Best refraction correction equations for the site and habitat units.

Data Group	Calibration	Validation
Site	$d = 1.21x + 0.09$ $R^2 = 0.62$	$d = 0.96x + 0.009$ $R^2 = 0.67$
Glide	$d = 0.67X + 0.14$ $R^2 = 0.12$	$d = 1.05X + 0.008$ $R^2 = 0.34$
Riffle	$d = 1.14x + 0.18$ $R^2 = 0.59$	$d = 0.69x + 0.11$ $R^2 = 0.34$
Pool	$d = 0.90x + 0.26$ $R^2 = 0.45$	$d = 0.87x + 0.21$ $R^2 = 0.46$

Spectral Depth Regression

To test the applicability of the spectral depth approach, the data were randomly divided into calibration and validation data sets for the whole channel, parts of the channel in shadow and not in shadow, and for the three habitat units (Table 11). The R^2 values range from 0.03 in the shadowed areas to 0.28 in riffles. The highest R^2 value associated with a data group that covers a majority of the channel is the non-shadow

group. Because of the low R^2 values for all the data groups, the best solution is to apply the non-shadow regression to estimate water depth, and use the site regression for areas in shadow. The relationship between these two water depth estimates are shown in Figures 12 and 13.

Table 11: Spectral Depth regressions and goodness of fit for the site and three habitat units. The best R^2 value and its corresponding regression equation are in bold for each data group. Obvious outliers were removed from the first calibration and validation data sets (columns two and three), and more outliers were removed from the second calibration data set (column 4).

Data Group	Calibration	Validation	Calibration, outliers removed	Validation, new calibration equation
Site: ½ calibration, ½ validation	d = 0.68X + 0.41 $R^2 = 0.09$	d = 1.29X - 0.09 $R^2 = 0.11$	d = 0.69X + 0.41 $R^2 = 0.09$	d = 1.26X - 0.07 $R^2 = 0.11$
Site: 2/3 calibration, 1/3 validation	d = 0.82X + 0.42 $R^2 = 0.11$	d = 0.77X + 0.11 $R^2 = 0.07$	d = 0.97X + 0.41 $R^2 = 0.17$	d = 0.66X + 0.17 $R^2 = 0.06$
Non-Shadow	d = 1.30X + 0.49 $R^2 = 0.24$	d = 0.89X - 0.04 $R^2 = 0.20$	d = 1.64X + 0.53 $R^2 = 0.35$	d = 0.61X + 0.07 $R^2 = 0.16$
Shadow	d = 0.03X + 0.49 $R^2 = 0.0001$	d = 5.54X - 2.41 $R^2 = 0.02$	d = 0.16X + 0.31 $R^2 = 0.05$	d = 2.18X - 0.39 $R^2 = 0.03$
Glide	d = 0.27X + 0.31 $R^2 = 0.06$	d = 0.83X + 0.007 $R^2 = 0.04$	d = 0.31X + 0.31 $R^2 = 0.09$	d = 0.71X + 0.05 $R^2 = 0.03$
Pool	d = 1.25X + 0.72 $R^2 = 0.11$	d = 1.09X - 0.06 $R^2 = 0.19$	d = 1.16X + 0.72 $R^2 = 0.09$	d = 1.18X - 0.11 $R^2 = 0.19$
Riffle	d = 0.61X + 0.35 $R^2 = 0.10$	d = 1.66X - 0.18 $R^2 = 0.28$	d = 0.67X + 0.36 $R^2 = 0.13$	d = 1.36X - 0.07 $R^2 = 0.21$

Site Spectral Depth Regression: Estimated vs. Measured Water Depths

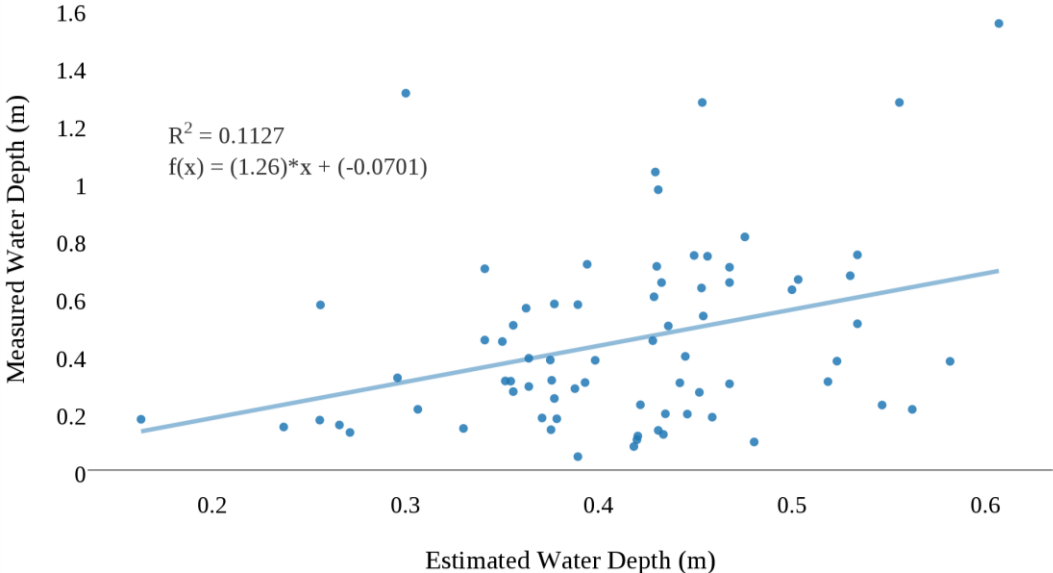


Figure 12: Scatter plot of the estimated water depths by the site spectral depth regression vs. measured water depths.

Non-Shadow Spectral Depth Regression: Estimated vs. Measured Water Depths

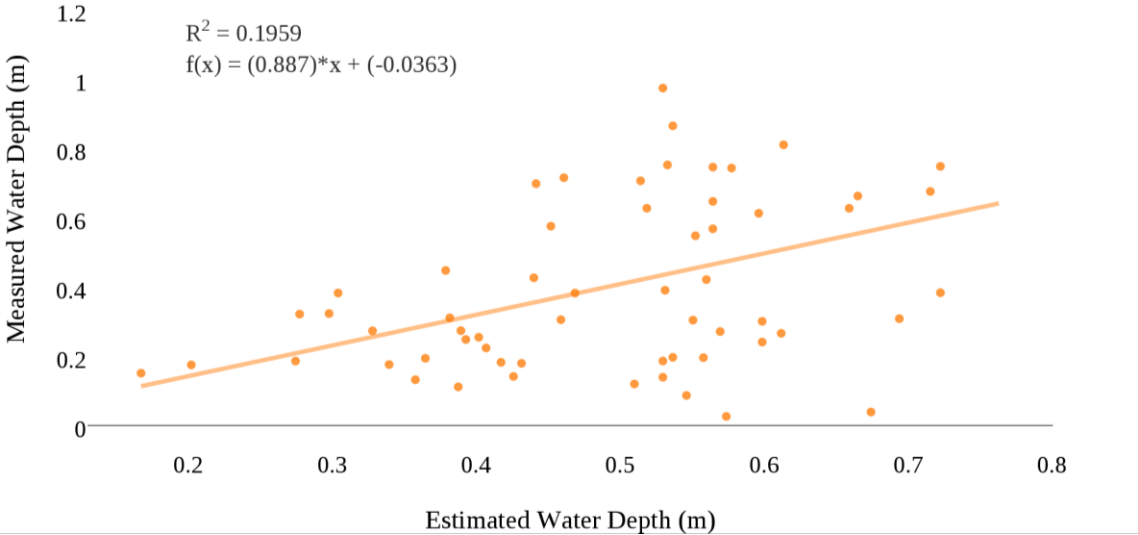


Figure 13: Scatter plot of the estimated water depths by the non-shadow spectral depth regression vs. measured water depths.

Comparison of Photogrammetric and Spectral Depth Approaches

Table 12 compiles the 2 photogrammetric and 2 spectral depth equations that produced the highest R^2 values. The error distributions between the estimated water depth after the correction and the observed water depth are displayed in histograms, density curves, and a box and whisker plot in Appendix D. In order to measure accuracy and precision, I calculated the mean error (ME) and mean absolute error (MAE) as indicators of systematic error, as well as the standard deviation of error (SD) as an indicator of random error (Table 13) (Westaway et al., 2001). The photogrammetric approach provides a water depth estimate prior to the refraction correction, and thus I could measure if the ME and SD significantly decreased after the refraction correction was applied to the data (Table 14). This comparison of ME was complicated by negative and positive errors; for example, the site-specific coefficient ME was negative before the correction and positive after the correction, and therefore a one-tailed t-test comparing the MEs cannot test if the error has significantly decreased after the correction. The only way to measure if the systematic errors have decreased is by comparing the non-directional error, or the MAE. Thus, a two-tailed t-test tested whether the before and after MEs are not significantly different from one another, and one-tailed t-tests measured if the MAE does not significantly decrease after the refraction correction. For both one and two tailed tests for the 1.34 coefficient, the p-value is less than 0.05, where only the one-tailed t-test for the site-specific coefficient has a significant p-value (Table 14). This indicates that the before and after MEs are significantly different, and that the MAE is significantly smaller only after the 1.34 refraction correction is applied, thereby significantly reducing the amount of error. Additionally, I used Levene's Test to test the

null hypothesis that the population variances are equal between the before and after refraction correction data. A significant result from the Levene's Test would indicate that the precision significantly increased after the correction. Both p-values were greater than 0.05, and thus the null hypothesis is accepted (Table 14). The reduction in ME and negligible change in the SD after the refraction correction procedure is similar to the results of other studies (Westaway et al., 2001).

Table 12: Comparison of photogrammetric and spectral depth approaches

Approach	Calibration	Validation
Photogrammetry (1.34 coefficient)	-	$d = 0.82x + 0.13$ $R^2 = 0.60$
Photogrammetry (Site-specific coefficient)	$d = 1.21x + 0.09$ $R^2 = 0.62$	$d = 0.96x + 0.01$ $R^2 = 0.67$
Spectral Depth (Non-shadow regression)	$d = 1.30x + 0.49$ $R^2 = 0.24$	$d = 0.89x - 0.04$ $R^2 = 0.20$
Spectral Depth (Site regression)	$d = 0.69x + 0.41$ $R^2 = 0.09$	$d = 1.26x - 0.07$ $R^2 = 0.11$

Table 13: Mean error and standard deviation values of two photogrammetric refraction corrections and two spectral depth regressions.

Approach	Validation data before correction (m)		Validation data after correction (m)		
	ME & MAE	SD	ME & MAE	SD	R^2
Photogrammetry (1.34 coefficient)	-0.16 0.18	0.179	-0.071 0.138	0.183	0.60
Photogrammetry (Site-specific coefficient)	-0.15 0.17	0.175	0.009 0.13	0.172	0.67
Spectral Depth (Non-shadow)	-	-	0.09 0.20	0.24	0.20
Spectral Depth (Site)	-	-	-0.036 0.22	0.30	0.11

Table 14: Changes in mean error and standard deviation after refraction correction

Approach	Two-tailed t-test: ME		One-Tailed t-test: MAE		Levene's Test	
	T-value	P-value	T-value	P-value	F Value	P-value
Photogrammetry (1.34 coefficient)	-4.56	0.000007	2.55	0.006	0.07	0.79

Photogrammetry (Site-specific coefficient)	-4.83	0.000004	1.49	0.07	0.24	0.62
--	-------	----------	------	------	------	------

Under the assumption that the site-specific coefficient best estimates water depth based on its high R^2 value, I wanted to test if its post-correction ME and SD values are significantly lower than those values of the other approaches. Table 15 shows the results of the two-tailed and one-tailed t-tests, where the null hypothesis for the two-tailed t-test is that the difference in ME between the site-specific coefficient and each of the other three approaches is equal to zero, and the null hypothesis for the one-tailed t-test is that the MAE of the site-specific coefficient is not less than that of the three remaining approaches. The p-values for the 1.34 coefficient show that its ME (-0.071 m) is significantly different from the site-specific coefficient ME (0.009 m), but that the MAE of the site-specific coefficient (0.13) is not significantly less than the MAE of the 1.34 coefficient (0.138). The MEs of the non-shadow spectral depth and site-specific coefficient are significantly different, and the MAE of the non-shadow spectral depth is significantly greater than the MAE site-specific coefficient. The site spectral depth ME is not significantly different from the site-specific coefficient ME, but its MAE is significantly greater than the site-specific coefficient MAE. The site-specific coefficient's MAE is significantly less than the spectral depth MAEs, however it is not significantly lower than the 1.34 coefficient MAE; only the MEs of the two photogrammetric coefficients are significantly different.

Table 15: T-tests measuring significant difference between mean error of site-specific coefficient and other approaches

Approach	Two-tailed t-test: ME		One-Tailed t-test: MAE	
	T-value	P-value	T-value	P-value
Photogrammetry (1.34 coefficient)	2.95	0.004	-0.25	0.40

Spectral Depth (Non-shadow)	-2.16	0.03	-2.81	0.003
Spectral Depth (Site)	1.07	0.29	-3.35	0.0006

The last step of the analysis is to assess if spatial autocorrelation of the mean errors exist. Only the validation data errors were used in this visual and statistical analysis, and therefore there were not enough data points to conduct a local statistic. Table 16 details the results of the Moran's I global statistic for each approach given a certain distance from which to calculate the average error, D. Given that the validation data were chosen randomly for each approach, each data set varied in the smallest distance that existed between two points. Nine meters was the smallest D value possible for two of the data sets, and so Moran's I was calculated with D = 9 m for all four approaches for consistency, and calculated the statistic again for approaches with a possible smaller D value. I removed one point from the non-shadow validation locations because it was approximately 15 meters away from any other point, which is a large distance to include as spatial neighbors in the calculation for a stream of this size (Appendix D). Table 16 shows that the site-specific coefficient is the only approach that does not have spatial autocorrelation in its error. The Moran scatterplots and visual error figures are in Appendix D.

Table 16: Moran's I statistic for 4 approaches to test for spatial autocorrelation of error. D is the distance from each point within which average error is calculated. D for the smallest distance possible is stated in meters in the cell above the value.

Approach	D = 9 meters		Smallest distance possible	
	Moran's I	P-value	Moran's I	P-value
Photogrammetry (Site-specific coefficient)	0.06	0.20	-	-
Photogrammetry (1.34 coefficient)	0.29	0.0000000000000002 (2.2e-16)	4 m 0.37	4 m 2.689 e-14

Spectral Depth (Non-shadow)	0.31	0.0001	5 m 0.41	5 m 0.0002
Site Spectral Depth	0.35	8.50 e-07	-	-

Given the above results and metrics in comparison with other methods, the site-specific photogrammetric correction is the highest quality approach to derive bathymetric data in this study. The site-specific correction had a higher R^2 value and lower SDE than the three other approaches, and was the only approach with a significantly low spatial autocorrelation of error. This method also resulted in a significantly lower MAE than the spectral depth approaches, and its validation slope was closest to 1 and its y-intercept was closest to zero in comparison to the other validation equations. The site-specific coefficient resulted in higher accuracy and precision, and a better goodness of fit validation equation.

Creating the Corrected DEM

The next step is to apply this refraction correction to the submerged DEM (Appendix D), and merge it to the dry DEM (Figure 14). Due to the cell sizes of the water surface, the cell size of the submerged DEM is different from the original DEM's cell size, and thus the submerged DEM was resampled to the original DEM cell size before merging the two. Figures 15 and 16 show the error distributions in the channel, based on measured water depths after the site-specific correction is applied. While the site-specific correction is the best approach in this study, Figure 16 shows that this method still has a systematic error: it predicts a smaller range of depths in comparison to ground truth values, because it over-predicts depths in shallow areas, and under-predicts water depths in deeper areas of the channel.

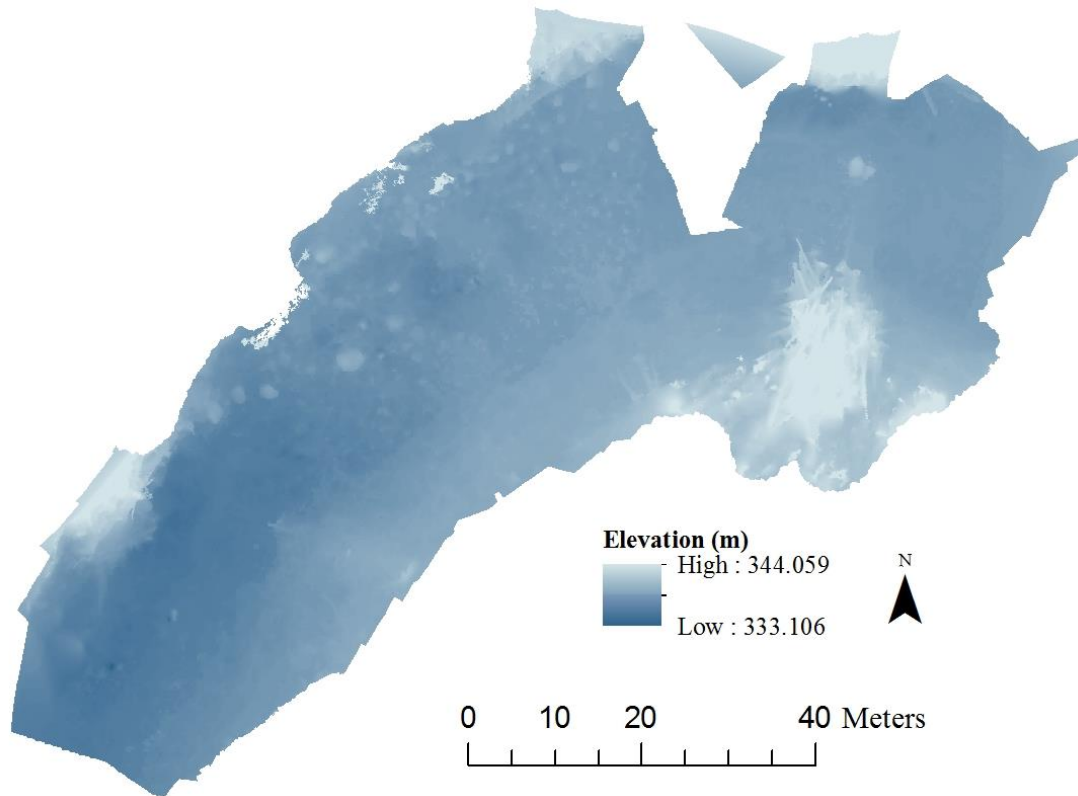


Figure 14: Final DEM after site-specific refraction corrected submerged channel DEM is merged to dry DEM. Spatial resolution of 1.50 cm.

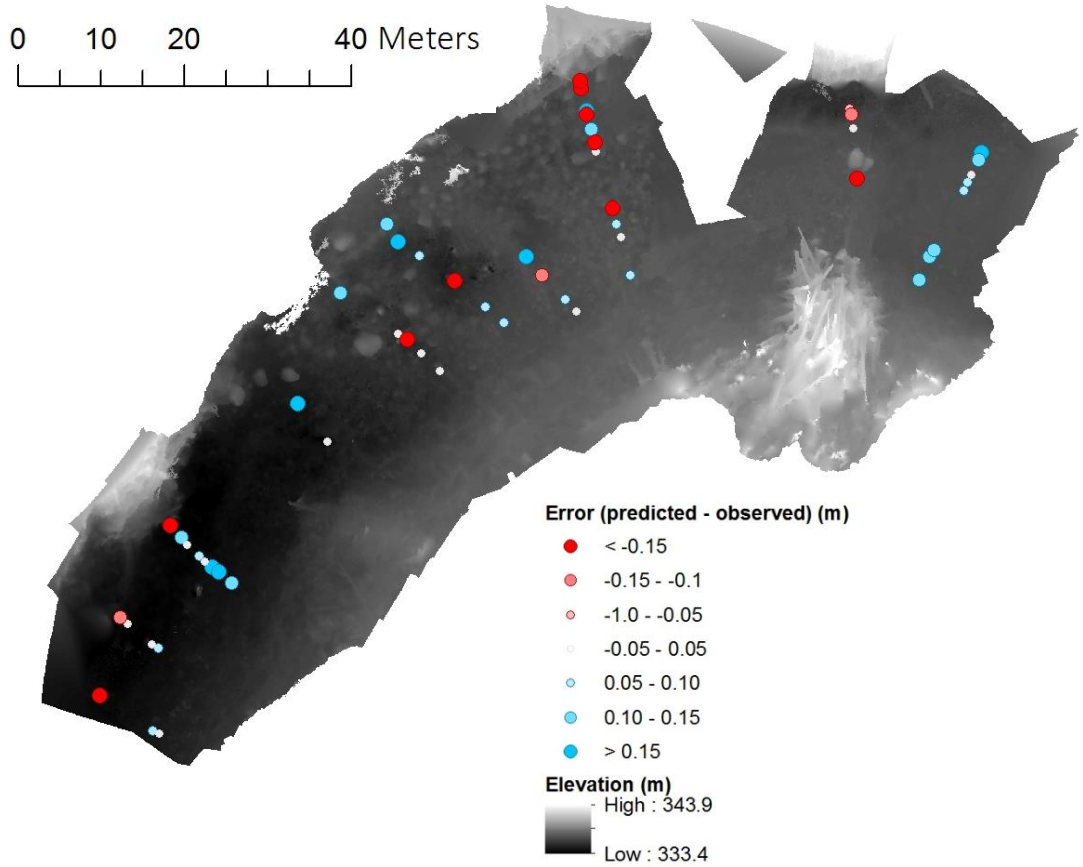


Figure 15: Error distributions between predicted depths from the site-specific correction and observed water depths.

Site Specific Refraction Correction: Depth Error

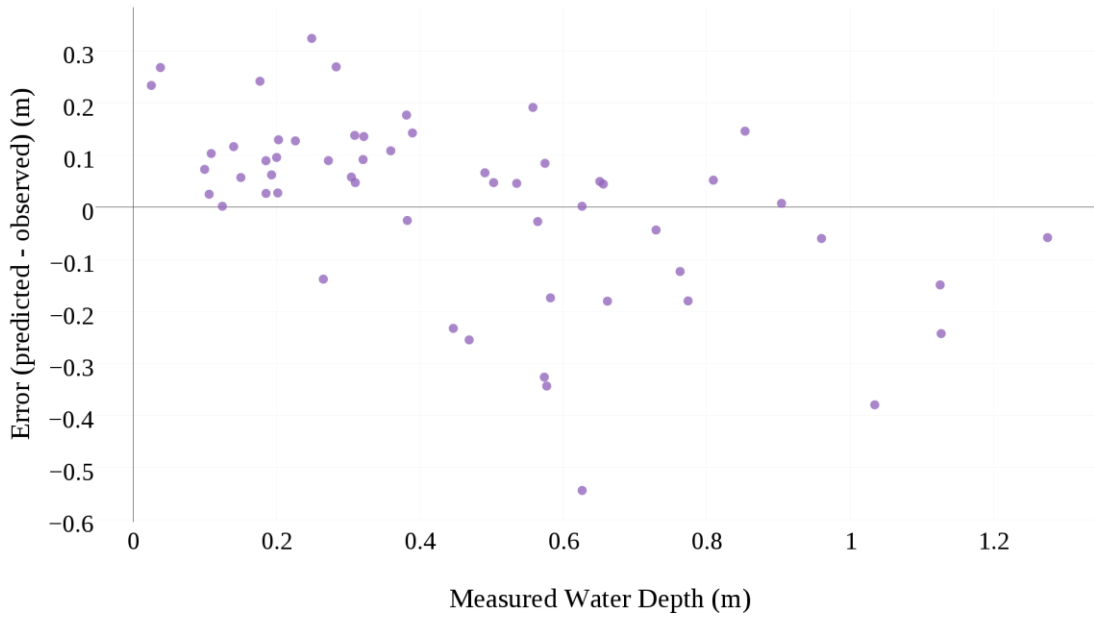


Figure 16: Residual plot of depth differences in measured water depths.

CHAPTER V

DISCUSSION

This chapter will examine the results found in the previous chapter. These sections include interpretations of the results and suggestions for how the methods could be improved in the future. The research questions are discussed in depth, and suggestions for river managers and scientists are given, along with these methods' limitations and considerations.

Image Acquisition

The proximity of the tall tree canopy to the wetted channel complicated image acquisition. In forested mountain drainage basins such as the Sandy River Basin, even a sunny, cloudless day may not guarantee better point clouds and DEMs because the tall tree canopy adjacent to the banks place parts of the submerged channel in shadow for a majority of the day. For example, in my site on the Salmon River, approximately the first 40 meters of the upstream section was in sunlight in the morning, but by the time a majority of the channel was in sunlight, the left bank upstream around the log structure was in shadow. Part of this shadowed area, particularly in the cross section directly downstream of the log structure, had inaccurate elevation predictions in the SfM output. The area on the right bank directly downstream of the second log structure also had a poor DEM. I believe it is because the first batch of photos collected here were in sunlight, and after taking pictures of the whole site and returning downstream 40 minutes later, the area was in shadow. Even though I collected imagery within one hour on the same day,

the tree canopy reduced the amount of time available to collect imagery with relatively even illumination.

Additionally, I only had access to four UAV batteries, giving me just under an hour to collect images. I used all four batteries, and still there is a large hole in the DEM and orthophoto on the right bank across from the first log structure. It is possible that the time limit of the UAV batteries prevented collecting enough photos, which contributed to PhotoScan not being able to develop a point cloud in this area. While it is possible to generally evaluate photo overlap in the field, the UAV battery is still a limitation. I captured the images on the last day of my field work, which was the only sunny day of the week. Leaving the field site to charge the batteries for another flight would have taken a minimum of three hours, and the change in the amount of channel in shadow would have certainly changed.

In areas of the channel with sufficient overlap and no shadow, submerged areas of the channel appeared clear in the orthophoto. The goal of the study was to capture bathymetry, so while I did not measure any quantitative results on dry land, I trust that the point cloud and DEM is accurate on the bar on river left, adjacent to the wetted channel and not underneath the canopy, given that the detail in the orthophoto is clear.

Water Surface Interpolation

The canopy also caused issues with the accuracy of the GPS data collection and the creation of the DEM. In areas where the canopy prevented the rtk-GPS from collecting an accurate GPS location, the canopy also reduced the amount of photo overlap and visibility. Consequently, there are large areas, particularly on the right bank, where

the DEM is inaccurate and there are no GPS locations to contribute to the water surface elevations. Even with GPS locations with relatively low errors, the rtk-GPS vertical error tends to be higher than horizontal error (Appendix B), and more error could have been introduced while using the equipment in the field. The cross sectional data, and therefore the edge-of-water elevations, were collected over two and a half days due to weather constraints, while the photos were collected within one hour. It is possible that using a combination of edge-of-water elevations and DEM water surface elevations over multiple days could have led to collecting and using slightly different water surface elevations. Multiple sources of small error could make a large difference in the accuracy of extracting submerged topography, especially in small, shallow streams where the vertical error may be equal to a large portion of the water depth.

I made the decision to slightly alter some of the water surface elevations to decrease in elevation in the downstream direction, but the effect of this change on the water surface accuracy, whether positive or negative, is unknown. While there is no way to guarantee that all GPS elevations will decrease in the downstream direction, in the future I would collect more edge-of-water elevations so that there are more data on which to base these decisions. More edge-of-water elevations could also improve the robustness of the quantitative test to determine which water surface represents the water surface more accurately.

The accuracy of the water surface affects both actual and predicted water depths, and therefore affects the accuracy of the linear relationship derived between the two depths. The ‘observed’ water depths were calculated by subtracting the GPS elevations from the water surface, and because the accuracy of the water surface is unknown, it is

unclear how much error exists in the ‘observed’ water depths due to the water surface and rtk-GPS errors, and therefore how well the mean error captures the accuracy and precision of the data. Due to the uncertainty of how SfM operates under water, the error between the predicted and actual water depths may not be the same, and thus the linear relationship derived from the calibration data and the R^2 may not describe the relationship adequately. This again supports the need for more edge-of-water elevations collected with high quality surveying equipment. On a site like the Salmon River, where the edge-of-water tends to be hidden between and under gravels and cobbles on the bar, relying on the DEM to extract these elevations will most likely overestimate the water surface elevation, as SfM is better at determining the elevations of the tops of cobbles and may not have visibility between cobbles. For the time being, the accuracy of the water surface in extracting submerged topography with little error requires field surveying of the water surface rather than relying on SfM alone.

Photogrammetric Approach

Between the 1.34 coefficient and the 4 site-specific coefficients, the site-specific coefficient with outliers removed proved to be the best fitting correction for these data, and applying this correction significantly reduced the mean error, or increased the accuracy by accounting for some of the light refraction. Removing more of the outliers from the calibration data set and applying this equation to all the validation data reduced systematic error further, as shown by the y-intercept and slope. While the accuracy was increased, the R^2 value remained the same, which may indicate an increase in the scatter of the data or the standard deviation of error. Using this same data set and removing

shallow depths did not improve the R^2 , but the slope was closer to 1 in all three cases. Further experiments are needed in order to understand this phenomenon of whether shallow depths may not need a refraction correction.

The highest achieved R^2 value of 0.67, indicating a moderately strong linear relationship, does not seem to be reflected when looking at the range of errors. The majority of the depth differences between the predicted and observed water depths occur between 0 and 0.15 meters (Appendix D), but the range spans from -0.55 to 0.35 meters. Upon examination of Figure 16, it is common for the refraction correction to over predict the depth in shallow waters (<0.4 m) by 50 – 100% of the measured depth, and to under predict depth in deeper waters (>0.6 m) by 30 – 50%. In a shallow stream such as the Salmon River, this is very problematic.

The idea that shallow waters may not need to be corrected for light refraction, along with my results of a site-specific coefficient, begs the question of the appropriateness of applying Snell's Law and 1.34 as the refractive index for every clear, shallow river. The higher accuracy of the site-specific coefficient does not disprove Snell's Law or suggest that 1.34 is not a suitable refractive index for some rivers; rather, it suggests that our lack of understanding of how SfM generates elevations underwater implies that we cannot be sure that Snell's Law holds true when SfM software aligns point clouds. It is possible that the site-specific coefficient may account for the point cloud alignment process, however no conclusions can be made without further experimentation. Even though refraction physically occurs in the same manner at the air-water interface, Butler et al. (2002) suggested that Snell's Law is inadequate to account for the refraction effect due to a number of factors that alter the magnitude of the

refractive index, such as the position, angle, and distance of the camera relative to the water surface. Thus, while we may not completely understand how SfM aligns submerged topography, the site-specific coefficient might account for the differences in alignment from one river to another. Additionally, Snell's Law only accounts for light refraction under the assumption of a planar water surface, and it is unclear how the varying angles and slopes of the water surface may alter the effects of refraction, and how SfM uses this information. Again, this is mere speculation and further experiments should be done to better understand how water surface topography and roughness affect apparent depth and how SfM processing functions in underwater environments.

The division of the data sets into habitat units also did not improve the goodness of fit of the refraction correction for the data. Photogrammetrically, the lower R^2 values in riffles and pools corroborate the physical environments in which SfM software has trouble identifying edges and creating point clouds, such as deeper water depths and reflective water surfaces. However, if the physical environments influence the accuracy, then it would be hypothesized that glides, with their shallow depths and smooth water surfaces, would result in a higher R^2 . It is possible that the within habitat unit variation is so great that dividing the data into groups emphasizes this variation and therefore doesn't improve the goodness of fit of the model. Assuming a homogeneous channel unit groups together features where large pixel-scale variability may exist. If the within-unit variation does exist, then a combination of errors could have accumulated to cause the variation, such as errors in the water surface layer and rtk-GPS locations. It is also possible that removing deeper apparent depth points could over-exaggerate depth where the water is shallow (Westaway et al., 2001). After removing more outliers from the calibration data

for the three habitat units, the R^2 values remained the same, but only the glide validation equation showed an increase in accuracy demonstrated by its slope and y-intercept being closer to 1 and 0. For pool and riffle habitats, the slopes and y-intercepts shifted farther away from 1 and 0, unveiling more systematic error. This may have occurred due to the smaller sample sizes in the pool and riffle habitats (45 and 34 points) in comparison to the glide habitat (88 points). This may imply that if the data set is large enough, removing more outliers from the calibration data to create a linear equation reduces systematic error represented in the slope and y-intercept but does not improve precision. This may or may not be true in this data set or for other data sets, but collecting more GPS points in a variety of water depths and water surface roughness areas throughout the site could help avoid this issue.

These results demonstrate that the site-specific coefficient, given its highest R^2 and lowest error, is the most appropriate refraction coefficient for this reach of the Salmon River. This implies that if this is a viable method to derive the most accurate water depths, then this method could be applied to other similar gravel-bed streams environments that are clear and shallow. However, the refractive index must be derived from data collected at the site of interest.

Spectral Depth Approach

The results of the spectral depth regressions clearly demonstrated that this approach most likely cannot be successful in a stream such as the Salmon River, where the environmental conditions lead to large errors and a poor depth estimation. This reach of the Salmon River contains local variations in substrate colors, surface turbulence

causing sun glint on the water surface, and a large amount of shadow between cobbles and gravels in the riverbed, which all contribute to producing different reflectance values captured by the sensor that greatly complicate depth mapping by changing the relationship between depth and image radiance (Marcus et al., 2003; Legleiter et al., 2009; Marcus et al., 2012; Carbonneau et al., 2012). These characteristics contributed to the low R^2 values for both the site-specific regression and the habitat unit regressions, where, similar to the photogrammetric habitat unit equations, it is possible that a combination of a greater within group variation and small sample size increased the error. While these facts are accepted in the remote sensing community, spectral depth results in depth mapping on streams such as the Salmon River are not published; rivers with brighter, homogeneous, and low-texture substrates and smooth water surfaces are chosen for spectral depth tests (Feurer et al., 2008). A larger range of fluvial environments should be surveyed using the spectral depth approach in order to develop the range of rivers and optical river environments where the spectral depth approach can and cannot be successful in bathymetric mapping.

In addition to the errors that accumulated from the GPS locations and water surface interpolation that affect both photogrammetric and spectral depth approaches, the radiometric resolution of the sensor adds another source of error that greatly affects the success of the spectral depth approach. Radiometric resolution, or a sensor's capacity to perceive small changes in radiance, often determines bathymetric precision (Legleiter and Roberts, 2009), where the amount of reflectance detected is dependent on the change in radiance exceeding the fixed amount of radiance represented by one digital number (Legleiter and Fonstad, 2012). Additionally, the range of digital values captured by a

sensor is significantly smaller for water than for land (Marcus and Fonstad, 2008), further reducing capacity of the sensor to detect changes in radiance. When examining the differences in digital number values of the green and red bands of the pixels used in the calibration and validation data sets, many of the green and red values were equal to each other at a wide range of depths, or the values only differed by a small amount in comparison to the possible range of digital number values for this sensor (256). This implies that the radiometric resolution of the sensor likely influenced the spectral depth relationship to have high variability, where similar LN(G/R) values were calculated at a large range of depths. It is possible that capturing images with a sensor that has finer radiometric resolution could produce a better spectral depth relationship, however the site and optical characteristics that complicate bathymetric mapping would still be present.

Regardless of the divisions and details, the spectral depth approach could not yield reliable and accurate results. This river environment is not amenable to using the spectral depth approach, and so analyzing the differences between the water depth errors in areas of shadow and non-shadow is not realistic. This is a question that would be best answered in rivers with characteristics that have allowed this approach success in previous studies.

Comparison of the approaches and applicability in surveying fish habitat

This research has shown that this reach of the Salmon River that is shallow, clear, and a gravel-bed stream is best surveyed for bathymetry using photogrammetric techniques by applying a refraction correction to predicted DEM elevations. The photogrammetric results had higher R^2 values, lower standard deviation of error values,

and significantly lower mean error than the spectral depth results. Between the 1.34 and site-specific coefficients, the latter estimated water depths with greater accuracy and precision than the former, represented by a validation slope closer to 1 and a y-intercept closer to 0, and a higher R^2 value. The high local variation in substrate sizes and colors created a high textured environment that facilitates SfM processing, and complicates spectral depth relationships. Depending on the sensitivity of the application to accuracy and precision, a photogrammetrist would provide a river manager with the data that provides the highest accuracy (the lowest mean error), the highest precision (lowest standard deviation of error), or both (Westaway et al., 2001).

When comparing the practicality of surveying using photogrammetric and spectral depth techniques, the main distinctions are dependent on the river environment and sometimes cost. Both techniques require the same data set and generally the same data processing, with the only difference being the use of RGB values or predicted depth in the calibration and validation data sets. Regardless of the technique, predicted depth and color values of each pixel can be collected and calculated with the same data set from image acquisition, GPS data collection, and processing the data with SfM software. The two methods are both affected by changing environmental conditions, although to varying degrees, such as weather, time of day, and shadow. In other words, both techniques perform best on cloudless, sunny days with minimal shadow, which is affected by sun angle and the proximity and height of the tree canopy. The river environment, as discussed above, is the main determinate of which technique would perform best in a given site. Photogrammetric methods can more easily extract bathymetric data in heterogeneous river environments and substrates of varying colors

and sizes, whereas homogeneous river environments with bright, low texture substrates, such as sand, are amenable to spectral depth methods. Cost may also be a factor, where spectral depth better predicts depth with a high radiometric resolution sensor, whereas photogrammetric techniques do not depend on this factor to the same degree. Regardless of the sensor, flying a UAV at a lower altitude can generally increase spatial resolution, whereas the level of radiometric resolution in a sensor cannot be changed.

When comparing the two approaches in their ability to provide high quality data for fish habitat surveys, the approach to choose depends on the river environment of the target fish species. For the Salmon River and other similar gravel-bed rivers in the Pacific Northwest, where native salmon species depend on gravels at various life stages and monitoring gravel recruitment is a common practice, the photogrammetric approach would most likely work best. This research has shown that photogrammetric methods provided higher quality data in this environment, most likely because of the high texture, heterogeneous substrates (Feurer et al. 2008).

Stream monitoring programs most commonly used in the Pacific Northwest have overlapping goals that are directly or indirectly related to evaluating fish habitat, including the Columbia Habitat Monitoring Program (CHaMP), Pacific Infish Biological Opinion Effectiveness Monitoring Program (PIBO), and Aquatic and Riparian Effectiveness Monitoring Program (AREMP). In order to determine if these monitoring programs could provide high quality data from photogrammetric surveys, I will compare the photogrammetric data to the type of data and the scale of the monitoring programs. Photogrammetric data can potentially provide high quality data at the reach scale for the

geomorphic aspects of fish habitat, along with some other observable characteristics, but not quantitative hydraulic or water quality metrics.

The goal of AREMP is to describe the ecological condition of aquatic ecosystems and watersheds by monitoring the ecosystem processes that shape and maintain habitats rather than smaller scale channel habitat features, such as number of pools or pieces of large wood (Reeves et al., 2004). Basin geomorphology is one of many ecological conditions that AREMP protocol is interested in collecting, including hydrologic patterns, water quality, and riparian forest conditions. Photogrammetry could provide high quality data for the geomorphological aspect of the protocol, however this research measured submerged topography at the mesohabitat scale. Logistical obstacles associated with these methods are collecting field validation measurements near the time of flight or photo acquisition, which is unfeasible at the watershed scale (Marcus and Fonstad, 2008). While aerial photos are always helpful in characterizing general form and patterns, AREMP may not be the best beneficiary of photogrammetric data from SfM software at the basin scale.

For monitoring programs that focus on collecting data on smaller scales, using SfM to collect topographic information related to fish habitat would provide high quality data required by PIBO and CHaMP surveys. While CHaMP is more of a fish-centric survey, both surveys are moderately data intensive, requiring the collection of reach length, cross-sections, delineating and measuring features of channel units, and a drawing of a reach map, among other topographically related data (Bouwes et al., 2011; Heitke et al., 2011). The CHaMP survey even emphasizes the use of aerial photography and remote sensing to improve the surveys and potentially provide spatially continuous data, and that

the topographic data collected with a total station should be used to produce high resolution DEMs and a water depth map. While photogrammetry can't provide stream characteristics such as discharge and water chemistry, the photogrammetric methods in this research can provide a majority of the topographic data necessary as a high resolution and spatially continuous data set, and even general descriptions of riparian structure, fish cover, and relative surface water speed. While the use of remote sensing to collect substrate information is outside the scope of this study, other studies have examined the use of close-range photogrammetry techniques in measuring grain sizes (Carbonneau et al., 2004; Verdu et al., 2005; Hedger et al., 2006; Dugdale et al., 2010).

Both PIBO and CHaMP surveys are conducted in wadable streams, and given other stream conditions such as low turbidity and shadow, photogrammetry could provide the same or better data for these or similar surveys that measure topographic variables related to fish habitat at the reach or mesohabitat scale. Photogrammetric data processed by SfM can produce high resolution DEMs that can be used to measure various aspects of the quantity and quality of stream habitat available to fish. While it doesn't eliminate the need for data collection and adds its own field work requirements, the higher resolution and spatially continuous data can improve the understanding of the connection between habitat attributes and salmonid life history requirements and therefore the ability and scope of these monitoring programs.

Suggestions for River Scientists and River Managers

Photogrammetric techniques in extracting bathymetric data still have a ways to go before reaching the point where they can be common monitoring methods for rivers.

However, for future studies and river managers in using a UAV to collect bathymetric data on a clear, shallow, gravel-bed stream like the Salmon River, the following section provides some improvements on these methods or factors to think about before and during surveying and data collection. Table 17 provides a set of best practices for collecting these data in the field. I believe that a large majority of my errors could be improved by having enough photo overlap in all areas of the submerged channel, less shadow, having an accurate water surface, and potentially altering GPS surveying techniques.

Table 17: Best field surveying practices.

	Best Practices
Collecting imagery	<ul style="list-style-type: none"> • Capture imagery at various heights. The highest photos should include the entire width of the channel and some of the bars and/or floodplain if possible. • When capturing closer imagery, zig-zag the sensor and take photos incrementally to ensure photo overlap (calculate beforehand the area included in the image given the sensor is at a certain height – this can inform the surveyor of the amount needed to move the sensor to capture 60% overlap. More overlap is always safer). • Collect imagery as close together in time as possible to reduce differences in illumination. • Plan photo acquisition for the time of day with as much sunlight covering the channel as possible. These methods are more successful when images are collected on a bright, cloudless day.
Ground control points	<ul style="list-style-type: none"> • Given site area, estimate a range of the number of photos you might take. Choose the higher number, and use at least one-tenth of that number for ground control points. • For underwater GCPs, place them in areas with a very smooth water surface. If you can't clearly see the point on the card that you will survey when it's underwater, then it shouldn't be used to georeference images. Record water depth with a stadia rod at underwater GCPs. • Draw a map of where you put the GCPs and what number they are.
Topographic surveying	<ul style="list-style-type: none"> • Validation bed elevations: Random surveying points are recommended, but if you choose to survey using cross sections, surveying points between cross sections is suggested. The density of

	<p>points is dependent on the channel characteristics (water depth, water surface roughness, etc).</p> <ul style="list-style-type: none"> • Validation elevations: Consider surveying on top of gravels and cobbles and not between them, particularly in gravel-bed streams where it is difficult to see in the dark crevices in between gravels. • Water surface elevations: Collect edge-of-water elevations at a regular spacing, or increase the density of points where slope changes more rapidly. The accuracy of the water surface will influence the accuracy of all subsequent calculations. Plan surveying so the water surface elevations are recorded the same day the imagery is collected.
Pilot Study	<ul style="list-style-type: none"> • Conducting a pilot study on a small area first will help avoid mistakes in data collection and improve the accuracy and precision of the results. The results of the pilot study will give a better indication of the best way to set up a sampling scheme. • Test different refraction correction techniques and mapping areas by habitat or shadow and non-shadow.

Photo overlap is key in generating a high-density point cloud, an accurate DEM, and therefore a potentially stronger relationship between predicted and actual water depth. Ensuring enough photo overlap in the images can be evaluated in the field by reviewing photographs. This suggestion should be considered within the context and goals of a study, as higher density point clouds are not always necessary or helpful. However, it is possible to reduce the resolution by merging DEM pixels with a low-pass filter if necessary, while increasing the resolution of the DEM is more difficult. Given my site and research goals, collecting more photos likely would have improved my results. If limited flying time is an issue, then a trade-off can be made between area of the stream captured and flying altitude. Similar to limited flying time, planning for image acquisition during the least amount of shadow in the channel may also be an issue, particularly if the orientation of the canopy limits the window of time in which photos can be collected with minimum shadow. Making observations at the site and planning a flight pattern prior to

data collection can mitigate the limitations created by the length of battery life and duration and location of shadows. If necessary, it might be useful to capture imagery in sections based on when certain sections will be in sunlight, but the effects of this in the photogrammetric processing is uncertain.

It is very likely that a large amount of errors stemmed from the inaccuracies of the interpolated water surface, and potentially from the implementation of surveying techniques. I collected validation data through cross section data, and only collected edge-of-water elevation data on each side of the cross section. In the future, I would survey points throughout the site with a generally even spacing, but even if cross sections are still used to collect data, I would also collect relatively evenly spaced edge-of-water elevations, with a greater density of elevations in areas where the slope changes. This increases the amount of water surface elevations available and reduces dependency on the SfM-produced DEM for elevations, which introduces more error. Additionally, I would consider placing the rtk-GPS pole on top of cobbles and gravels instead of the between cobbles, which is a common tendency and practice (Westaway et al., 2001), where light may not reach and muddle the detection of edges in SfM software. If the end goal is to provide accurate and precise bathymetric data, the surveying of submerged topography should be in locations that SfM software, and spectral depth techniques, can better detect and predict elevations, which in turn could potentially improve the strength of the predicted to actual water depth relationship.

In addition to observing site conditions prior to data collection, it may also behoove the researcher to complete a pilot study to improve data collection at the study site in order to improve the depth prediction, such as understanding the spatial

autocorrelation structure of the river and the amount and type of sampling needed. I calculated the Moran's I statistic, which is not ideal because it is a global statistic and my data were too far apart to draw strong conclusions or implications. Three of the four approaches that I tested for spatial autocorrelation produced low, although statistically significant, spatial autocorrelation of error between the estimated and observed water depths. The low spatial autocorrelation does not allow any concrete conclusions, but understanding the spatial autocorrelation of error in a river could improve the depth prediction.

Limitations and Considerations

The same limitations exist for these methods that have been discussed in previous sections and explained thoroughly in published literature (article here... Westaway et al., 2001; Woodget et al., 2014), such as the water depth limit, shadow, and water surface roughness. There are other limitations and considerations that affect current practices in the field regarding SfM processing, the way we think about and apply Snell's Law, whether accuracy and precision values are representative of the area of interest, and the range of river environments that these techniques can successfully extract bathymetric data.

Applying a simple refractive index to correct for light refraction in water is appealing for various applications because of its ease of use and repeatability. However, simplifying this procedure for a majority of streams while using SfM is contradictory in terms of their underlying processes and assumptions. SfM functions by producing 3D point clouds from overlapping, converging images from different angles and distortion

can be reduced by using imagery collect at varying distances (Westoby et al., 2012; Fonstad et al., 2013), but the degree of the refraction correction required increases with radial distance from the sensor (Butler et al., 2002). Any single refractive index functions under the assumption of a planar water surface, which is rarely the case in natural streams, and thus requires a different refractive index for water surface roughness that introduces varying angles of the surface that also changes from image to image. If the angle of the water surface is constantly changing and different in each image captured, this also questions how SfM can align submerged points that appear in a different location in each image. This implies that the refractive index would not only be different in each image based on factors such as water surface roughness and the distance between the water surface and the sensor, but the refractive index may be different throughout one image. Assuming that SfM can align submerged points under a non-planar water surface and that one refraction correction can be applied to a site and act as an average correction for all the different refractive indexes needed across the images, then the average refraction correction depends on the range of refractive indexes, which will be different for every site and every data set. Therefore, while 1.34 may be a physically correct refractive index, the refractive index used for SfM-derived DEMs should average the refractive indexes that exist in the images in order to encompass both refraction at the air-water interface and any other processes causing more errors to occur. In other words, the refraction correction should be site and image specific in the same way that the correlation between spectral properties and depth is specific for each site and set of images. The refraction phenomena should be further studied to determine if it is affected by more than just the air-water interface in photogrammetric outputs, such as depth,

water surface roughness, and the alignment of point clouds in SfM software, or if the refractive index used to correct submerged elevation encompasses the correction of other errors and not only refraction.

Fluvial remote sensing studies report error, accuracy, and precision metrics in the form of mean error, standard deviation, R^2 , and percent correct value that only represents the validation data. The two questions that arise from this are 1) can these quantitative indicators be extrapolated to the entire channel as a whole or do they only describe the individual validation data collected (Westaway et al., 2001); and 2) can these metrics actually be used and compared to a subjective threshold to determine a ‘better’ method based on minimal theory about the accuracy and precision levels necessary for specific applications (Marcus and Fonstad, 2008)? Every study uses a different amount of validation data that could result in varying levels of accuracy and that may or may not be representative of the submerged topography as a whole. This makes comparison of research results difficult, or at least implies that choosing a method shouldn’t be chosen based solely on these metrics. Additionally, the range of amenable environments in which we can expect certain levels of accuracy and precision from these methods is unknown. This lack of knowledge needs to be resolved by testing both methods on all different types of streams to establish where these methods can be applied in order to establish the levels of accuracy and precision required for different applications.

The methods and results in this research also highlight the gaps of knowledge in the literature. Researchers have not quantitatively examined the effects of using different water surface interpolation methods. For both photogrammetry and spectral depth approaches, researchers tested these methods on sites with ideal conditions and often

used elevation data to validate predicted water depths to measure error, thereby reducing reported error. Most articles using spectral depth to estimate water depth tested the method on rivers with homogeneous substrates, smooth water surfaces, and low turbidity that improve the spectral depth relationship (Winterbottom and Gilvear, 1997; Lejot et al., 2007). To my knowledge, there are no articles published with R^2 values as low as the values from my spectral depth regression equations. Testing spectral depth on ideal sites does not establish a range of environments that are amenable to this technique. For the photogrammetric studies, the comparison of the measured and estimated topographic data measures the strength of the refractive index, when in reality the use of the elevation data instead of water depths introduces a bias that improves the R^2 value due to the inherent relationship that elevation decreases downstream. Spectral depth studies compare measured and predicted water depths, but cannot be compared to photogrammetrically derived bathymetric data. Both types of approaches should be tested on a wider range of streams and use the same measure of accuracy and precision in order to be comparable.

CHAPTER VI

CONCLUSION

This research has shown the differences in methods and results of using photogrammetric and spectral depth methods in extracting bathymetry from a gravel-bed, shallow, clear stream. The results showed that the photogrammetric site-specific refraction coefficient was the best fitting model for the data and resulted in higher accuracy and precision in comparison to the other photogrammetric and spectral depth tests. The photogrammetric methods clearly produced higher R^2 values, accuracy, and precision than the spectral depth approaches. The low accuracy and precision produced by the spectral depth results implies that this type of river environment is not amenable for the use of spectral properties in deriving water depths. That being said, many of the estimated depth errors from the photogrammetric method are proportionally high for a shallow stream. These errors could be potentially minimized by improving the water surface accuracy, surveying on top of cobbles instead of in between them, and ensuring relatively equal lighting during image acquisition. This site-specific coefficient could be applied to similar stream environments from images and data collected at the site of interest and under ideal illumination conditions.

This research demonstrates the importance for the fluvial remote sensing community to produce more studies that quantitatively test the accuracy and compare the methods that produce bathymetric data. In particular, the interpolation of water surfaces and the refraction effects on photogrammetric processes should be tested in robust studies. Other methods not currently published, such as a site- or habitat-specific refractive index, should be evaluated in their ability to extract bathymetry in a wider

range of fluvial environments. This technique can be improved by testing at various sites with different depths and hydraulic characteristics in order to develop guidelines for where this method can and cannot be applied, and to develop best practices for this method.

APPENDIX A
STRUCTURE-FROM-MOTION

AGISOFT PHOTOSCAN WORKFLOW

- 1) Workflow > add original jpeg photos downloaded from UAV (ensure that the image quality is above 0.6)
- 2) Convert (button above loaded images on left) the photo coordinate system if the photos are geotagged.
- 3) Align photos (Medium accuracy, Disabled pair preselection; Advanced options left as default)
- 4) Select all photos that did not align, 'reset camera alignment', then 'align selected cameras'
- 5) Zoom out from sparse point cloud and disable cameras that are not in the right place
- 6) Select any points that are located outside of the point cloud and remove.
- 7) Import GCP text file with name, lat, long, and altitude
 - a. If the camera/UAV image locations are in decimal degrees, then import your GCP text file under the correct geographic coordinate system (ie, WGS 84)
 - b. Make sure the lat and long in your text file are already converted in decimal degrees, or whatever the camera coordinate system is set to
- 8) Select all the photos in the Cameras section (reference pane) and uncheck all geotagged photos.
- 9) Locate and assign GCPs to your images (right click point on image, place marker, and select correct GCP)
 - a. To get an idea of if this will work, choose a few GCPs spread throughout the image, and place markers on them in at least 3 images. Save then click update. If the error (m) and error (pix) are still low for those markers, then continue to assign GCPs
- 10) Once you are done locating and placing GCP flags on all your pictures, Save.
- 11) Click the optimize button, then check your errors. Uncheck any markers that have high error, then click optimize again.
- 12) Once you are happy with your error, build your dense point cloud (medium quality if lots of pictures, aggressive depth filtering)
- 13) Build Mesh. Select Height Field for the surface type if your final product is a DEM, Dense Cloud for the source data, and Medium face count. Select Enabled interpolation.
- 14) Build texture. Adaptive orthophoto as the mapping mode, mosaic as the blending mode, and the texture size/count was left at default number. 'Enable color correction' was left unchecked.
- 15) Export DEM or orthophoto – ensure the projection is the same. Leave defaults, and click export.

APPENDIX B

RTK-GPS CHANNEL CROSS-SECTION DATA

FID	Northing	Easting	Elevation (m)	HRMS (m)	VRMS (m)	HDOP	VDOP	Solution
0	5023809.145	577617.787	337.101	0.006	0.011	1.127	2.395	2.113
1	5023810.434	577618.107	336.849	0.007	0.011	1.09	2.179	1.887
2	5023810.778	577617.794	335.602	0.012	0.018	0.98	1.991	1.733
3	5023811.984	577618.457	335.536	0.009	0.012	1.195	2.085	1.708
4	5023814.028	577619.17	335.595	0.008	0.012	1.158	2.045	1.686
5	5023816.178	577620.391	336.859	0.008	0.011	1.353	2.33	1.897
6	5023817.332	577620.869	336.872	0.007	0.01	1.314	2.246	1.822
7	5023818.713	577621.287	336.917	0.007	0.011	1.249	2.199	1.81
8	5023819.873	577621.562	336.93	0.007	0.01	1.309	2.256	1.837
9	5023821.616	577622.135	336.948	0.007	0.01	1.246	2.209	1.824
10	5023823.038	577622.657	337.033	0.008	0.011	1.244	2.215	1.832
11	5023824.782	577623.156	337.053	0.008	0.011	1.242	2.22	1.84
12	5023826.207	577623.492	336.943	0.008	0.011	1.352	2.337	1.906
13	5023827.512	577623.9	336.903	0.014	0.019	1.252	2.273	1.897
14	5023829.134	577624.335	337.381	0.01	0.012	1.486	2.571	2.098
15	5023830.207	577624.568	336.854	0.013	0.02	1.337	2.396	1.989
16	5023831.278	577624.878	337.019	0.009	0.012	1.336	2.451	2.055
18	5023812.625	577607.649	337.192	0.006	0.015	1.046	2.799	2.596
19	5023813.524	577608.119	337.093	0.006	0.014	1.025	2.606	2.396
20	5023814.455	577608.471	336.923	0.006	0.014	1.007	2.413	2.193
21	5023815.365	577608.845	336.993	0.006	0.013	1.02	2.53	2.315
22	5023816.251	577609.34	336.992	0.006	0.013	1.019	2.505	2.289
23	5023817.088	577609.859	336.953	0.006	0.013	1.049	2.409	2.169
24	5023818	577610.338	336.931	0.006	0.014	1.093	2.956	2.747
25	5023818.884	577610.77	337.032	0.006	0.012	1.141	2.74	2.491
26	5023819.799	577611.159	336.993	0.006	0.014	1.093	2.969	2.761
27	5023820.688	577611.638	337.111	0.006	0.016	1.052	3.323	3.152
28	5023821.63	577612.017	336.962	0.006	0.015	1.052	3.309	3.138
29	5023822.468	577612.495	337.067	0.006	0.015	1.077	3.301	3.12
30	5023823.365	577612.951	337.078	0.007	0.015	1.256	3.342	3.097
31	5023824.26	577613.449	336.964	0.006	0.015	1.301	3.395	3.136
32	5023825.169	577613.87	337.007	0.01	0.025	1.204	3.338	3.114
33	5023826.057	577614.376	336.966	0.007	0.015	1.298	3.443	3.189
34	5023826.989	577614.714	337.016	0.014	0.028	1.386	3.494	3.208
35	5023827.841	577615.283	336.955	0.011	0.018	1.666	3.222	2.758
36	5023827.824	577615.23	337.041	0.009	0.015	1.648	3.205	2.748
37	5023828.732	577615.63	337.083	0.014	0.023	1.772	3.477	2.991
38	5023829.662	577616.086	336.931	0.015	0.024	1.837	3.501	2.98

39	5023830.564	577616.471	336.865	0.012	0.019	1.826	3.428	2.901
40	5023816.962	577600.2	337.164	0.007	0.012	1.237	2.601	2.288
41	5023818.294	577600.161	336.868	0.007	0.014	1.237	2.607	2.295
42	5023819.676	577600.133	337.231	0.007	0.013	1.237	2.613	2.301
43	5023824.328	577600.526	336.786	0.006	0.01	1.021	2.073	1.804
44	5023825.635	577600.623	336.84	0.007	0.012	1.236	2.635	2.327
45	5023829.214	577600.329	336.882	0.006	0.011	1.041	2.161	1.894
46	5023830.423	577600.33	336.889	0.007	0.012	1.097	2.301	2.022
47	5023831.721	577600.175	336.736	0.007	0.014	1.233	2.701	2.403
48	5023832.596	577600.016	336.581	0.007	0.014	1.233	2.716	2.42
49	5023833.16	577600.047	336.263	0.007	0.014	1.232	2.721	2.426
50	5023833.366	577600.001	336.098	0.007	0.014	1.232	2.725	2.431
51	5023833.663	577599.823	335.945	0.006	0.011	0.96	1.922	1.665
52	5023834.024	577599.742	335.942	0.006	0.01	0.961	1.923	1.666
53	5023811.94	577586.282	337.084	0.006	0.011	1.084	2.242	1.962
54	5023813.288	577585.948	337.043	0.006	0.011	1.084	2.244	1.964
55	5023814.933	577585.46	336.974	0.006	0.011	1.085	2.246	1.967
56	5023816.311	577585.048	336.872	0.006	0.012	1.085	2.248	1.969
57	5023817.576	577584.615	336.883	0.006	0.011	1.085	2.25	1.972
58	5023818.925	577584.211	336.806	0.006	0.011	1.085	2.253	1.974
59	5023820.068	577583.737	336.82	0.006	0.01	1.011	1.966	1.686
60	5023821.317	577583.366	336.834	0.006	0.011	1.086	2.256	1.978
61	5023822.758	577582.923	336.846	0.006	0.012	1.164	2.605	2.331
62	5023823.82	577582.5	336.865	0.006	0.011	1.087	2.262	1.983
63	5023825.308	577581.954	336.811	0.006	0.012	1.087	2.264	1.986
64	5023826.632	577581.665	336.73	0.006	0.012	1.087	2.266	1.988
65	5023827.774	577581.402	336.736	0.006	0.011	1.087	2.268	1.99
66	5023828.973	577581.116	336.707	0.012	0.029	1.401	3.446	3.149
67	5023830.305	577580.754	336.752	0.008	0.017	1.394	3.091	2.759
68	5023831.445	577580.327	336.732	0.013	0.028	1.405	3.127	2.793
69	5023832.537	577579.992	336.436	0.008	0.017	1.252	2.887	2.602
70	5023833.519	577579.582	336.459	0.008	0.018	1.2	2.848	2.583
71	5023834.318	577579.191	336.397	0.007	0.017	1.31	2.894	2.58
72	5023835.293	577578.864	336.435	0.013	0.029	1.228	2.89	2.616
73	5023836.347	577578.569	336.578	0.013	0.029	1.197	2.839	2.574
74	5023837.292	577578.143	336.562	0.008	0.017	1.427	3.206	2.871
75	5023838.082	577577.81	336.556	0.014	0.027	1.44	3.24	2.903
76	5023839.252	577577.448	336.612	0.014	0.026	1.328	2.941	2.624
78	5023841.621	577576.356	337.049	0.008	0.015	1.422	2.878	2.503

79	5023842.174	577576.261	337.189	0.008	0.015	1.384	2.723	2.345
80	5023837.742	577567.31	336.95	0.008	0.013	1.277	2.336	1.957
81	5023837.358	577567.444	336.625	0.009	0.015	1.278	2.339	1.96
82	5023836.508	577567.567	336.534	0.008	0.014	1.383	2.748	2.374
83	5023835.678	577567.738	336.456	0.008	0.013	1.383	2.748	2.375
84	5023834.631	577567.908	336.44	0.008	0.014	1.383	2.749	2.376
85	5023833.805	577568.281	337.16	0.008	0.014	1.383	2.749	2.376
86	5023833.342	577568.257	336.605	0.008	0.014	1.383	2.749	2.376
87	5023832.418	577568.582	336.632	0.007	0.012	1.283	2.354	1.974
88	5023831.53	577568.833	336.975	0.007	0.011	1.284	2.356	1.975
89	5023830.771	577569.089	336.75	0.007	0.011	1.285	2.358	1.978
90	5023829.964	577569.24	336.59	0.007	0.01	1.286	2.36	1.979
91	5023828.853	577569.426	336.606	0.007	0.01	1.286	2.361	1.98
92	5023827.98	577569.46	336.673	0.007	0.011	1.287	2.364	1.982
93	5023827.156	577569.772	337.187	0.007	0.01	1.288	2.366	1.984
94	5023826.69	577569.845	336.708	0.007	0.011	1.289	2.367	1.985
95	5023825.911	577570.098	336.512	0.007	0.011	1.29	2.369	1.987
96	5023825.119	577570.286	337.052	0.007	0.01	1.291	2.37	1.988
97	5023824.506	577570.576	336.626	0.007	0.01	1.292	2.372	1.989
98	5023823.7	577570.76	336.965	0.007	0.01	1.292	2.373	1.99
99	5023823.002	577571.097	336.738	0.007	0.011	1.293	2.374	1.991
100	5023822.087	577571.389	336.695	0.007	0.011	1.294	2.376	1.993
101	5023821.092	577571.639	336.895	0.006	0.01	1.079	2.122	1.827
102	5023820.177	577571.87	337.012	0.006	0.01	1.007	1.92	1.635
103	5023818.657	577572.363	337.065	0.006	0.01	1.077	2.103	1.806
104	5023817.791	577572.57	337.051	0.006	0.01	1.004	1.906	1.621
105	5023816.979	577572.805	337.045	0.006	0.009	1.004	1.905	1.618
106	5023815.787	577573.13	337.152	0.006	0.01	1.073	2.066	1.765
107	5023814.887	577573.301	337.253	0.007	0.011	1.308	2.393	2.003
108	5023814.115	577573.5	337.003	0.007	0.011	1.39	2.727	2.346
109	5023813.563	577573.497	336.951	0.01	0.016	1.04	1.959	1.66
110	5023812.659	577573.823	337.141	0.01	0.015	1.046	1.957	1.654
111	5023808.933	577567.723	336.984	0.006	0.007	0.961	1.693	1.394
112	5023809.696	577566.989	336.872	0.006	0.008	1.007	1.805	1.498
113	5023810.444	577566.323	336.798	0.006	0.008	0.968	1.692	1.388
114	5023811.145	577565.648	336.939	0.006	0.008	0.971	1.691	1.384
115	5023813.422	577563.671	336.835	0.008	0.008	1.233	1.854	1.385
116	5023814.082	577562.945	336.735	0.007	0.008	1.23	1.846	1.376
117	5023814.865	577562.326	336.724	0.008	0.01	1.615	2.655	2.107

118	5023815.606	577561.565	336.688	0.008	0.008	1.34	2.039	1.536
119	5023816.299	577561.029	336.936	0.007	0.008	0.994	1.681	1.356
120	5023817.189	577560.368	337.019	0.006	0.008	0.997	1.679	1.352
121	5023817.952	577559.735	337.057	0.012	0.013	1.595	2.48	1.898
122	5023818.732	577559.131	336.743	0.008	0.009	1.221	1.819	1.348
123	5023819.555	577558.499	337.013	0.007	0.008	1.005	1.675	1.339
124	5023820.284	577557.876	336.975	0.007	0.008	1.217	1.808	1.337
125	5023821.067	577557.221	336.917	0.007	0.009	1.142	1.912	1.534
126	5023821.754	577556.544	336.661	0.007	0.008	1.06	1.817	1.475
127	5023822.671	577556.07	336.884	0.007	0.008	1.018	1.666	1.319
128	5023823.478	577555.553	336.881	0.014	0.012	1.688	2.445	1.769
129	5023824.227	577554.893	336.892	0.007	0.008	1.05	1.701	1.338
130	5023825.08	577554.154	336.478	0.008	0.01	1.383	2.114	1.598
131	5023825.792	577553.53	336.567	0.013	0.017	1.394	2.2	1.701
132	5023826.618	577552.963	336.863	0.012	0.017	1.559	2.424	1.856
133	5023790.687	577539.845	335.792	0.006	0.01	1.032	2.054	1.776
134	5023791.62	577539.192	335.497	0.007	0.011	1.276	2.442	2.082
135	5023792.325	577538.613	335.452	0.007	0.011	1.31	2.455	2.076
136	5023792.915	577538.004	335.326	0.008	0.012	1.39	2.494	2.071
137	5023793.331	577537.476	335.385	0.008	0.011	1.389	2.488	2.064
138	5023794.092	577537.188	335.333	0.007	0.012	1.27	2.411	2.049
139	5023794.695	577536.765	335.26	0.007	0.011	1.389	2.472	2.044
140	5023795.4	577536.385	335.26	0.008	0.011	1.389	2.461	2.031
141	5023795.912	577536.02	335.357	0.008	0.011	1.388	2.45	2.019
142	5023796.572	577535.283	335.268	0.007	0.012	1.309	2.489	2.117
143	5023797.276	577534.74	335.203	0.012	0.019	1.292	2.4	2.022
144	5023798.009	577534.192	335.216	0.008	0.013	1.399	2.456	2.019
145	5023798.68	577533.682	335.369	0.007	0.011	1.252	2.319	1.951
146	5023799.033	577533.428	335.537	0.007	0.011	1.251	2.311	1.943
147	5023799.695	577532.837	335.662	0.008	0.012	1.25	2.304	1.936
148	5023800.565	577532.166	335.718	0.009	0.013	1.387	2.376	1.93
149	5023801.511	577531.218	335.732	0.008	0.011	1.387	2.371	1.923
150	5023802.474	577530.653	335.79	0.009	0.013	1.345	2.516	2.127
151	5023803.408	577530.043	335.906	0.013	0.018	1.45	2.773	2.364
152	5023804.385	577529.528	335.922	0.011	0.016	1.338	2.476	2.083
153	5023812.537	577537.992	336.41	0.013	0.02	1.256	2.525	2.191
154	5023811.911	577538.763	336.526	0.008	0.012	1.246	2.303	1.937
155	5023811.389	577539.5	336.33	0.011	0.02	1.272	2.623	2.294
156	5023810.662	577540.425	335.879	0.007	0.012	1.244	2.299	1.933

157	5023810.294	577541.143	335.93	0.007	0.012	1.285	2.358	1.977
158	5023809.704	577541.943	336.059	0.006	0.011	0.972	2.132	1.897
159	5023809.127	577542.74	336.107	0.007	0.011	1.129	2.227	1.92
160	5023808.393	577543.591	336.041	0.007	0.012	1.243	2.294	1.928
161	5023807.729	577544.487	336.241	0.012	0.021	1.235	2.467	2.135
162	5023807.012	577545.626	335.846	0.007	0.013	1.289	2.569	2.223
163	5023806.34	577546.731	335.76	0.007	0.014	1.29	2.564	2.215
164	5023805.45	577547.597	335.801	0.008	0.018	0.999	2.801	2.617
165	5023804.684	577548.442	336.014	0.007	0.013	1.06	2.446	2.205
166	5023803.902	577549.266	335.908	0.006	0.012	1.109	2.454	2.189
168	5023802.622	577550.674	336.289	0.01	0.022	1.027	2.404	2.173
169	5023801.842	577551.375	336.323	0.006	0.013	0.938	2.355	2.16
170	5023801.117	577551.936	336.31	0.005	0.012	0.938	2.351	2.156
171	5023805.396	577561.968	336.972	0.006	0.009	1.081	1.955	1.629
172	5023806.374	577560.872	336.823	0.006	0.008	1.04	1.654	1.287
173	5023807.235	577559.781	336.858	0.006	0.009	1.098	1.89	1.538
174	5023808.44	577558.368	336.728	0.006	0.008	1.099	1.89	1.538
175	5023809.414	577557.305	336.703	0.006	0.008	1.012	1.741	1.417
176	5023810.291	577556.106	336.537	0.006	0.008	1.008	1.771	1.456
177	5023810.998	577555.327	336.303	0.006	0.007	1.044	1.645	1.271
178	5023811.929	577554.023	336.024	0.007	0.009	0.999	1.722	1.403
179	5023812.618	577553.285	335.897	0.006	0.008	1.001	1.725	1.405
180	5023813.421	577552.392	335.669	0.006	0.008	1.003	1.727	1.406
181	5023814.365	577551.109	335.56	0.006	0.008	1.006	1.73	1.408
182	5023815.142	577549.958	335.695	0.007	0.009	1.008	1.733	1.409
183	5023815.892	577549.135	336.024	0.007	0.008	1.197	1.752	1.279
184	5023816.452	577548.238	336.183	0.013	0.017	1.076	2.104	1.808
185	5023816.797	577547.454	336.012	0.013	0.016	1.081	1.993	1.674
186	5023817.512	577546.488	335.949	0.009	0.01	1.152	1.997	1.632
187	5023818.113	577545.672	336.483	0.015	0.013	1.718	2.523	1.848
188	5023818.922	577545.005	336.637	0.009	0.01	1.225	2.117	1.726
189	5023820.117	577544.414	336.661	0.011	0.01	1.761	2.446	1.697
190	5023821.204	577543.916	336.686	0.009	0.01	1.236	2.109	1.709
191	5023822.022	577543.301	336.863	0.008	0.01	1.251	2.178	1.783
192	5023820.25	577544.267	336.704	0.008	0.01	1.274	2.343	1.966
193	5023773.941	577529.439	335.837	0.007	0.011	1.248	2.317	1.952
194	5023774.538	577528.596	335.764	0.007	0.01	1.284	2.384	2.008
195	5023775.192	577527.869	335.556	0.008	0.01	1.49	2.496	2.003
196	5023775.89	577527.149	335.771	0.008	0.01	1.428	2.411	1.942

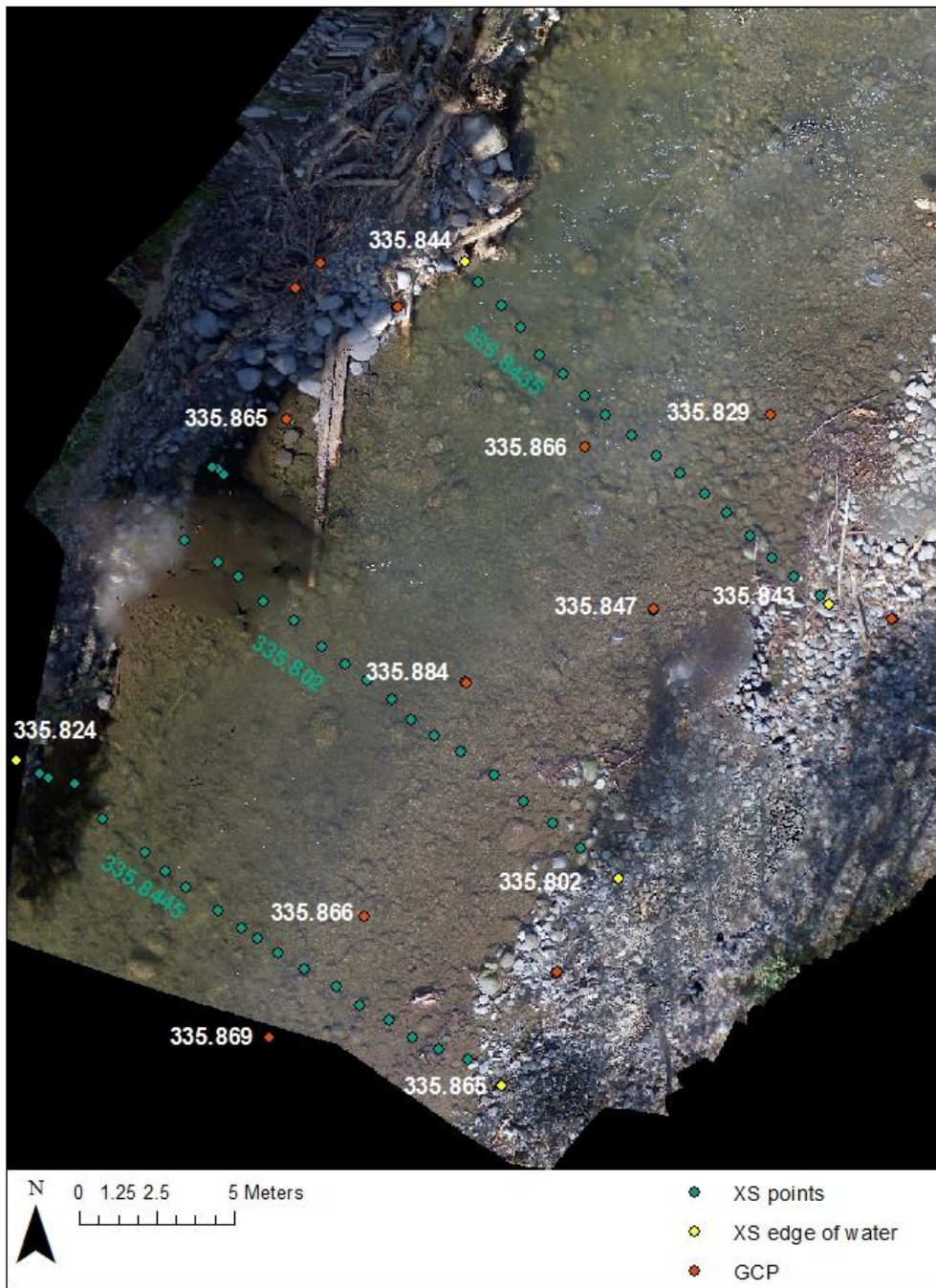
197	5023776.625	577526.428	335.421	0.008	0.01	1.485	2.475	1.98
198	5023777.27	577525.712	335.411	0.009	0.015	1.403	2.859	2.491
199	5023777.924	577524.917	335.347	0.008	0.012	1.362	2.647	2.27
200	5023778.5	577524.148	335.413	0.008	0.011	1.513	2.463	1.943
201	5023779.143	577523.355	335.514	0.007	0.011	1.286	2.313	1.923
202	5023779.798	577522.488	335.144	0.008	0.011	1.521	2.473	1.95
203	5023780.423	577521.835	334.996	0.007	0.01	1.256	2.234	1.847
204	5023781.154	577521.091	335.106	0.008	0.011	1.256	2.223	1.834
205	5023781.77	577520.358	334.913	0.008	0.01	1.528	2.42	1.877
206	5023782.635	577519.737	334.974	0.008	0.014	1.403	2.834	2.462
207	5023783.347	577519.129	334.644	0.008	0.013	1.418	2.901	2.531
208	5023784.104	577518.362	334.712	0.008	0.014	1.405	2.834	2.462
209	5023765.73	577521.651	335.658	0.007	0.012	0.994	2.042	1.783
210	5023766.544	577520.795	335.553	0.008	0.012	1.392	2.635	2.238
211	5023767.272	577519.825	335.432	0.008	0.013	1.333	2.599	2.231
212	5023768.094	577518.856	335.326	0.008	0.012	1.391	2.622	2.223
213	5023768.873	577517.79	335.245	0.008	0.013	1.293	2.535	2.181
214	5023769.41	577516.915	335.122	0.007	0.012	1.291	2.527	2.173
215	5023769.92	577516.181	335.051	0.008	0.013	1.389	2.599	2.196
216	5023770.573	577515.579	334.966	0.009	0.013	1.287	2.515	2.161
217	5023771.203	577514.764	334.93	0.008	0.013	1.387	2.57	2.164
218	5023771.725	577514.019	335.04	0.008	0.014	1.279	2.487	2.133
219	5023772.296	577513.277	335.024	0.008	0.013	1.31	2.502	2.132
220	5023773.141	577512.379	335.01	0.011	0.016	1.498	2.796	2.36
221	5023773.729	577511.369	334.916	0.013	0.02	1.179	2.324	2.002
222	5023774.544	577510.56	335.246	0.01	0.014	1.388	2.491	2.069
223	5023775.026	577509.909	335.215	0.012	0.017	1.466	2.803	2.389
225	5023777.894	577510.125	334.298	0.012	0.015	1.473	2.331	1.806
226	5023778.046	577509.921	334.542	0.01	0.012	1.446	2.276	1.757
227	5023778.128	577509.736	334.74	0.012	0.011	2.029	2.779	1.899
228	5023768.169	577504.132	335.774	0.012	0.011	1.914	2.61	1.774
229	5023768.015	577504.417	335.463	0.015	0.014	2.067	2.746	1.807
231	5023766.703	577506.198	334.936	0.01	0.022	1.07	2.609	2.38
232	5023765.573	577507.529	334.914	0.01	0.02	0.919	2.058	1.841
233	5023764.99	577508.214	334.843	0.007	0.014	1.221	2.826	2.549
234	5023764.472	577508.887	335.064	0.009	0.013	1.713	3.09	2.571
235	5023763.688	577509.904	334.977	0.007	0.011	0.913	2.082	1.871
236	5023763.13	577510.674	335.237	0.006	0.01	0.9	1.936	1.714
237	5023762.794	577511.182	335.141	0.007	0.013	1.184	2.786	2.522

238	5023762.325	577511.866	335.104	0.006	0.01	0.901	1.929	1.705
239	5023761.784	577512.735	335.228	0.006	0.01	0.901	1.925	1.701
240	5023761.241	577513.75	335.272	0.006	0.011	0.902	1.92	1.695
241	5023760.606	577514.527	335.579	0.006	0.013	1.095	2.721	2.491
242	5023760.166	577515.451	335.453	0.01	0.021	1.099	2.709	2.477
243	5023759.56	577516.23	335.593	0.006	0.013	1.095	2.695	2.463
244	5023759.216	577517.056	335.589	0.006	0.013	1.192	2.737	2.464
245	5023758.868	577518.016	335.756	0.006	0.012	1.043	2.638	2.424

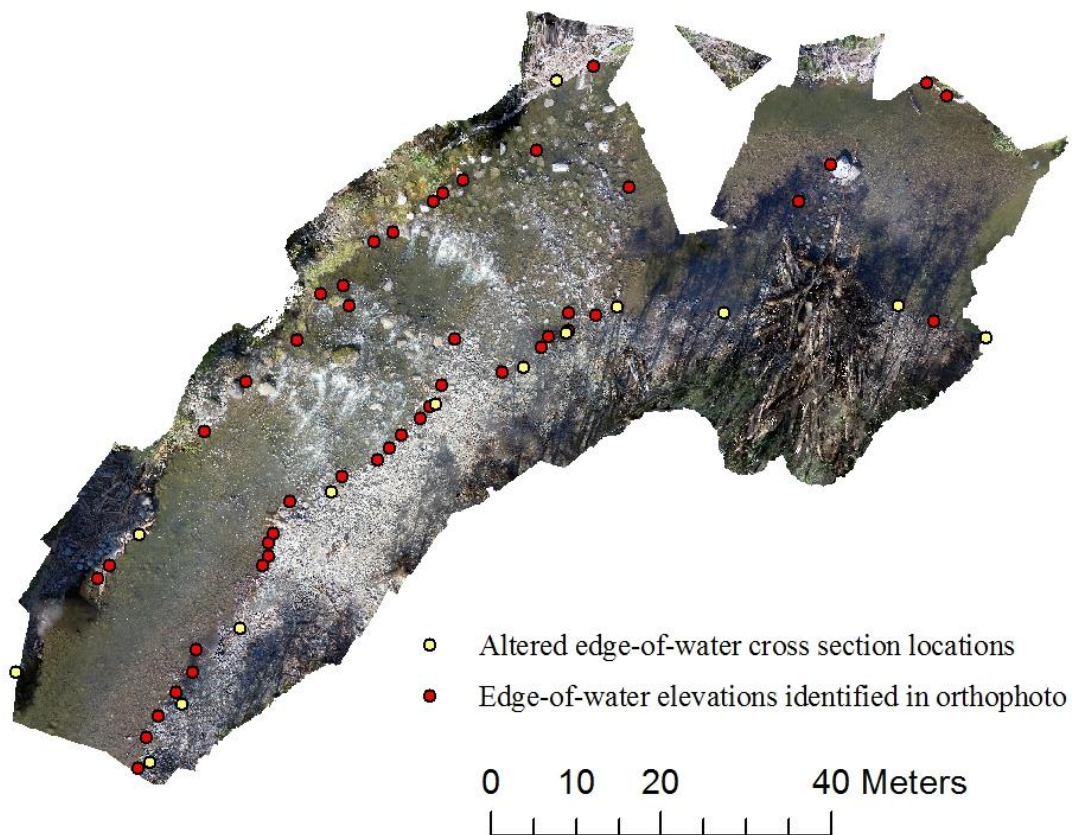
APPENDIX C

WATER SURFACE INTERPOLATION

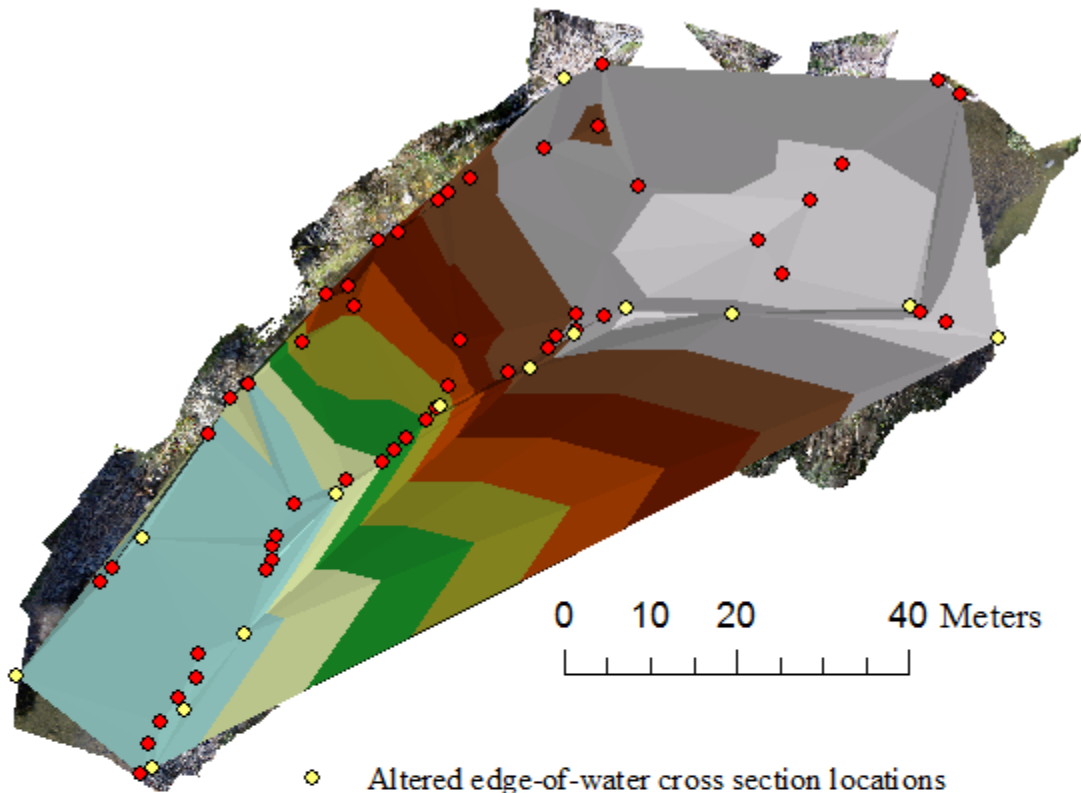
WATER SURFACE ELEVATIONS MEASURED IN THE FIELD AT CROSS SECTIONS 10, 11, AND 12



EDGE-OF-WATER ELEVATION LOCATIONS



TIN 1 OF WATER SURFACE

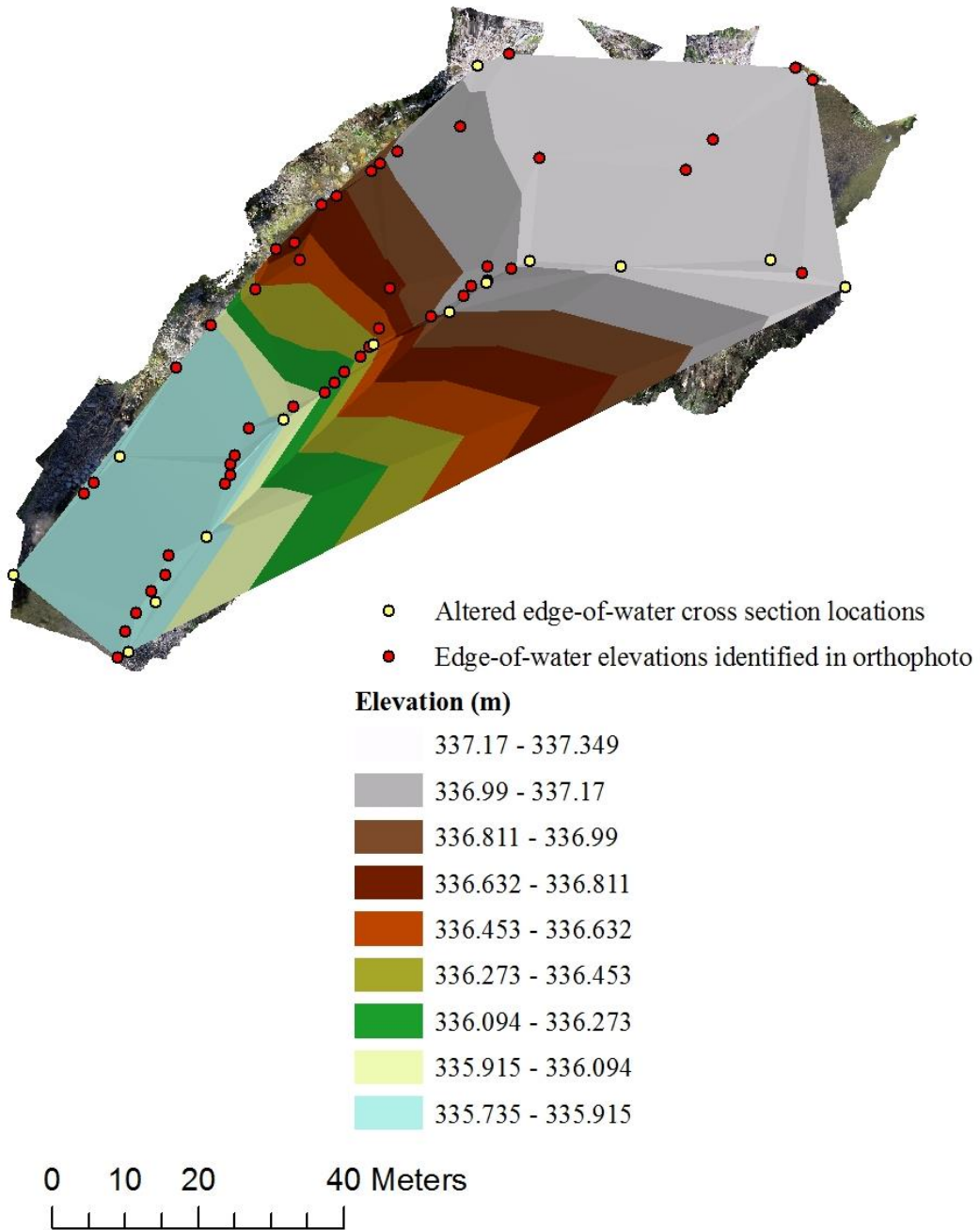


- ◆ Altered edge-of-water cross section locations
- Edge-of-water elevations identified in orthophoto

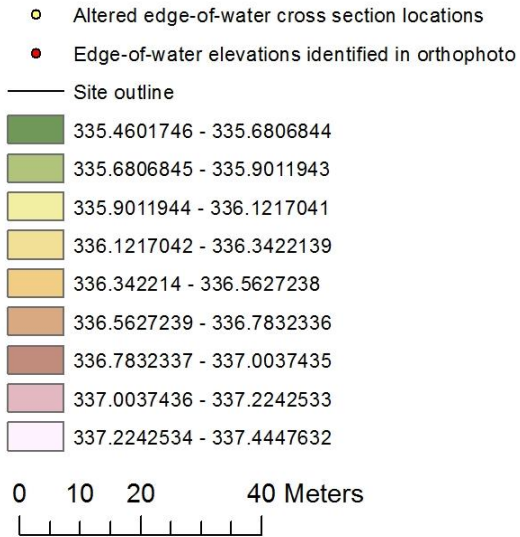
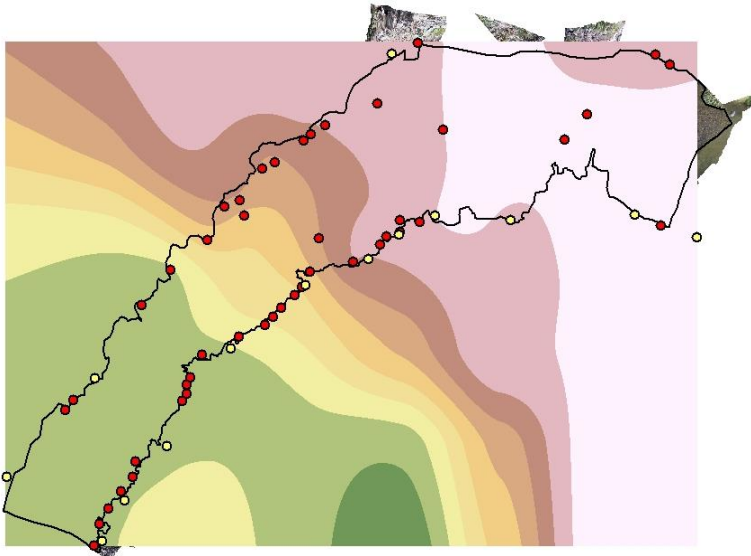
Elevation (m)

◆	337.253 - 337.443
■	337.063 - 337.253
■	336.874 - 337.063
■	336.684 - 336.874
■	336.494 - 336.684
■	336.304 - 336.494
■	336.115 - 336.304
■	335.925 - 336.115
■	335.735 - 335.925

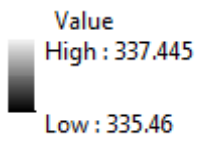
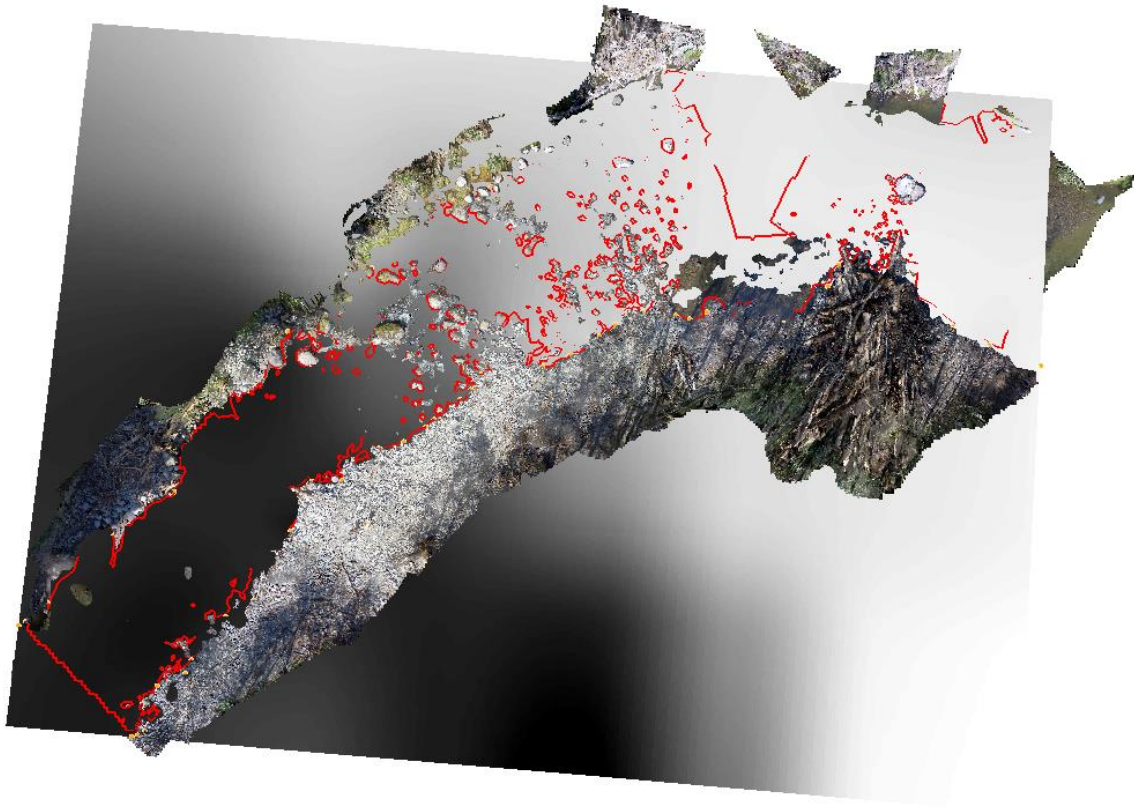
TIN 2 OF WATER SURFACE



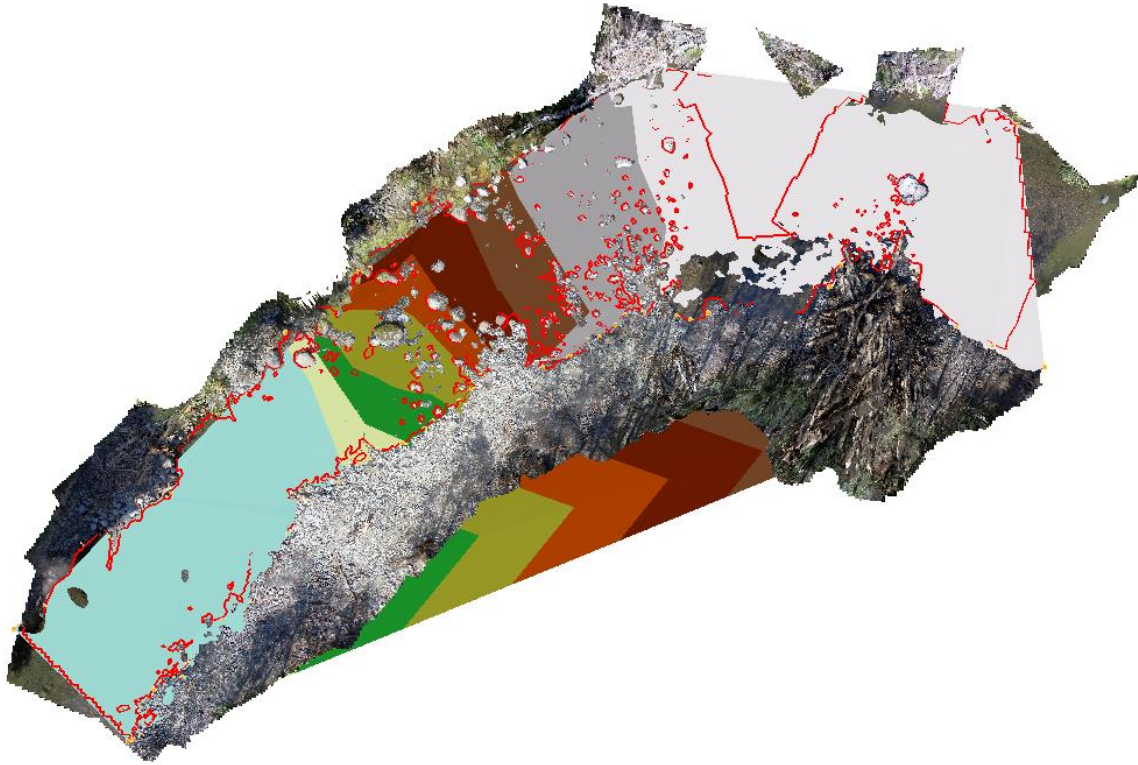
SPLINE OF WATER SURFACE



3D VIEW OF SPLINE WATER SURFACE



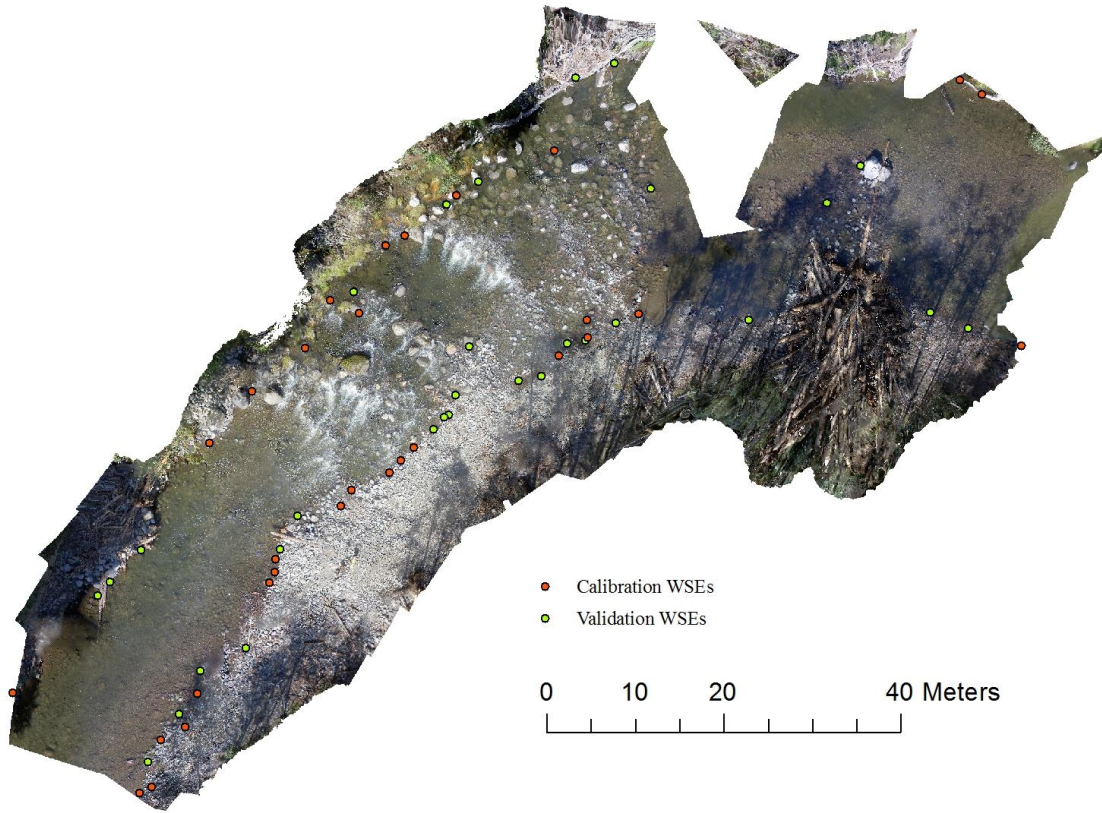
3D VIEW OF TIN 2 WATER SURFACE



Elevation

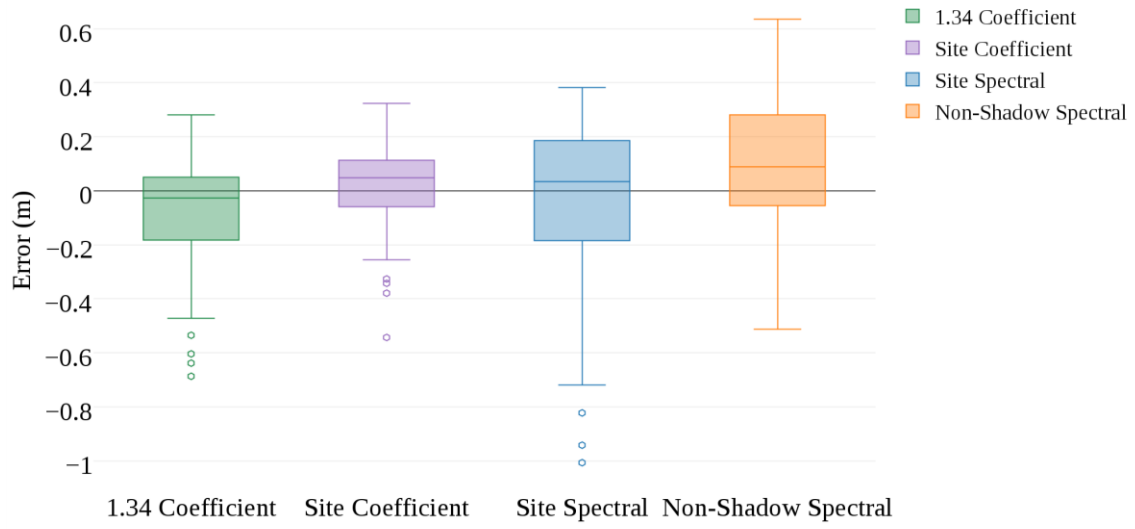
337.17 - 337.349
336.99 - 337.17
336.811 - 336.99
336.632 - 336.811
336.453 - 336.632
336.273 - 336.453
336.094 - 336.273
335.915 - 336.094
335.735 - 335.915

SPATIAL DISTRIBUTION OF WSE DATA FOR QUANTITATIVE COMPARISON
OF WATER SURFACE INTERPOLATION ACCURACY

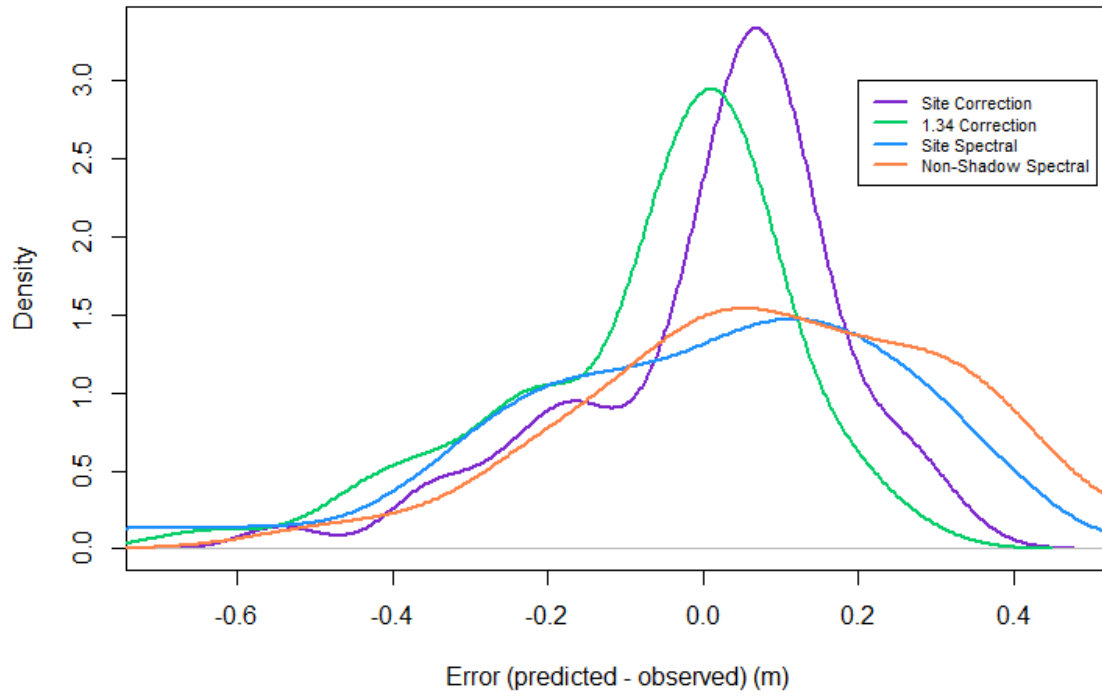


APPENDIX D
ERROR DISTRIBUTIONS

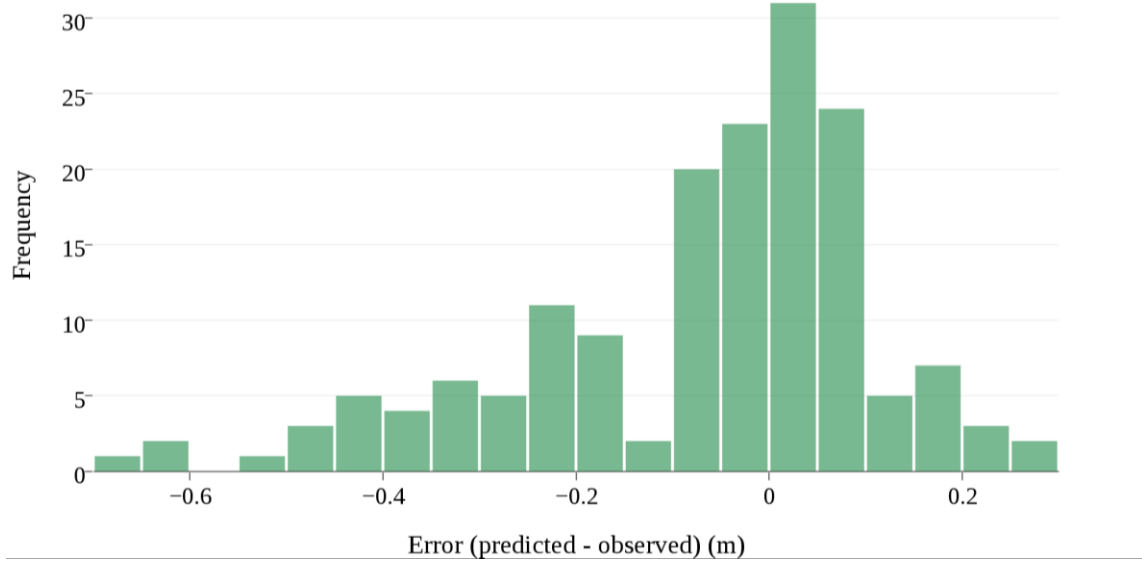
COMPARISON OF DEPTH ERROR BETWEEN METHODS



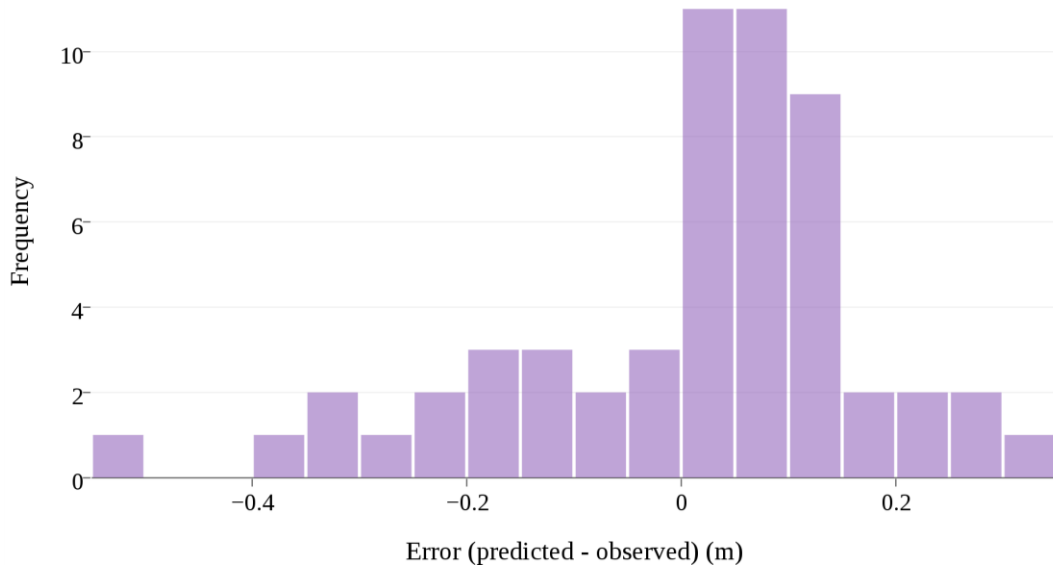
ERROR DENSITY CURVES FOR FINAL CORRECTIONS



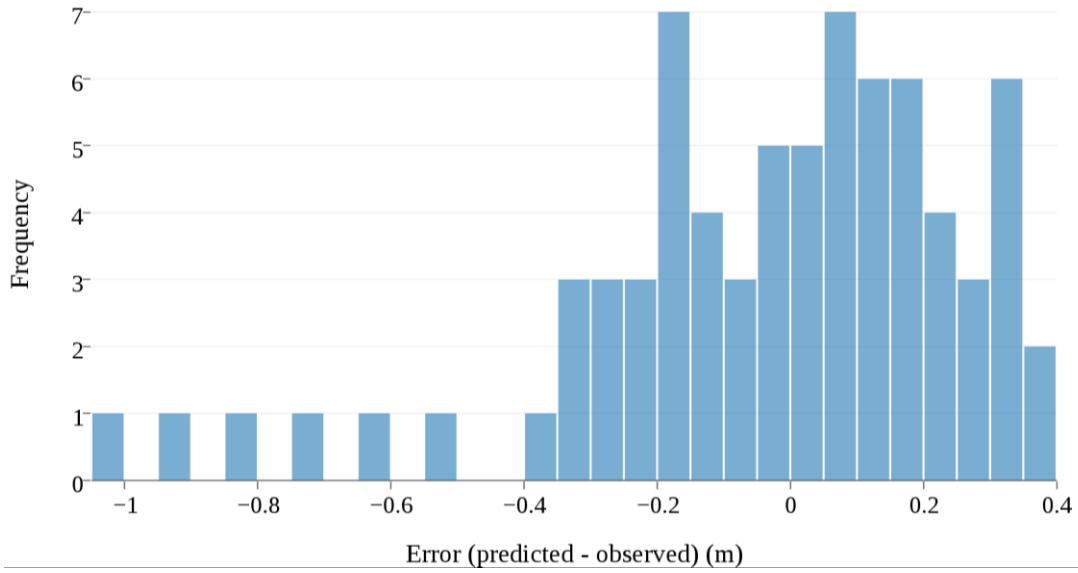
1.34 REFRACTION CORRECTION: DEPTH ERROR DISTRIBUTION



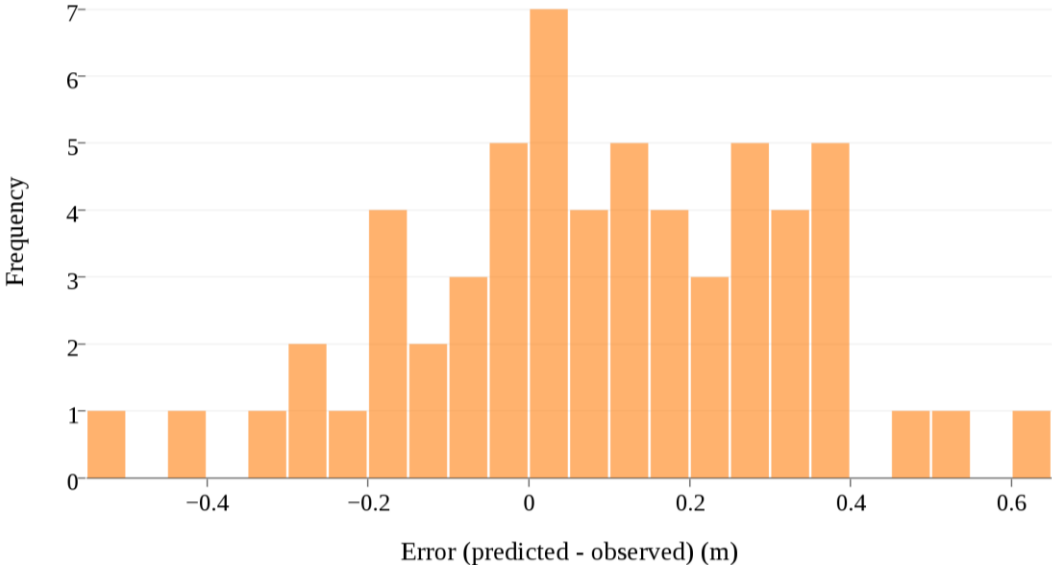
SITE-SPECIFIC REFRACTION CORRECTION: DEPTH ERROR DISTRIBUTION



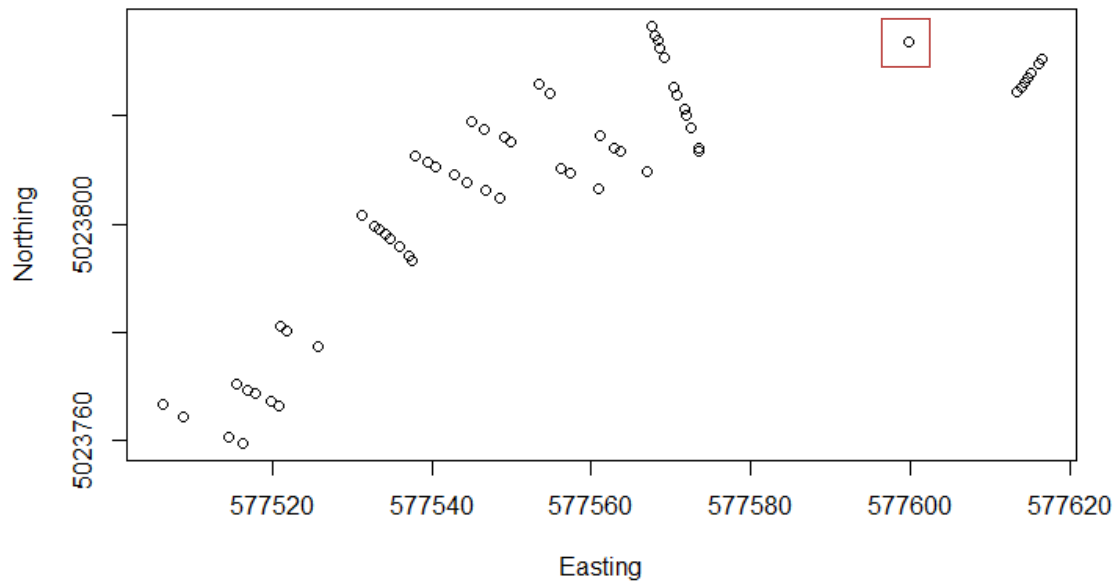
SPECTRAL SITE REGRESSION: DEPTH ERROR DISTRIBUTION



NON-SHADOW SPECTRAL REGRESSION: DEPTH ERROR DISTRIBUTION

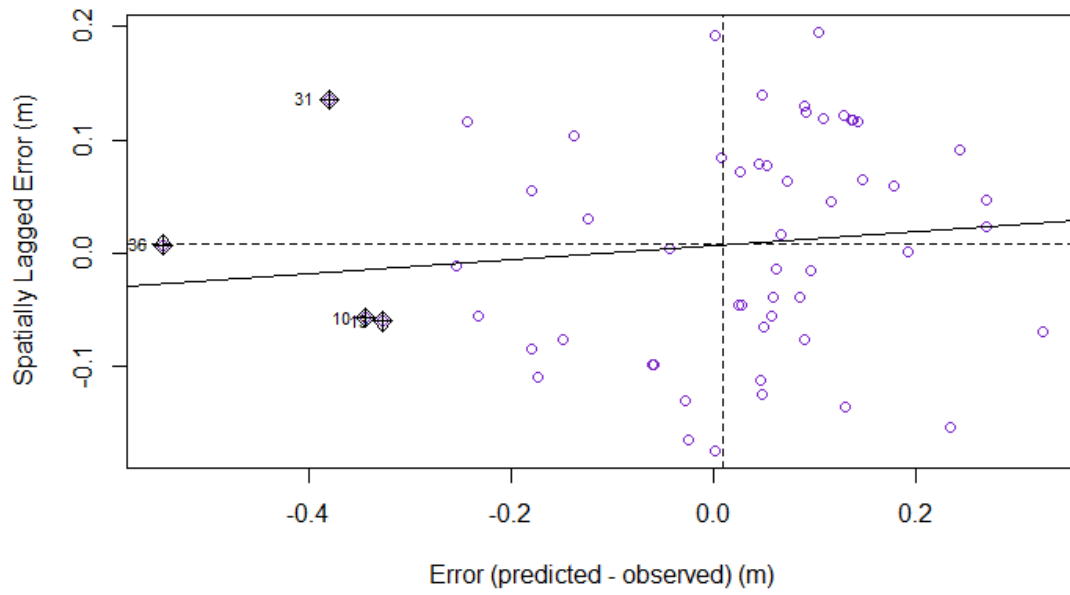


DATA POINT REMOVED PRIOR TO CALCULATING MORAN'S I FOR NON-SHADOW VALIDATION DATA

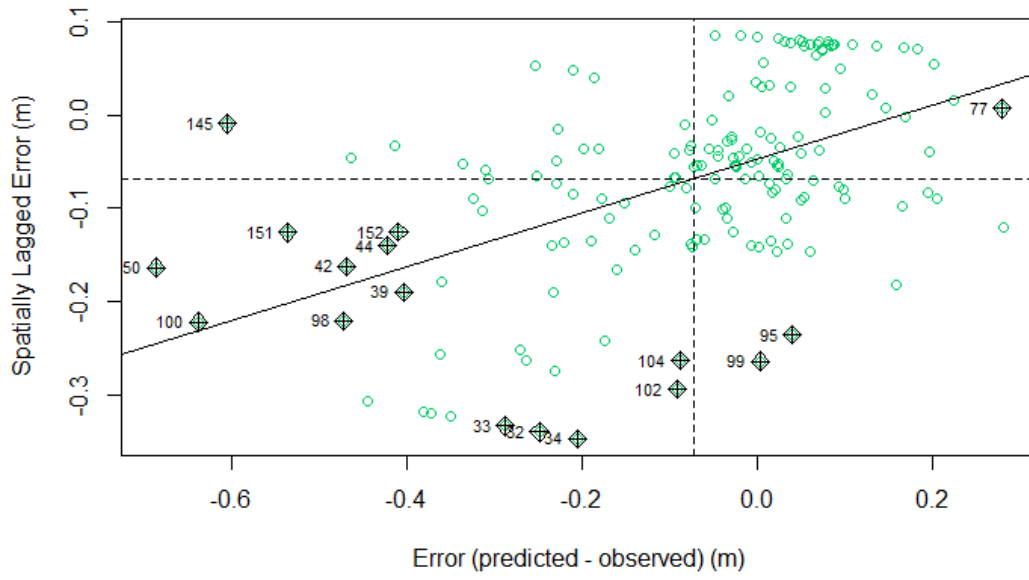


□ Data point removed

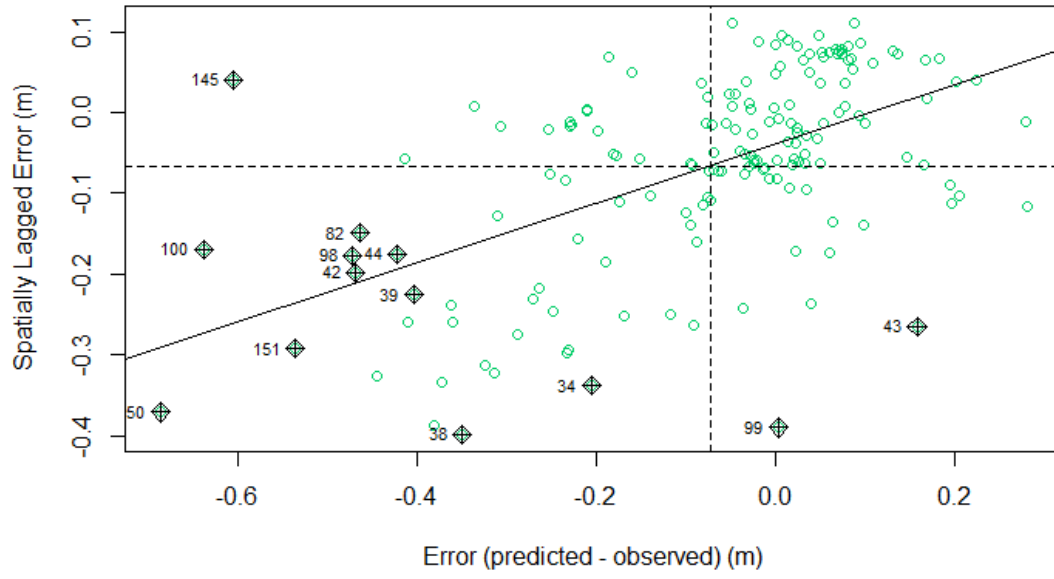
SITE-SPECIFIC COEFFICIENT: MORAN SCATTERPLOT, D = 9



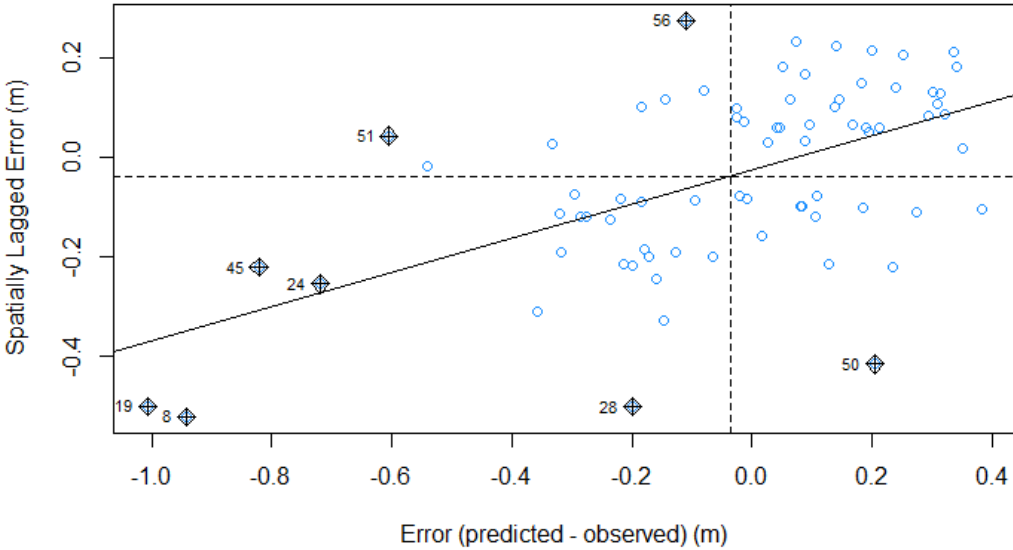
1.34 COEFFICIENT: MORAN SCATTERPLOT, D = 9



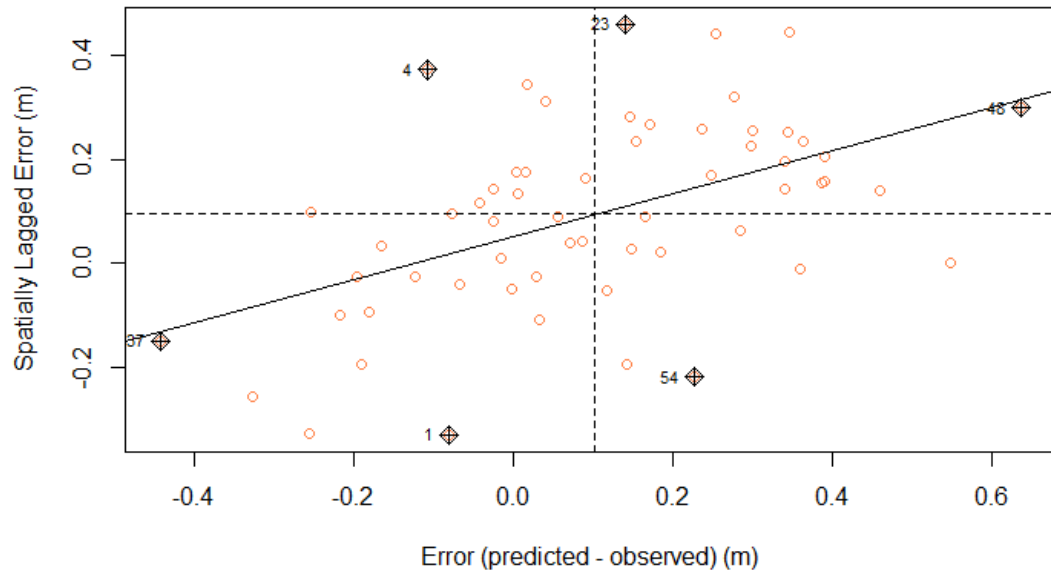
1.34 COEFFICIENT: MORAN SCATTERPLOT, D = 4



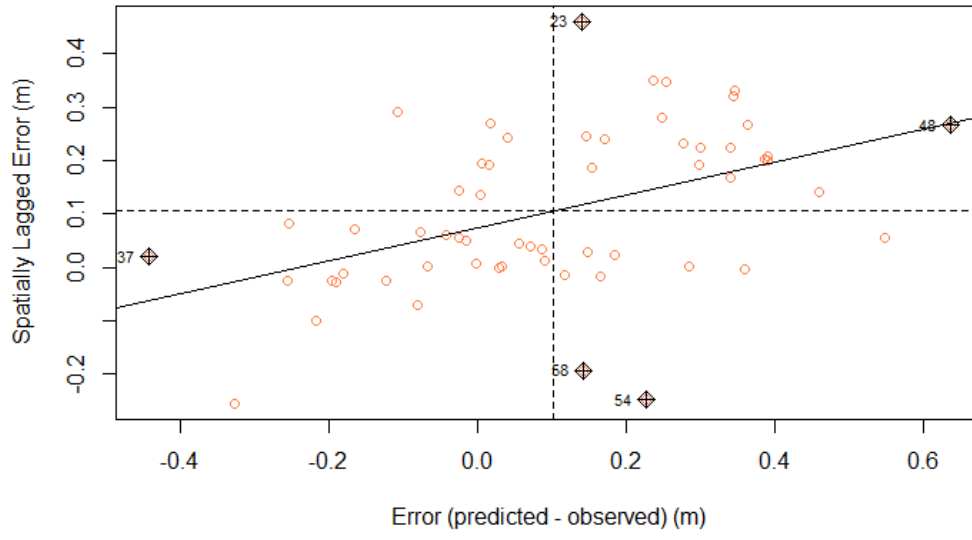
SPECTRAL SITE REGRESSION: MORAN SCATTERPLOT, D = 9



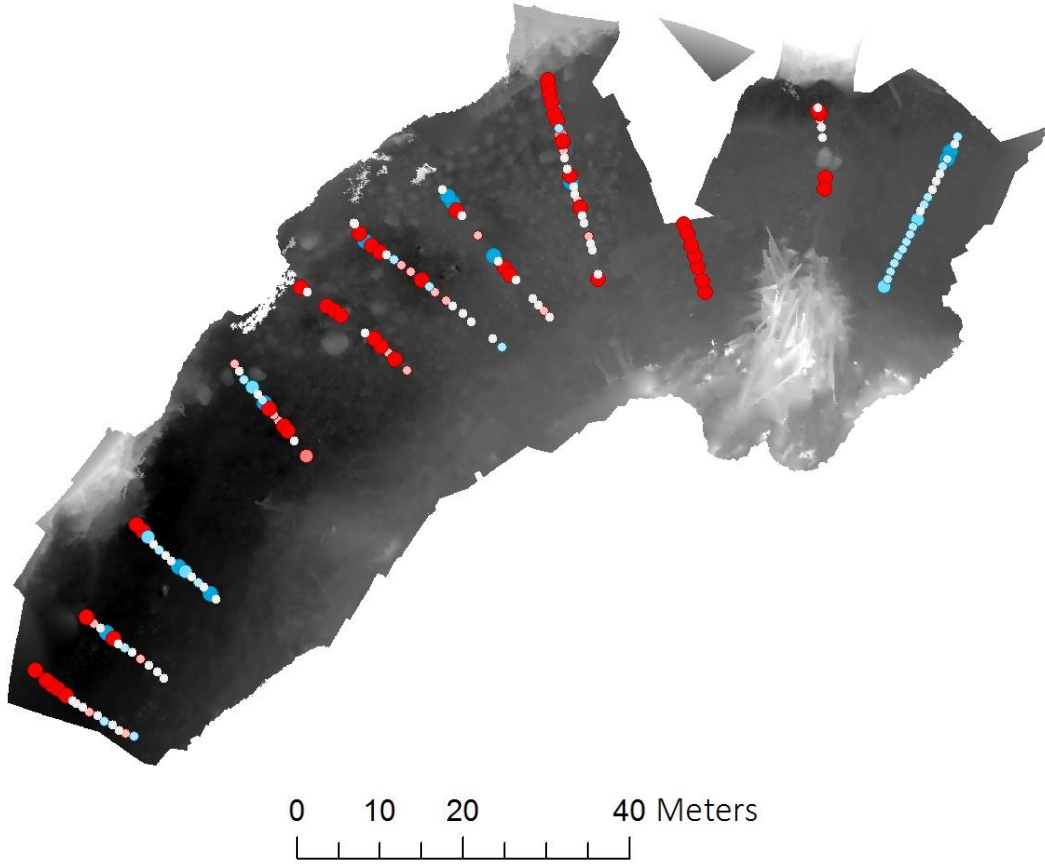
NON-SHADOW SPECTRAL REGRESSION: MORAN SCATTERPLOT, D = 5



NON-SHADOW SPECTRAL REGRESSION: MORAN SCATTERPLOT, D = 9



MAGNITUDE OF ERROR AFTER APPLYING THE 1.34 REFRACTION COEFFICIENT



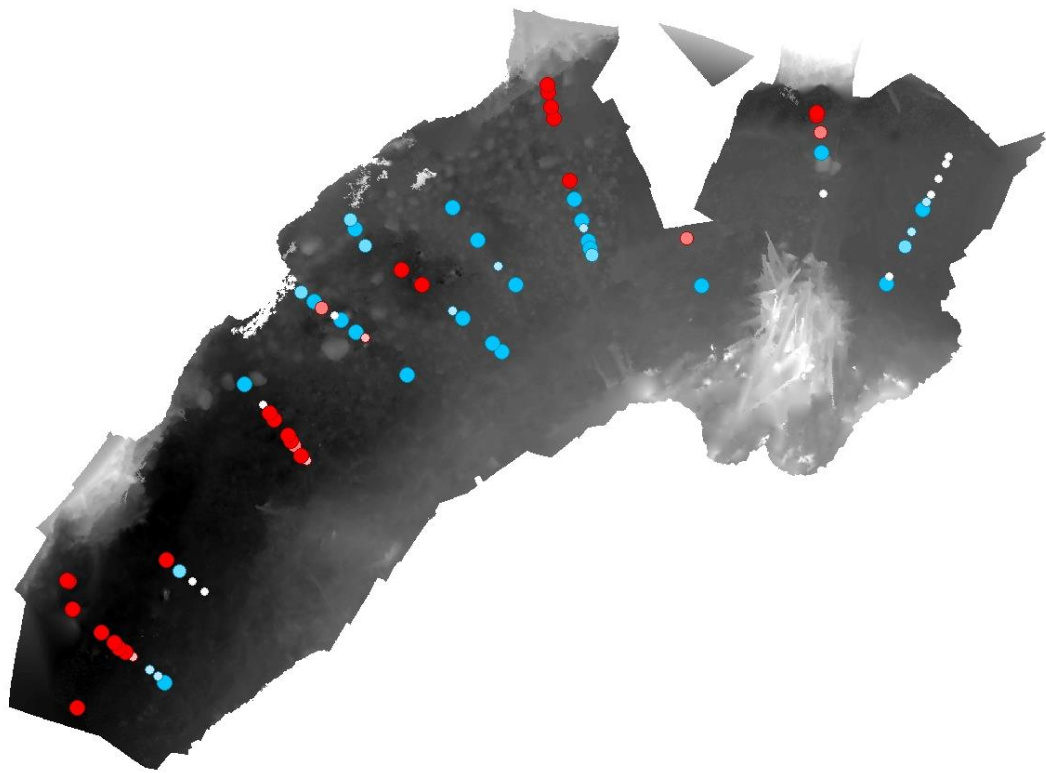
Error (predicted - observed) (m)

- < -0.15
- -0.15 - -0.1
- -0.10 - -0.05
- -0.05 - 0.05
- 0.05 - 0.10
- 0.10 - 0.15
- > 0.15

Elevation (m)

High : 343.9
Low : 333.4

MAGNITUDE OF ERROR AFTER APPLYING THE SITE SPECTRAL DEPTH REGRESSION



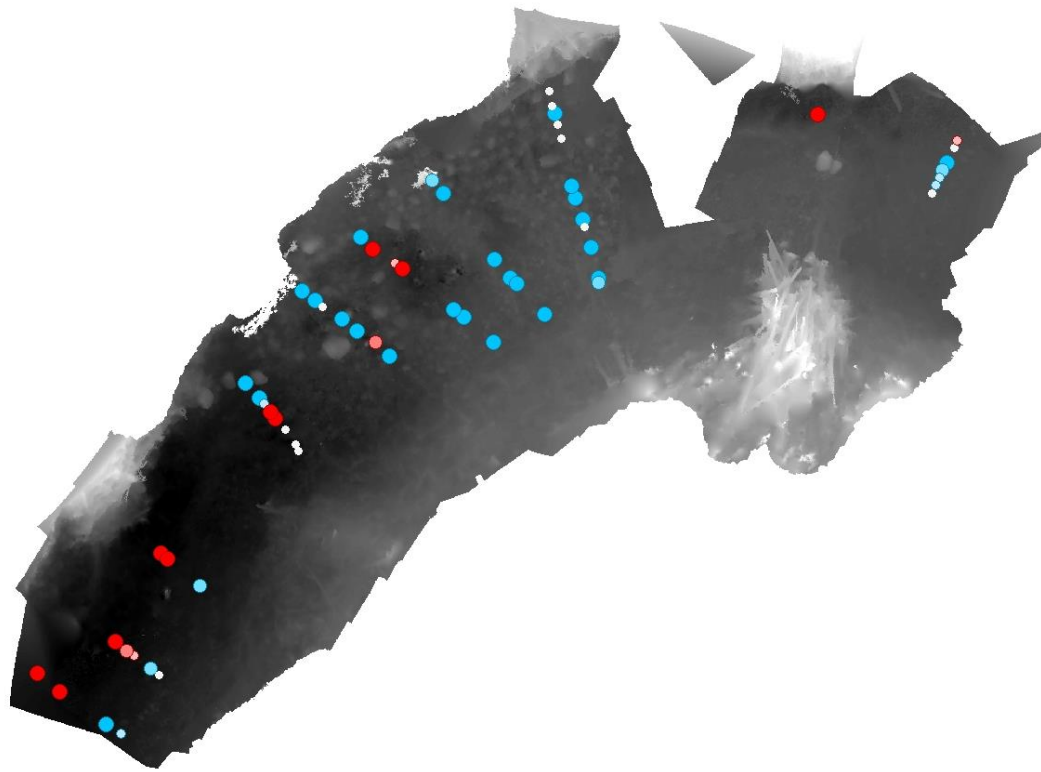
Error (predicted - observed) (m)

- < -0.15
- -0.15 - -0.1
- -0.10 - -0.05
- -0.05 - 0.05
- 0.05 - 0.10
- 0.10 - 0.15
- > 0.15

Elevation (m)

High : 343.9
Low : 333.4

MAGNITUDE OF ERROR AFTER APPLYING THE NON-SHADOW SPECTRAL DEPTH REGRESSION



0 10 20 40 Meters

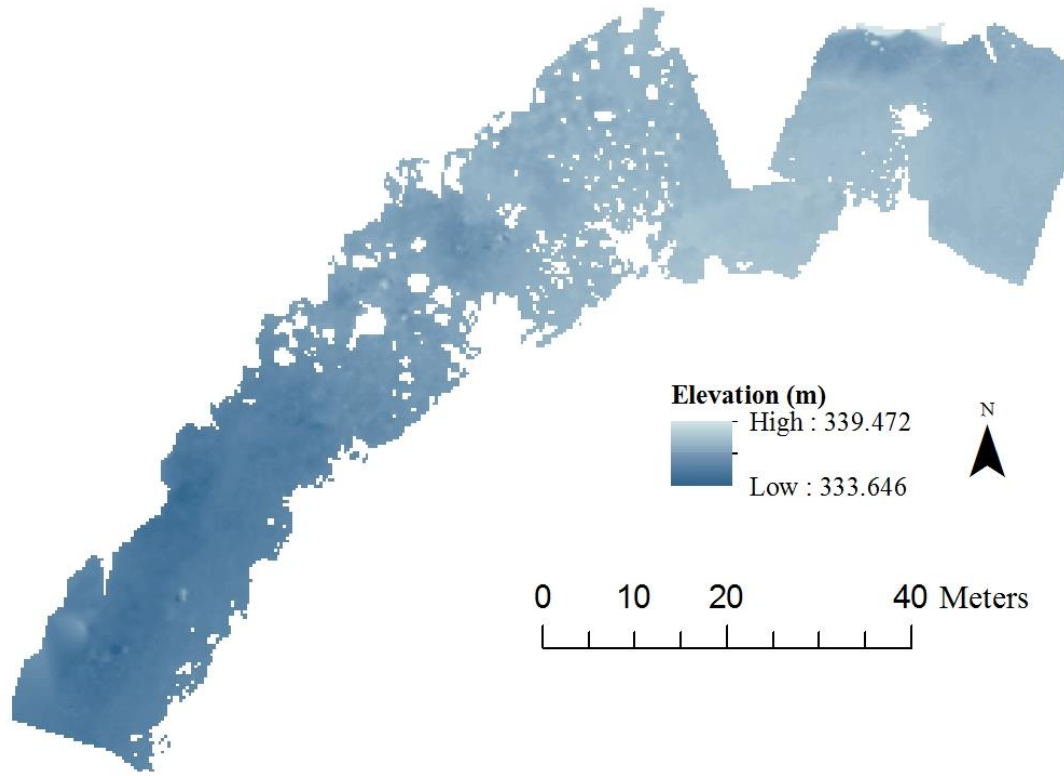
Error (predicted - observed) (m)

- < -0.15
- -0.15 - -0.1
- -0.1 - -0.05
- -0.05 - 0.05
- 0.05 - 0.10
- 0.10 - 0.15
- > 0.15

Elevation (m)

High : 343.9
Low : 333.4

ADJUSTED DEM IN SUBMERGED CHANNEL AFTER SITE SPECIFIC CORRECTION



REFERENCES CITED

- AgiSoft LLC. 2015. PhotoScan Professional Edition v.1.2.3. St. Petersburg, Russia [online] Available from: www.agisoft.com.
- Bangen, S. G., Wheaton, J. M., Bouwes, N., Bouwes, B., & Jordan, C. 2014. A methodological intercomparison of topographic survey techniques for characterizing wadeable streams and rivers. *Geomorphology*, 206(1), 343–361.
- Bergeron, N. & Carbonneau, P. E. 2012. Geosalar: Innovative Remote Sensing Methods for Spatially Continuous Mapping of Fluvial Habitat at Riverscape Scale. In *Fluvial Remote Sensing for Science and Management*, John Wiley & Sons, 193–213.
- Bouwes, N., Moberg, J., Weber, N., Bouwes, B., Bennett, S., Beasley, C., Jordan, C. E., Nelle, P., Polino, M, Rentmeester, S., Semmens, B., Volk, C., Ward, M. B., & White, J. 2011. Scientific protocol for salmonid habitat surveys within the Columbia Habitat Monitoring Program. Prepared by the Integrated Status and Effectiveness Monitoring Program and published by Terraqua, Inc., Wauconda, WA. 118 pages.
- Butler, J. B., Lane, S. N., Chandler, J. H., & Porfiri, E. 2002. Through-water close range digital photogrammetry in flume and field environments. *Photogrammetric Record*, 17(99), 419–439.
- Carbonneau, P. E., Lane, S. N., & Bergeron, N. 2006. Feature based image processing methods applied to bathymetric measurements from airborne remote sensing in fluvial environments. *Earth Surface Processes and Landforms*, 31(11), 1413–1423.
- Carbonneau, P. E., Piegay, H., Lejot, J., Dunford, R., & Michel, K. 2012. Hyperspatial Imagery in Riverine Environments. In *Fluvial Remote Sensing for Science and Management*, John Wiley & Sons, 163-191.
- Carbonneau, P.E. & Piegay, H. 2012. The Growing Use of Imagery in Fundamental and Applied River Sciences. In *Fluvial Remote Sensing for Science and Management*, John Wiley & Sons, 1-18.
- Dietrich, J. T. 2016. Riverscape mapping with helicopter-based Structure-from-Motion photogrammetry. *Geomorphology*, 252(1), 144–157.
- Dugdale, S. J., Carbonneau, P. E., & Campbell, D. 2010. Aerial photosieving of exposed gravel bars for the rapid calibration of airborne grain size maps. *Earth Surface Processes and Landforms*, 35(6), 627–639.

- Feurer, D., Bailly, J.-S., Puech, C., Le Coarer, Y., & Viau, A. A. 2008. Very-high-resolution mapping of river-immersed topography by remote sensing. *Progress in Physical Geography*, 32(4), 403–419.
- Flener, C., Lotsari, E., Alho, P., & Kayhko, J. 2012. Comparison of empirical and theoretical remote sensing based bathymetry models in river environments. *River Research and Applications*, 28, 118–133.
- Fonstad, M. A., Dietrich, J. T., Courville, B. C., Jensen, J. L., & Carbonneau, P. E. 2013. Topographic structure from motion: A new development in photogrammetric measurement. *Earth Surface Processes and Landforms*, 38(4), 421–430.
- Fonstad, M. A. & Marcus, W. A. 2005. Remote sensing of stream depths with hydraulically assisted bathymetry (HAB) models. *Geomorphology*, 72(1), 320–339.
- Harvey, G. L., Clifford, N. J., & Gurnell, A. M. 2008. Towards an ecologically meaningful classification of the flow biotope for river inventory, rehabilitation, design and appraisal purposes. *Journal of Environmental Management*, 88(4), 638–650.
- Hedger, R. D., Dodson, J. J., Bourque, J. F., Bergeron, N. E., & Carbonneau, P. E. 2006. Improving models of juvenile Atlantic salmon habitat use through high resolution remote sensing. *Ecological Modelling*, 197(3), 505–511.
- Heitke, J. D., Archer, E. K., Leary, R. J., & Roper, B. B. 2011. Effectiveness monitoring for streams and riparian areas: sampling protocol for stream channel attributes.
- James, M. R. & Robson, S. 2012. Straightforward reconstruction of 3D surfaces and topography with a camera: Accuracy and geoscience application. *Journal of Geophysical Research: Earth Surface*, 117, 1-17.
- James, M. R., & Robson, S. 2014. Mitigating systematic error in topographic models derived from UAV and ground-based image networks. *Earth Surface Processes and Landforms*, 39(10), 1413–1420.
- Javernick, L., Brasington, J., & Caruso, B. 2014. Modeling the topography of shallow braided rivers using Structure-from-Motion photogrammetry. *Geomorphology*, 213, 166–182.
- Jerlov, N. G. 1976. *Marine Optics*. Elsevier: Amsterdam.
- Legleiter, C. J. 2012. Remote measurement of river morphology via fusion of LiDAR topography and spectrally based bathymetry. *Earth Surface Processes and L*, 499–518.

- Legleiter, C. J. 2015. Calibrating remotely sensed river bathymetry in the absence of field measurements: Flow REsistance Equation-Based Imaging of River Depths (FREEBIRD). *Water Resources Research*, 51, 2865–2884.
- Legleiter, C. J., Roberts, D. A., Marcus, W. A., & Fonstad, M. A. 2004. Passive optical remote sensing of river channel morphology and in-stream habitat: Physical basis and feasibility. *Remote Sensing of Environment*, 93(4), 493–510.
- Legleiter, C. J., Roberts, D. A., & Lawrence, R. L. 2009. Spectrally based remote sensing of river bathymetry. *Earth Surface Processes and Landforms*, 34(8), 1039-1059.
- Legleiter, C. J. & Roberts, D. A. 2009. A forward image model for passive optical remote sensing of river bathymetry. *Remote Sensing of Environment*, 113(5), 1025-1045.
- Legleiter, C.J. & Fonstad, M,A. 2012. An Introduction to the Physical Basis for Deriving River Information by Optical Remote Sensing. In *Fluvial Remote Sensing for Science and Management*, John Wiley & Sons, 43–69.
- Lejot, J., Delacourt, C., Piégay, H., Fournier, T., Trémélo, M., & Allemand, P. 2007. Very high spatial resolution imagery for channel bathymetry and topography from an unmanned mapping controlled platform. *Earth Surface Processes and Landforms*, 32(11), 1705–1725.
- Lyzenga, D. R. (1978). Passive remote sensing techniques for mapping water depth and bottom features. *Applied Optics*, 17(3), 379–383.
- Marcus, W. A. and Fonstad, M. A. 2008. Optical remote mapping of rivers at sub-meter resolutions and watershed extents. *Earth Surface Processes and Landforms*, 33(1), 4-24.
- Marcus, W. A., Legleiter, C. J., Aspinall, R. J., Boardman, J. W., & Crabtree, R. L. 2003. High spatial resolution hyperspectral mapping of in-stream habitats, depths, and woody debris in mountain streams. *Geomorphology*, 55(1), 363-380.
- Marcus, W. A., Fonstad, M. A., & Legleiter C. J. 2012. An Introduction to the Physical Basis for Deriving River Information by Optical Remote Sensing. In *Fluvial Remote Sensing for Science and Management*, John Wiley & Sons, 19–41.
- Montgomery, D. R., & Buffington, J. M. 1998. Channel processes, classification, and response. In Naiman, R. J., and Bilby, R. E. (eds.) *River Ecology and Management: Lessons from the Pacific Coastal Ecoregion*, Springer-Verlag, New York, 13-42.
- Reeves, G. H., Hohler, D. B., Larsen, D. P., Busch, D. E., Kratz, K., Reynolds, K., Stein, K. F., Atzet, T., Hays, P., & Tehan, M. 2004. Effectiveness Monitoring for the Aquatic and Riparian Component of the Northwest Forest Plan: Conceptual

- Framework and Options. Gen. Tech. Rep. PNW-GTR-577. Portland, OR: U.S. Department of Agriculture, Forest Service, Pacific Northwest Research Station. 71 pages.
- Tamminga, A., Hugenholtz, C., Eaton, B., & Lapointe, M. 2015. Hyperspatial remote sensing of channel reach morphology and hydraulic fish habitat using an unmanned aerial vehicle (UAV): A first assessment in the context of river research and management. *River Research and Applications*, 31, 379–391.
- Verdu, J. M., Batalla, R. J., and Martinez-Casasnovas, J. A. 2005. High-resolution grain-size characterization of gravel bars using imagery analysis and geo-statistics. *Geomorphology*, 72(1), 73-93.
- Walther, S. C., Marcus, W. A., & Fonstad, M. A. 2011. Evaluation of high-resolution, true-colour, aerial imagery for mapping bathymetry in a clear-water river without ground-based depth measurements. *International Journal of Remote Sensing*, 32(15), 4343–4363.
- Wanner, G. Personal communication. Mar. 2015.
- Westaway, R. M., Lane, S. N., & Hicks, M. D. 2001. Remote Sensing of Clear-Water, Shallow, Gravel-Bed Rivers Using Digital Photogrammetry. *Photogrammetric Engineering & Remote Sensing*, 67(11), 1271–1281.
- Westoby, M. J., Brasington, J., Glasser, N. F., Hambrey, M. J., & Reynolds, J. M. 2012. ‘Structure-from-Motion’ photogrammetry: A low-cost, effective tool for geoscience applications. *Geomorphology*, 179, 300–314.
- Williams, R. D., Brasington, J., Vericat, D., & Hicks, D. M. 2014. Hyperscale terrain modelling of braided rivers: fusing mobile terrestrial laser scanning and optical bathymetric mapping. *Earth Surface Processes and Landforms*, 39(2), 167–183.
- Winterbottom, S. J. & Gilvear, D. J. 1997. Quantification of channel bed morphology in gravel-bed rivers using airborne multispectral imagery and aerial photography. *Regulated Rivers-Research & Management*, 13(6), 489–499.
- Woodget, A. S., Carbonneau, P. E., Visser, F., & Maddock, I. P. 2014. Quantifying submerged fluvial topography using hyperspatial resolution UAS imagery and structure from motion photogrammetry. *Earth Surface Processes and Landforms*, 40(1), 47–64.